"In presenting the dissertation as a partial fulfillment of the requirements for an advanced degree from the Georgia Institute of Technology, I agree that the Library of the Institution shall make it available for inspection and circulation in accordance with its regulations governing materials of this type. I agree that permission to copy from, or to publish from, this dissertation may be granted by the professor under whose direction it was written, or such copying or publication is solely for scholarly purposes and does not involve potential financial gain. It is understood that any copying from, or publication of, this dissertation which involves potential financial gain will not be allowed without written permission.

("

_____

BEHAVIOR OF CURVED BEAMS UNDER IMPACT LOADING

A THESIS

Presented to

the Faculty of the Graduate Division

Georgia Institute of Technology

In Partial Fulfillment

of the Requirements for the Degree

Master of Science in Civil Engineering

By

Arthur Remington White, Jr.

August 1954

BEHAVIOR OF CURVED BEAMS UNDER IMPACT LOADING

Approved:

Date Approved by Chairman:

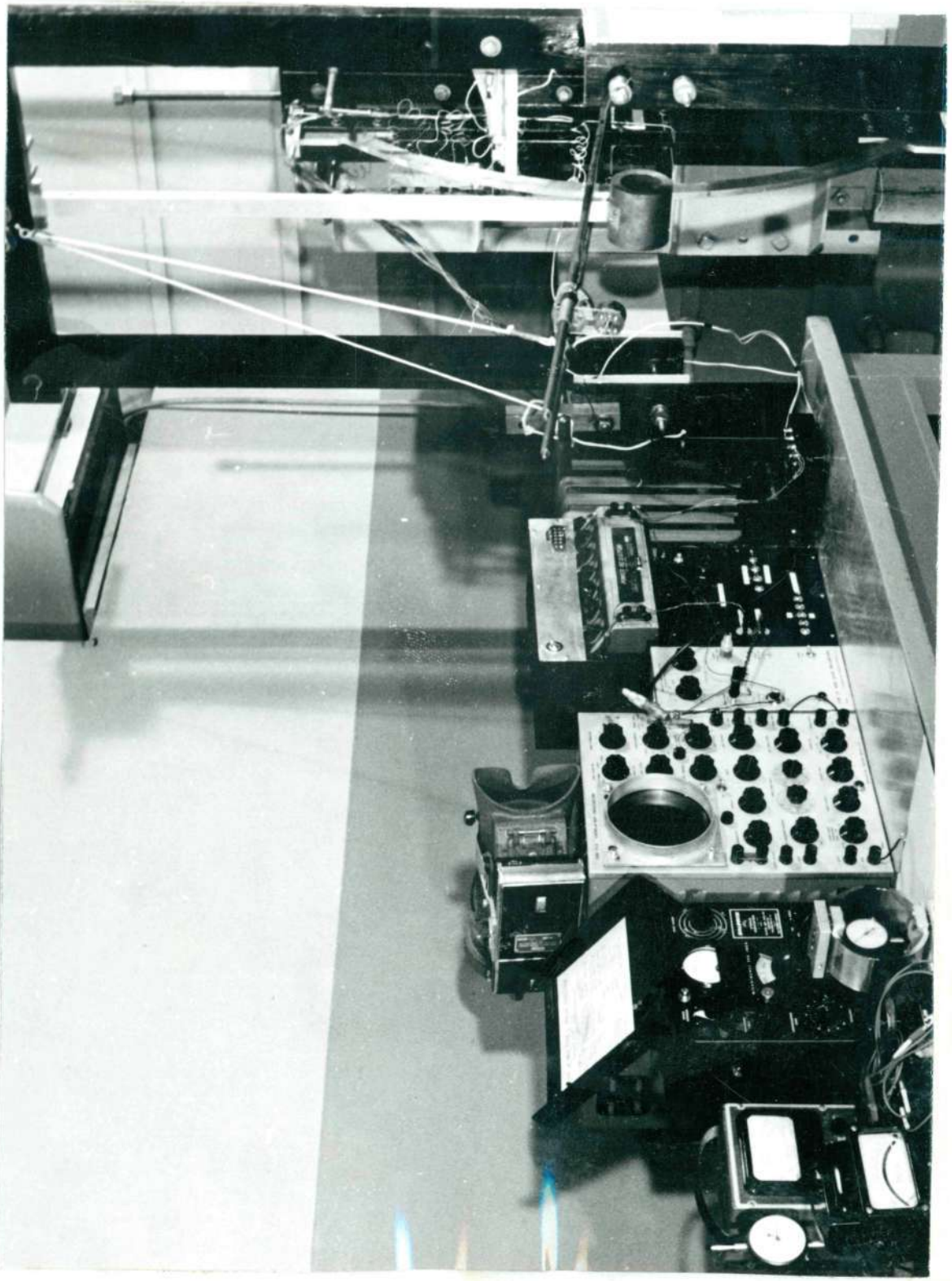

Frontispiece

PREFACE

The purpose of this investigation is two-fold; first to begin a study of the behavior of curved beams under dynamic loading, with special reference to arches in civil engineering use. The secondary purpose is to begin the study of structural dynamics in the Civil Engineering Department of the Georgia Institute of Technology by establishing experimental techniques which would aid future investigators. For this reason a detailed account of the instrumentation and experimental procedures is included in the text.

With the advent of nuclear weapons much attention has recently been paid to the effect of blast loading upon building structures. With this revived interest in dynamic loadings, engineers have begun to examine more critically such loadings as wind, earthquake, and vehicular impact; long considered as "equivalent" static loads, but actually known to be dynamic effects. For some reason bridge structures have received little attention with regards to dynamic loadings. In view of the almost complete lack of available information regarding the dynamic behavior of the arch, the experimental work was confined to this particular type of structure. In addition an approximate theoretical analysis of this same structure was performed. The experimental data was then used as a check on the validity of the theoretical analysis. Due to the complexity of the problem under

consideration, the objectives of the investigation were limited. It was anticipated, however, that once the groundwork for the problem had been established, it would serve as a starting point for future study. Recommendations for this further investigation are made at the end of this thesis.

The writer is indebted to Professor H. C. Saxe, his thesis advisor, for his invaluable assistance and advice. In addition, he would also like to express his thanks to Mr. J. C. Butterworth, of the Engineering Experiment Station for his assistance with the electronic instrumention; and to Professors B. J. Dasher, and F. O. Nottingham of the Electrical Engineering Department for their help in making available their time and equipment. Further acknowledgment is made to Mr. Frank M. Gordon, fellow student in the Civil Engineering Department, for his help in the considerable amount of photographic work involved.

TABLE OF CONTENTS

Page

LIST OF TABLES

LIST OF ILLUSTRATIONS

BEHAVIOR OF CURVED BEAMS UNDER IMPACT LOADING (122)

By: Arthur Remington White Jr.

Advisor: Dr. Harry C. Saxe

The purpose of this thesis is to develop an approximate theory which would facilitate the analysis of stresses produced in a curved bar when subjected to impact loading. The solutions given by this method of analysis are compared with known exact solutions. An experimental investigation was made and this data compared with the results of the approximate theory.

A fixed-end model aluminum arch was selected for experimental study. The bending and thrust strains along the length of the arch were measured with SR-4 wire resistance strain gages and a cathode ray oscilloscope as the model was subjected to a blow from a heavy pendulum. Photographs of the strain-time traces obtained are given in the Appendix. The apparatus and instrumentation techniques are described in detail.

Four factors were analyzed: (1) the maximum stress during impact, (2) the length of time the striking mass is

in contact with the model, (3) the natural frequencies of the bar, and (4) the modes of full vibration of the bar. Solutions exist for the first two factors. The theory by which the latter two are analyzed is original with the writer.

The study lead to the following conclusions: (1) conventional theory gives good results for the maximum stress during impact; (2) the time of contact may be predicted with good accuracy by common methods; (3) the approximate theory of free vibrations of curved bars gives an accurate analysis for bars of small central angles such as would occur in normal bridge and roof structures.

Approved:_____

Date of Approval:_____

CHAPTER I

INTRODUCTION

This study deals with the behavior of an elastic structure when subjected to the impact of a moving mass. At the instant of contact of such a mass with an elastic system, motion ensues. The portion of the system in the vicinity of the point of impact moves first, the more remote portions experiencing no movement due to the inertia of the elastic structure. As the shock wave propagates through the structure, these remote points also experience motion. As the structure deflects it exerts an increasing force on the striking mass which causes a decceleration of the mass until it stops. Then the mass is accelerated in the opposite direction until it leaves contact with the structure at a velocity comparable to its initial velocity. During this cycle the structure itself deflects approximately as the shape of the static-load deflection curve. Superimposed upon this deflection curve, however, is the free vibration of the structure. After the mass is "ejected" from contact with the structure the structure will oscillate in its natural modes of vibration. This vibration is gradually attenuated.

A rigorous general treatment of these phenomena is possible, but would be inordinately complex. A few of the

more important variables include: relative inertia of the structure to that of the mass; velocity of the mass; geometry of the structure; geometry of the contact surfaces; physical properties of the material; effects of plastic action, both local and general; and so on. In order to decrease the variables to a minimum one specific case was selected for study. Aluminum was chosen as the elastic material due to its comparatively low modulus of elasticity and consequent high strain for a given stress. The symmetrical arch, a common bridge structure, was selected due to its difficulty in dynamic analysis a factor justifying experimental study of the problem. One weight of striking mass was used throughout the entire study. The dynamic load was applied at two points, one being the crown of the arch, the other at three-eights point of the span from the left end.

Under each loading the strains due to bending and due to axial force at sixteen selected points on the arch were recorded by means of SR-4 wire resistance strain gages and a cathode-ray oscilloscope. These strains shown with respect to time are given in Appendix A.

The study of this experimental evidence in light of the theoretical considerations developed in the text is made with respect to:

(a) magnitude of maximum stress

(b) length of time of the contact cycle, referred to as the "time of contact"

(c) natural frequencies of the arch

(d) modes of free vibration of the arch

As mentioned in the preface, this study is not complete, but is more of the nature of an interim report. However, the data taken is given in detail and further study of these data is recommended as mentioned in the final chapter of this writing.

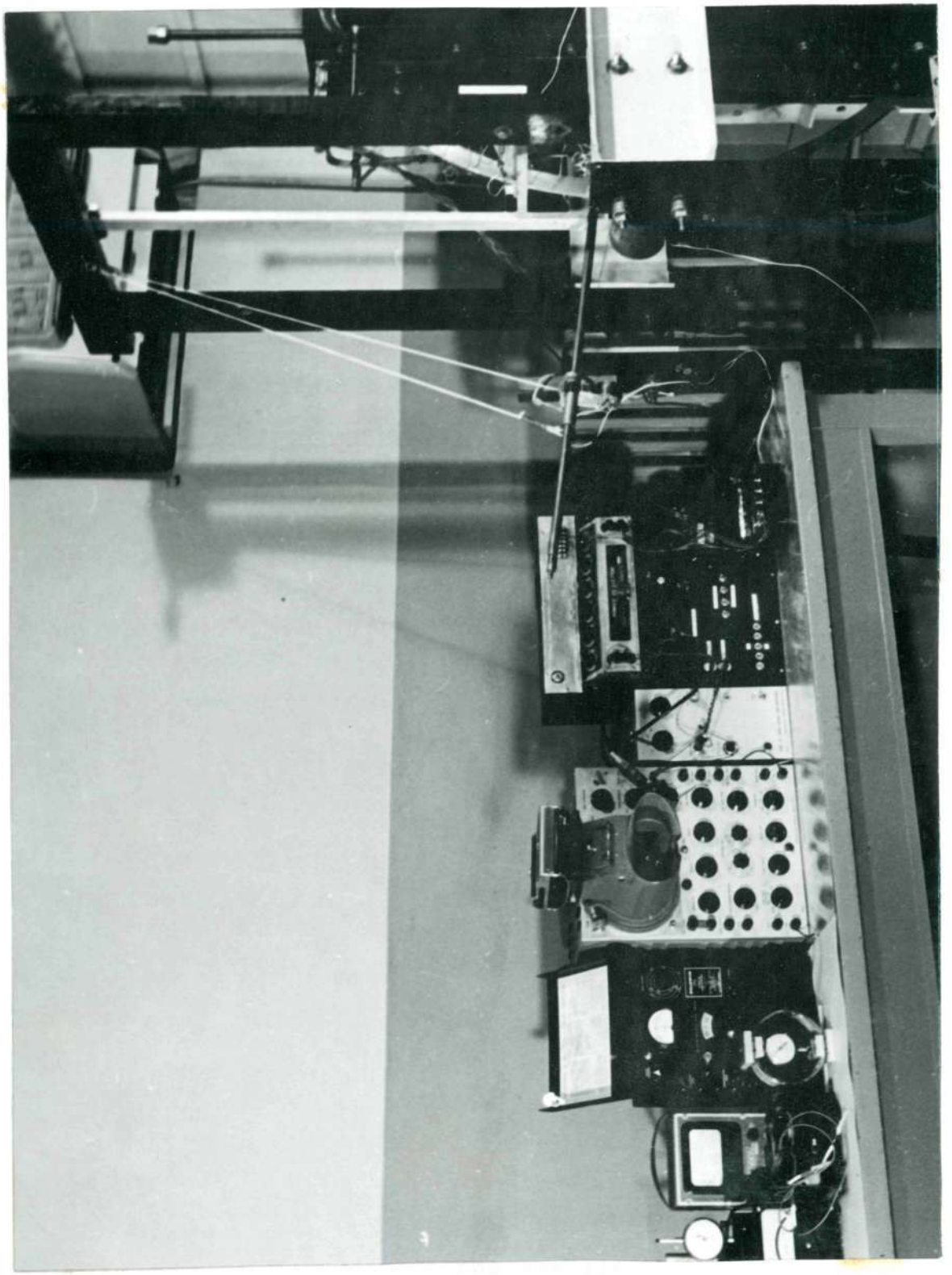

Fig. 1 Overall View of Apparatus

CHAPTER II

APPARATUS AND INSTRUMENTATION

An overall view of the equipment used may be seen in Fig. 1. From right to left:

(a) frame

(b) model with its normally horizontal axis placed vertically to receive the pendulum blow

(c) the pendulum and pendulum release

(d) the DC strain gage power supply

(e) the switching unit

(f) the oscilloscope amplifier

(g) the oscilloscope with photographic attachment

(h) the static strain indicator

(i) the proving ring

(j) miscellaneous electrical equipment

The frontispiece is a slightly better view of the entire apparatus, showing the oscilloscope screen with the camera removed and placed on top of the oscilloscope. In this photograph the strain gages may be seen with the associated wiring as well as the trigger mechanism used to start the sweep of the electron beam of the oscilloscope.

Various features of the apparatus will now be discussed in detail:

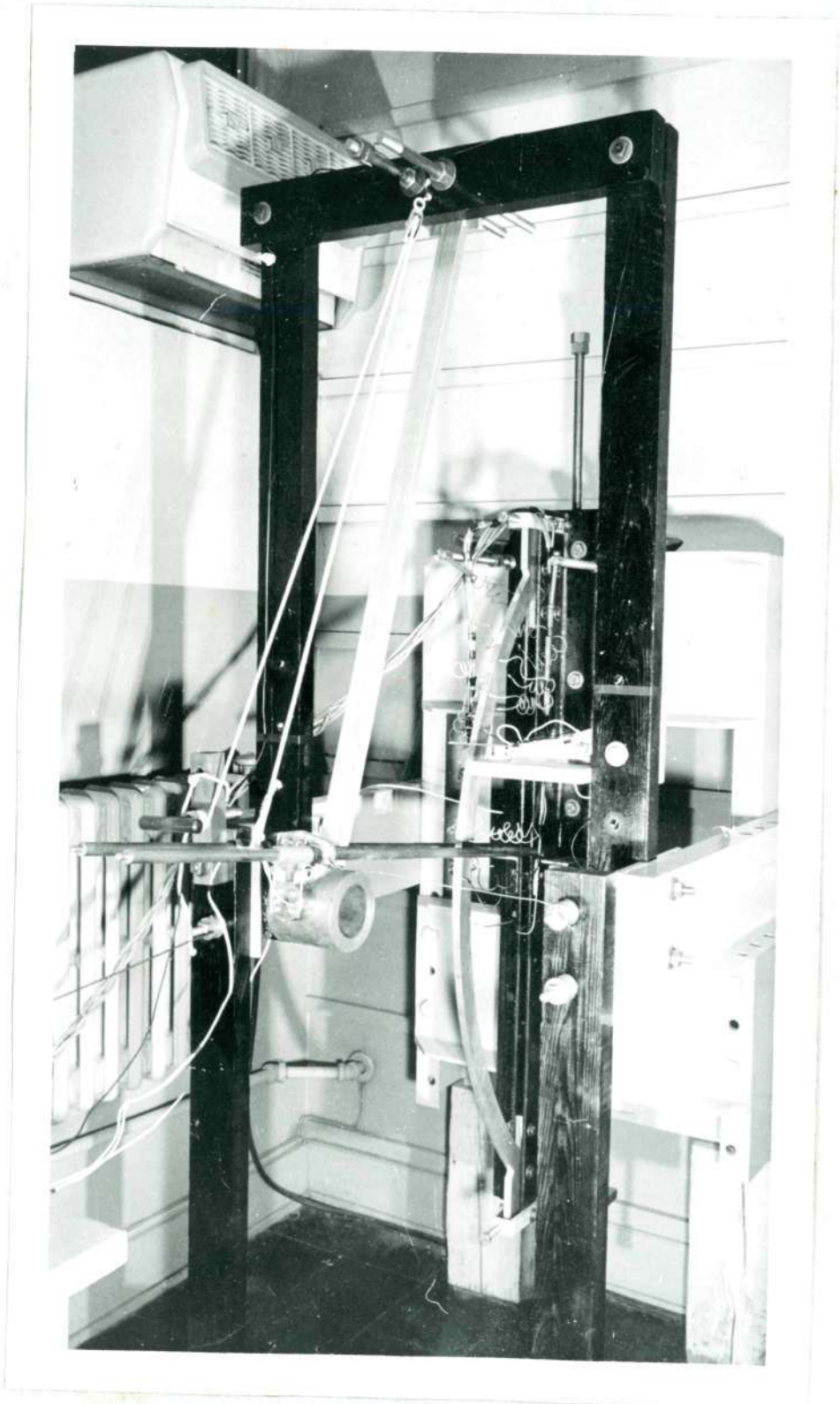

Fig. 2 Detail View of Model Showing Pendulum

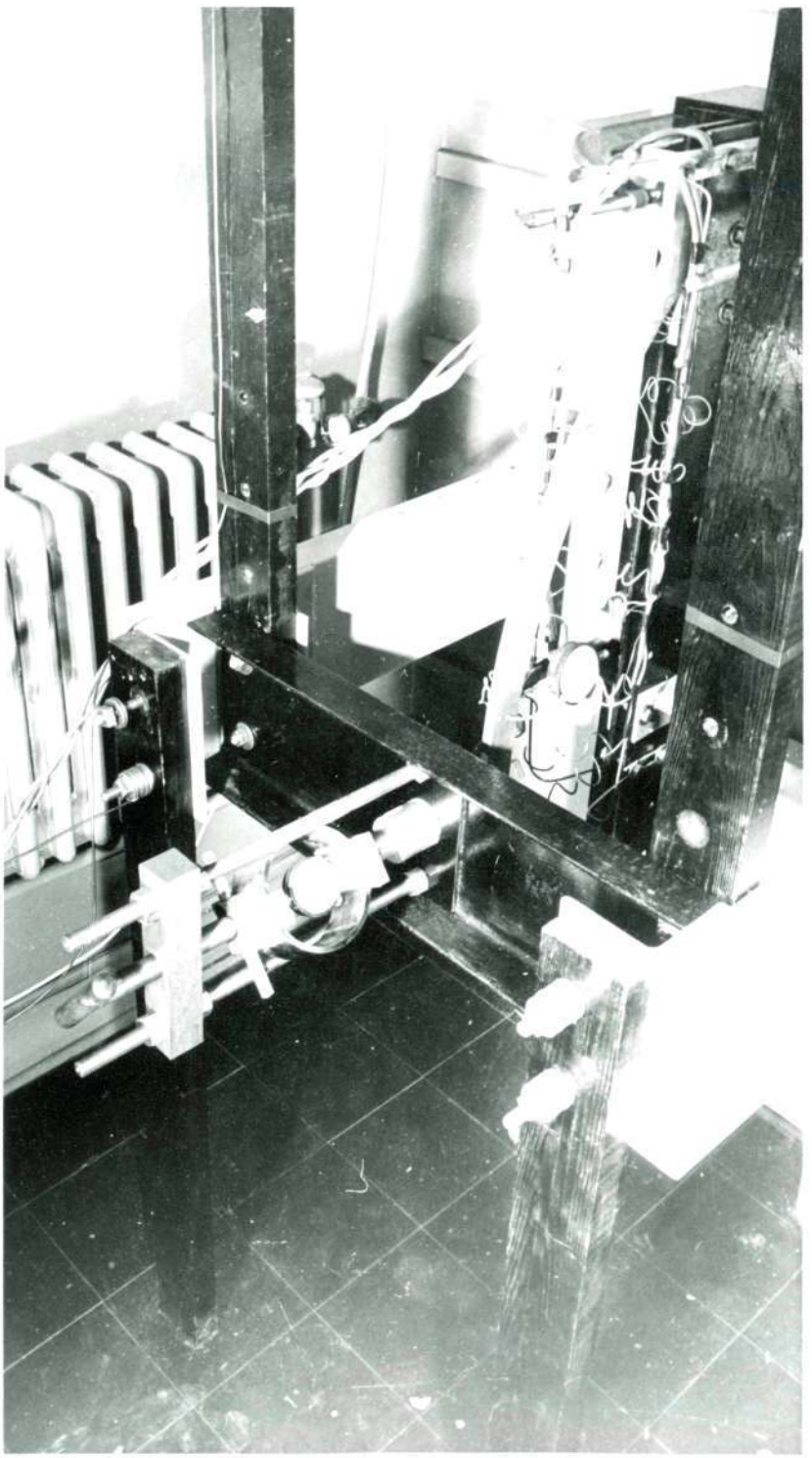

Fig. 3 Detail View of Model Showing Static Load Device

Frame.--The frame had two distinct parts: (a) the base holding the model, and (b) the frame which supported this base and provided a means of applying the load. The base for the model consisted of two very heavy clip angles between which the ends of the model were rigidly bolted. These clip angles were bolted to a heavy channel section with plates welded on the ends with large bolts through these plates to provide for vertical adjustment of the entire base and model assembly with respect to the frame. The flexural rigidity of this base was about two-hundred times that of the model itself.

The frame consisted of channel sections bolted together to provide adaptability when dealing with different models. The entire assembly was designed to permit the loading of the model at any point. A detailed photograph is shown in Fig. 2.

Static Load Device.--The device for applying a static load to the arch is shown in Fig. 3. A channel was bolted across the frame in front of the model. Set in this channel was a lubricated brass bushing through which a steel pin with a rounded point was inserted in make contact with the model. The calibrated proving ring was placed between this pin and the threaded pin which was turned by hand to apply the load. Loads up to 1500 pounds with an accuracy of ± 1 per cent were obtained with this device. When a load was applied to the model, the pin was tapped lightly with a hammer to eliminate

the effect of friction between the pin and the guide. An Ames dial gage, visible beneath the model, was used to measure the deflections of the model to 0.001 in.

Dynamic Load Device.--The dynamic load device consisted of a simple pendulum shown in Fig. 2. The pendulum itself was a heavy steel cylinder fastened to the end of a light aluminum hollow rectangular shaft. The shaft rotated on a lubricated pin attached to a plate which was in turn fastened to the two threaded bolts visible at the top of the frame in Fig. 2. The plate could be moved to any position along the length of these bolts and then locked in position by four nuts. Before each loading sequence the plate was adjusted so that the pendulum was barely in contact with the model in order that as the pendulum fell and came into contact with the arch its motion would be horizontal.

Two long steel rods supported the electromagnet which was used to hold the pendulum and release it at the desired time. The magnet was powered by dry-cell batteries. The release switch is visible on the control panel.

The weight of the steel cylinder was 9.44 lbs, that of the shaft was 1.26 lbs. If the head, or cylinder, moved at a velocity v, the center of gravity of the shaft would move at a velocity of 1/2v. The total kinetic energy would therefore be $\frac{9.44v^2}{2} + \frac{1.26v^2}{8}$. Equating this to $\frac{M_e v^2}{2}$, where M_e is the "effective" weight of the pendulum concentrated at the end to deliver the same kinetic energy as

the actual pendulum, it is found that M_e is 9.75 lbs. This is the weight of the pendulum used in the computations following.

The length of the pendulum was 41.18 in. The chord distance from the position of the pendulum against the electromagnet to the position of the pendulum when in contact with the model was measured and is referred to in the following as the "pendulum distance". By trigonometry it may be shown that the vertical height of fall of the pendulum mass is the square of the pendulum distance divided by twice the length of the pendulum. Denoting h as the height of fall, then the velocity of the pendulum at the bottom of its swing is given by

$$v = 2gh = \frac{gx^2}{41.18}, \qquad (1)$$

where g is the acceleration of gravity and x is pendulum distance. Knowing the velocity of the pendulum and its effective mass, the kinetic energy delivered to the model by the pendulum for any given pendulum distance may be found.

Model.--The model was a 24 S-T aluminum alloy constant-section circular arch of 28 in. radius. The span was 40.00 in. and the rise equal to 8 1/2 in. The stress strain curve of the material representing the average of three specimens taken from the same plate as the model is shown on Fig. 4.

The arch itself was marked into twenty equal arc lengths and each space numbered consecutively from left to

right. The SR-4 strain gages were placed at the center of selected spaces on the left side of the arch, eight gage sets being used in all. Readings could then be taken at sixteen points on the arch by first loading one side of the arch and then loading the corresponding point on the opposite side of the centerline with an identical load. A detailed drawing of the model and the location of the strain gages is shown by Fig. 5.

Strain Gages and Gage Arrangement.--The SR-4 strain gage consists of an extremely fine metallic wire cemented between two stiff strips of paper. These gages were cemented firmly to the model. As the model underwent strain the fine wire was also strained with a consequent change in length, change in cross section, and change in the resistive properties of the gage wire, resulting in a change in the electrical resistance of the gage. This change in resistance is found to vary linearly with the strain and each particular type of gage may be calibrated. Changes in temperature also affect the resistance of the gage. Compensation for this effect will be discussed more fully in subsequent paragraphs. The gage is manufactured by the Baldwin-Lima-Hamilton Corporation, Philadelphia, Pennsylvania, and the reader is referred to the publications of the manufacturer or to (Reference 9) for more complete discussion of the gage. The gage is available commercially in a variety of gage lengths varying from 1/16th of an inch to 4 in. The sensitivity of the gage is not materially

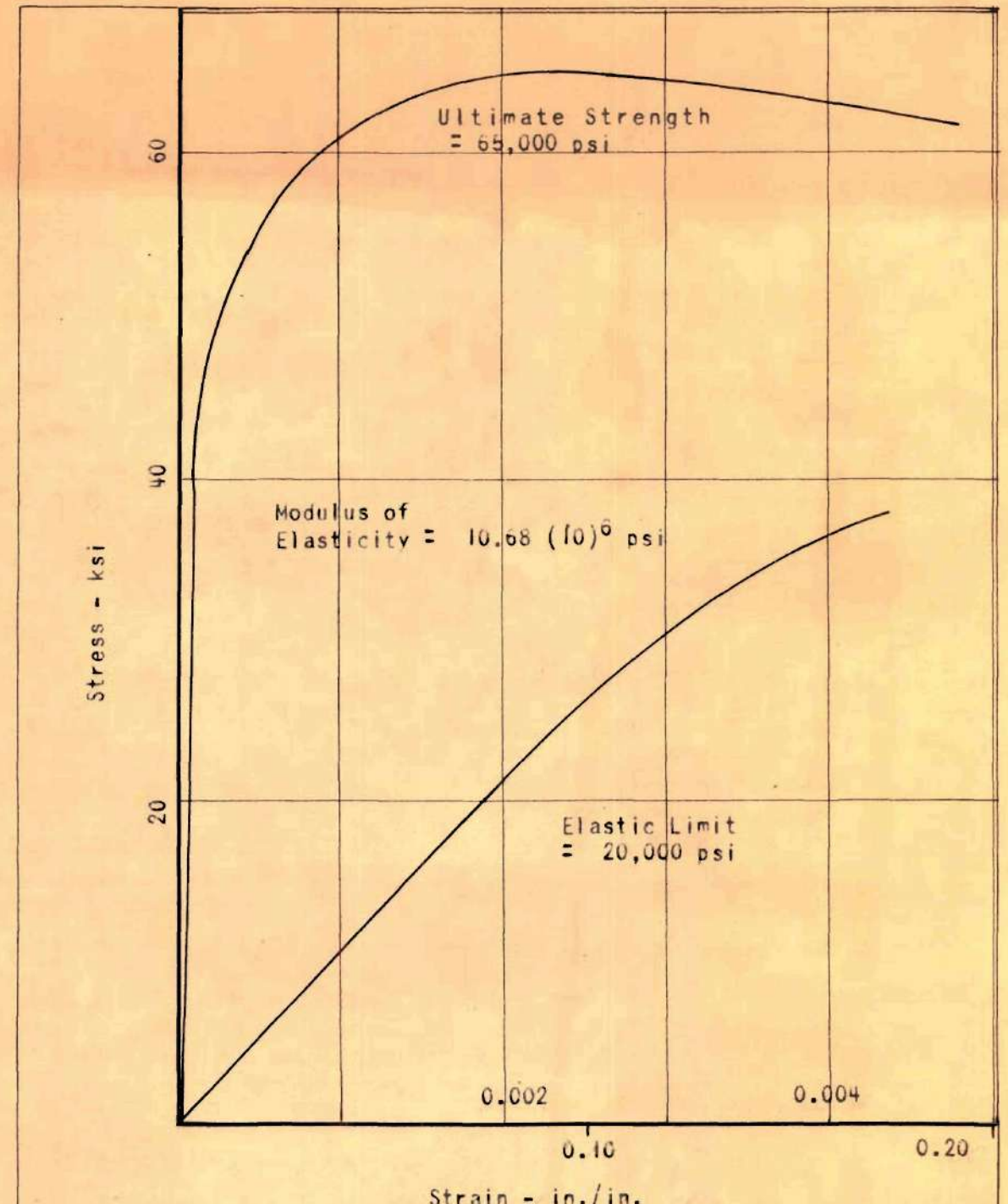

FIG. 4 STRESS - STRAIN CURVE FOR SPECIMEN OF MODEL, 24ST ALUMINUM IN TENSION

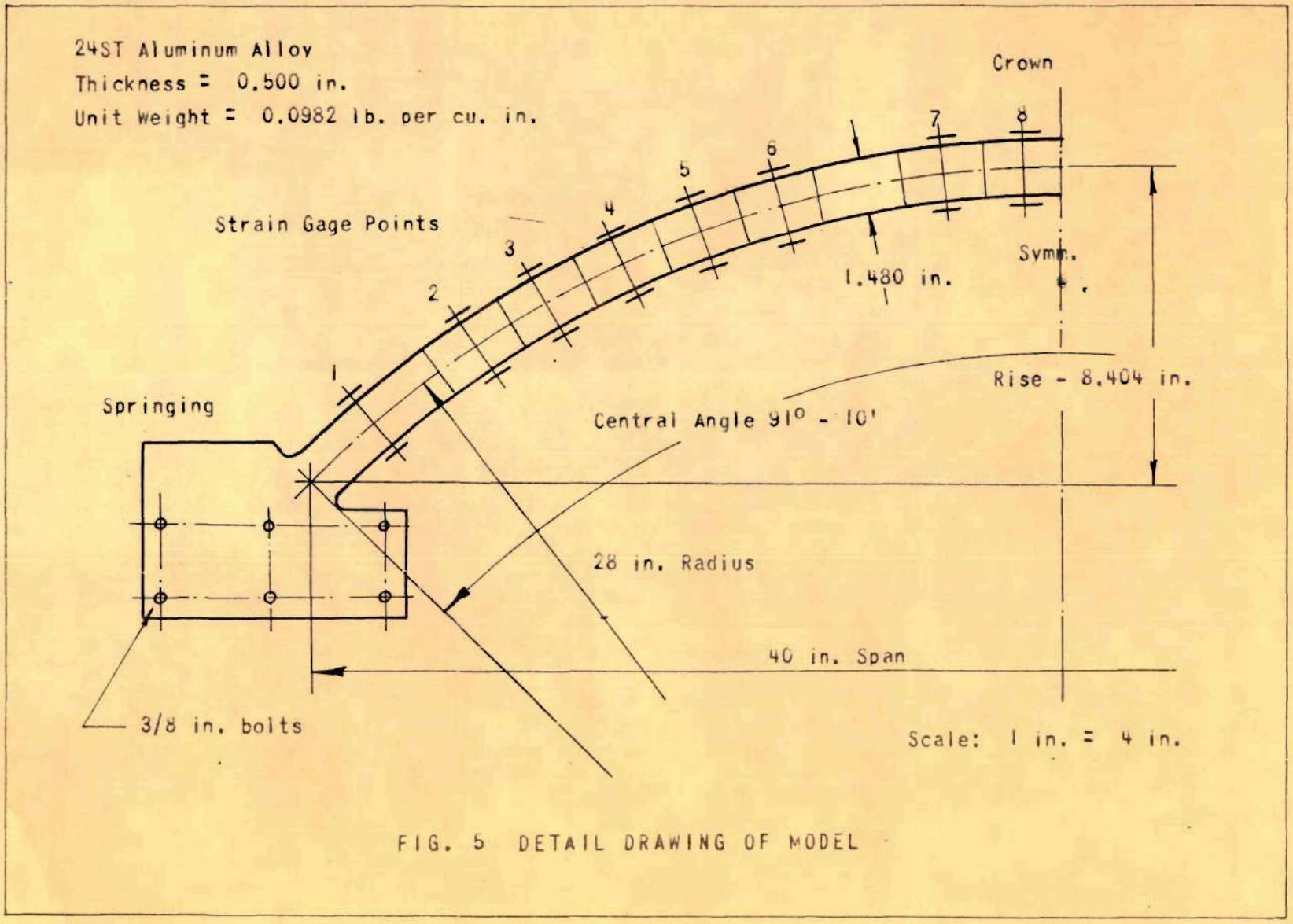

FIG. 5 DETAIL DRAWING OF MODEL

affected by the gage length. Gages are also available in various resistances, and various alloys depending upon the use to which the gage is to be put.

The resistance and the calibration factor for each gage are given by the manufacturer to an accuracy of ± 2 per cent. This calibration factor is known as the gage factor G, and is given by

$$G = \frac{\Delta R/R}{e} \quad , \tag{2}$$

where ΔR is the change in resistance, R the initial resistance, (both in ohms), and e is the unit strain. This gage factor has a range of values from 1.5 to 3.5, so it may be seen that the change in resistance to be measured is quite small. Two types of gages were used on the model, the A-18 and the CD-7 (manufacture numbers). The A-18 is an all purpose short gage length, medium output gage of a resistance of 120.5 ohms, and a gage factor of 1.76, and a gage length of 1/8th in. The CD-7 gage is a gage designed for the measurement of dynamic strains with a very high output and resistance; the resistance being 500 ohms, the gage factor 3.27, and the gage length of 1/4 in. The gages will be referred to as the "A" gages and the "D" gages respectively.

This change in resistance due to strain is ordinarily measured by a potentiometer or Wheatstone bridge type circuit. The Baldwin Corporation manufactures a package

unit for the measurement of static strains known as the Strain Indicator, which when used with a standard circuit records directly the strain in micro-inches per inch. This piece of equipment was used in this study for the measurement of static strains. The standard circuit for this potentiometer type instrument is for one gage, called the active gage, to measure strain on one side of the potentiometer, and an identical gage mounted on a similar unstrained piece of material on the adjacent side of the potentiometer. This latter gage is called the "dummy" or temperature compensating gage. Then as any temperature strains become evident, both gages are affected equally and the voltages induced cancel each other. Such a circuit is a temperature compensated circuit. The more recent models of the Strain Indicator include provision for the use of an external bridge made up of a series of gages. There are certain types of bridges which are advantageous for use in come cases due to increased output. These are discussed below.

In this investigation it was desired to measure separately the bending strains and the strains due to axial thrust at various points on the model. The Wheatstone bridge circuit was used and the two types of circuits are shown schematically at the upper right hand corner of Fig. 6. The "M" circuit was used to measure the strains due to bending moment and the "T" circuit to measure the strains due to thrust. For each gage set, one active gage was on the intrados, and one active gage was on the extrados of the

model. One pair of identical gages was used for the dummy gages in the moment circuit. The same pair plus two fixed resistors was used in the thrust circuit. The disadvantage of these fixed resistors is discussed subsequently.

The control box or switching unit, the wiring diagram for which is shown in Fig. 6, was built so that any gage point could be selected by the upper rotary switches, the proper dummy gages applied by the middle bank of switches, and the type of circuit (M or T) selected by the bottom bank of switches. The bridge power and the bridge output plugs are as shown. Not shown in the drawing is the pendulum release switch. Variations in contact resistance of the switches becomes an important factor in the design of such a unit. Therefore the finest grade switches were used and the experimental procedure was such that no switches were moved during the loading sequence.

The installation of the gages so that the lead wiring to the gages would not affect the vibrations of the model may be seen in Figs. 2 and 3. Two brass rods attached to the frame were placed parallel to the model and the wiring attached. This wiring then ran as a spiral to the gages where it was soldered to the gage leads. This soldering was kept to a minimum as the weight of the solder imposes high stresses on the fragile gage lead wires as the model is subjected to impact, resulting in fatigue failure of these lead wires. Several fatigue failures of the gage leads did occur but fortunately it was possible to repair

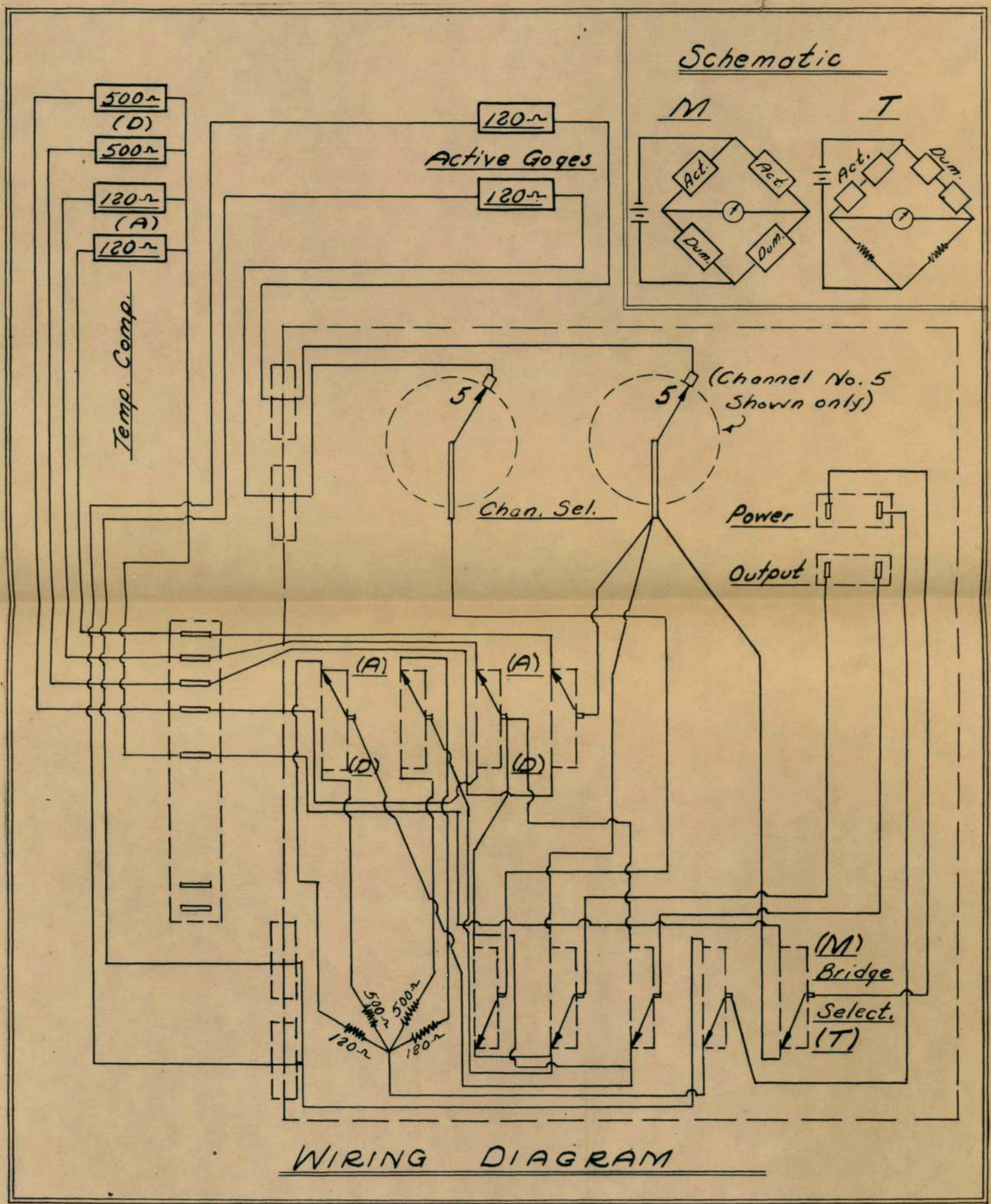

FIG. 6 CONTROL BOX WIRING DIAGRAM

this damage. The lead wires were then coated with rubber cement in the vicinity of the model to prevent the possibility of one of the wires coming in contact with the model during impact with consequent grounding of the circuit.

The output of the Wheatstone bridge in terms of bridge input voltage E, bridge output voltage E', the gage factor G, and the unit strain e will now be evaluated. Considering the schematic M circuit shown in Fig. 6, and calling the resistors R_1, R_2, R_3, R_4, respectively, beginning at the upper left and proceeding clockwise, it shall be taken that only R_1 and R_2 change in resistance by a very small amount ΔR_1 and ΔR_2. It may be shown for all practical purposes by Kirchoff's Law that the change in output voltage $\Delta E'$ may be given by

$$\Delta E' = E\left[\frac{(R_1+\Delta R_1)(R_3) - (R_2+\Delta R_2)(R_4)}{(R_1+R_2)(R_3+R_4)}\right] . \qquad (3)$$

If all of the resistances in the circuit are equal and expressed by R the equation above may be simplified to read

$$\Delta E' = \frac{E}{4R}\left[\Delta R_1 - \Delta R_2\right] . \qquad (3a)$$

But from Eq. (2) $\quad Ge = \frac{\Delta R}{R}$,

Thus $$\Delta E' = \frac{GE}{4}\left[e_1 - e_2\right] . \qquad (4)$$

It is noted that should $e_1 = -e_2$, then Eq. (4) would read

$$\Delta E' = \frac{CEe_m}{2} \quad , \tag{4a}$$

where e_m is the bending strain. The bending strain meets such a requirement, hence Eq. (4a) gives the output for the moment circuit in volts per certain amount of strain. It is also to be noted that if $e_1 = e_2$, such as would be experienced from temperature strains, then the output would be zero. Hence the circuit is compensated for temperature strains.

Should the gages be arranged as in the T circuit of Fig. 6, it is seen that the e_2 term no longer exists in Eq. (4), and the moment strains cancel, leaving only the strains due to thrust. The output of this circuit is given by

$$\Delta E' = \frac{GEe_t}{4} \quad , \tag{4b}$$

where e_t is the strain due to thrust. It may also be seen that this circuit is also compensated for temperature strains if the dummy gages are placed as shown. Note that this circuit has only half of the output of the moment circuit for any given bridge voltage E. However, the limiting factor is not the bridge voltage but the current per gage, a maximum used in this work being 50 milliamperes. It may be seen that the T circuit has twice the resistance of the M circuit and hence twice the bridge voltage may be safely used giving the T circuit the same sensitivity as the

M circuit, but with twice the bridge voltage, E.

It should be pointed out that the T circuit is the "standard" circuit used for the Strain Indicator. This instrument furnishes a constant bridge voltage, thus when the M circuit is used with the Strain Indicator all readings should be divided by two, and when the T circuit is used, the strain readings should be taken directly.

By inspection of Eq. (4) the advantages of D gages over the A gages becomes apparent. Due to the higher resistance of the D gages, slightly more than four times the bridge voltage may be applied to this type without exceeding the permissable current. Also by using an alloy for the gage wire which has more pronounced temperature characteristics, which is permissible in dynamic use, but would be disadvantageous in static work, the gage factor of the D gages is almost twice that of the A gages. Thus the D gages have about eight times the output of the A gages. None of these advantages are realized however if the Strain Indicator is used.

Strain Gage Power Supply.--The power supply for the measurement of static strain was built into the Strain Indicator and needs no further mention. Dry cell batteries of 45 volts were used for the strain gage power supply to obtain a steady voltage with respect to time. The circuit was arranged so that any voltage could be applied to the gage circuits up to 45 volts. The circuit is shown in Fig. 7. A

precision voltmeter was used with calibrated resistive multipliers inserted in series with the voltmeter to give the proper scale on the voltmeter. With such multipliers in the circuit the voltmeter will read the portion of the total voltage in proportion to voltmeter resistance divided by the sum of the voltmeter resistance and the multiplier resistance.

Measurement of Dynamic Strains.--A Tektronix type 511 cathode ray oscilloscope was used in recording dynamic strains. This is an excellent instrument, well adapted to strain gage work. It is not the purpose here to deal in detail with theory of such electronic equipment, but an explanation of the general principles is worthwhile. Essentially a cathode ray oscilloscope consists of a vacuum tube, at one end of which is a filament that emits a stream of electrons when heated. These electrons are channeled into a beam which impinges on the widened opposite end of the tube. This end of the tube is flattened forming a screen and coated on the interior with a material which fluoresces under the impact of these electrons. Four plates are placed along the length of the tube, two, being vertical, on each side; and two, horizontal at the top and bottom of the tube. When one vertical plate is charged the electron beam is deflected toward it. As the other is charged the beam is drawn across the screen. By varying these respective charges the speed at which the beam moves across the screen may be varied. This is referred to as the sweep speed and is variable in this instrument from 0.01

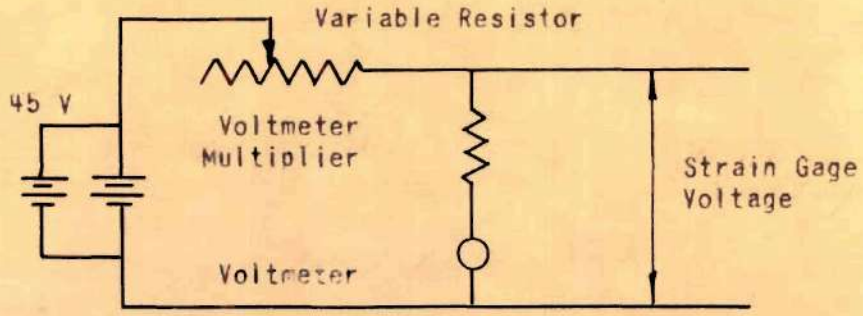

FIG. 7 STRAIN GAGE POWER SUPPLY

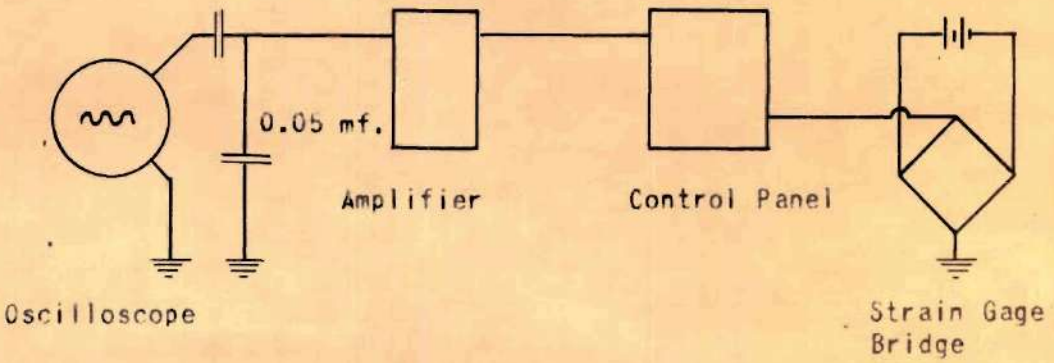

FIG 8 OVERALL CIRCUIT

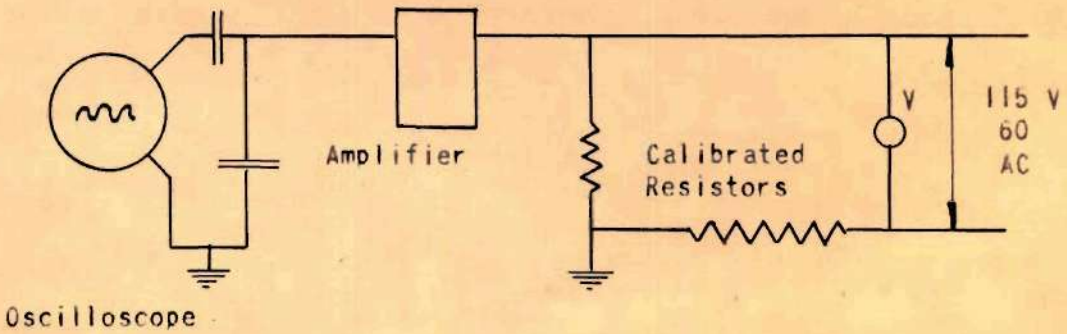

FIG. 9 CALIBRATION CIRCUIT FOR OSCILLOSCOPE

seconds per cm to 0.1 micro-seconds per cm, which gives a very wide range of application and can be used for virtually any mechanical vibration faster than 30 c.p.s. As the beam or sweep is drawn across the screen, variations in charge on the horizontal plates will cause the beam to deflect vertically. This charge is proportional to any voltage applied. Consequently a voltage-time trace is obtained, with time measured on the horizontal axis and voltage measured along the vertical axis. This measured voltage may be due to any cause. In this case it was the strain gage output.

In recording transient phenomena such as impact strains, it was necessary to have some method of beginning the sweep at the proper instant and of allowing only one passage of the sweep across the screen. Such a device is called a trigger and was used extensively in these tests. It is important that such a device be incorporated in the oscilloscope for work of this nature. The trigger circuit is generally such that as the circuit is either completed or broken the sweep is sent across the screen for only one passage. A mechanical device may be used to trigger the sweep, the one used in these tests shown by Fig. 2. It consisted of a simple lever which ordinarily completed the circuit. As the pendulum fell the pendulum shaft struck the lever breaking the circuit and starting the sweep. The lever was so adjusted that the shaft struck the lever

when the pendulum was about 1/4 in. from the model allowing the sweep to travel for about 0.001 second before contact with the model was made.

There were several ranges of magnification available on the oscilloscope itself, the maximum sensitivity being about 0.27 volts per cm. As the gage outputs were of the order of only a few millivolts, amplification was required. The amplifier used was an AC instrument of x100 multiplication. At this multiplication ratio, sensitivities of about 2.5 mv per vertical cm of deflection were then available.

It was also important to maintain a high impedance for such an instrument, as a low impedance instrument would affect the strain gage output. The impedance of this instrument and of the amplifier was 1 megohm shunted by 40 mmfd (micro-microfarads). This was enough to consider the instrument impedance infinite in the calculation of the gage output.

Some type of photographic device was necessary to record the traces. A Dumont Polaroid Land Camera was used. The camera may be seen on top of the oscilloscope in the frontispiece. The procedure used in photographing the trace was to set the trigger mechanism, release the pendulum, open the camera shutter, and then close the shutter after impact. The camera was so arranged that by opening a plate, the screen could be conveniently observed without exposing film. In this manner, five traces were recorded on one photograph.

The oscilloscope circuit is shown by Fig. 8. The

capacitance, in series with the oscilloscope, was used to block static strains, or slowly varying strains. Then this circuit could be used with a slightly unbalanced bridge which always occurs unless variable ballast resistors, and variable capacitors are used on the dummy side of the bridge circuit. The parallel capacitor of 0.05 micro-farad will be discussed in more detail under the discussion of interference.

It was considered necessary to calibrate the oscilloscope and amplifier. The circuit used for this is shown by Fig. 10. Measured line voltage of 60 cycle AC 115 volts was applied to two calibrated resistors in series, one a large ballast resistor and the other a very small resistor. The voltage drop across the very small resistor was the line voltage multiplied by the ratio of the small resistor to the total resistance of the circuit; this voltage was applied to the amplifier and the oscilloscope. The time of the sweep was calibrated by observing the 60 c.p.s. sine wave from the induced voltage. It was found that the sweep was about 4 per cent too fast.

When the calibrating voltage is applied it must be remembered that "peak to peak" voltages are read on the screen. Voltage computations, however, deal with the effective values of the voltage, or the "root mean square" (r.m.s.) value. The peak to peak value for a sine wave is 1.414 times the r.m.s. value. The system was calibrated at a number of voltages, and at a number of magnification

settings on the instruments themselves. The circuit was found to be perfectly linear with a maximum sensitivity of 2.31 millivolts per cm. The screen was found to be linear up to 2.25 cm deflection on either side of the axis. At 2.50 cm deflection the deflection was 4 per cent low and at a deflection of more than this the error increases quite rapidly.

Whenever low level voltage measurements such as these are attempted, provision will have to be made to eliminate the inevitable interference caused by the electromagnetic waves always present. These random waves may be caused by operating electrical machinery, fluorescent lights, making or breaking of any nearby electrical circuit, and probably the most important source - radio and television waves. These waves when crossing any open wiring will induce voltages in the wiring. To give some idea of the importance of this interference, before any provision was made in the equipment to eliminate the interference, the magnitude of the interference voltage was about one hundred times the expected voltage to be measured. It seems there is little that may be analytically predicted concerning the magnitude of such interference, or the type of it. Elimination of the interference is then done by a trial and error process. The methods used in this work to eliminate it are discussed below.

If the interference is of a much higher frequency than the frequencies to be measured the cause is probably radio

and television waves. One solution is to work in the early hours of the morning when the various stations are not broadcasting. The other solution is to place a variable condensor in parallel with the oscilloscope. This capacitance which offers low impedance to high frequency waves will effectively "ground out" such frequencies, allowing the lower frequency signals to be registered by the oscilloscope. The capacitance should be kept as small as possible as the impedance varies inversely as the capacitance. The capacitance should be varied to obtain the optimum condition. When condensers are used, they should be installed with lead wires less than 1/2 in. or they may have an opposite effect with respect to interference.

Should the interference have a frequency of the same magnitude as the one to be measured, shielding must be used. The idea of shielding is to cover all wires with a grounded metallic shield. This shield then intercepts the waves and eliminates the voltages. Ideal shielding would be a metallic cage around the entire area connected to the individual shielding of each wire and instrument. This is sometimes impractical. If shielded cable is not used in the wiring, all of the exposed wiring should be brought to a common point and braided together. This is at times just as effective as shielded cable. This was done in this investigation and is evident in the various photographs. All instruments, batteries, wiring, etc. should be housed in metal cabinets. All of these cabinets should be connected by firmly soldered

leads and grounded. It is helpful to place all of these cabinets on a copper screen, or as was used a large aluminum plate seen in the frontispiece.

The grounding of such shielding is quite important. At times it will be found that when some portions of the equipment are not grounded the results will be best. This can only be found by trial. It may be found that grounding to a water line will increase the interference due to stray ground currents. This was the case with this equipment. It was found best to ground all cabinets and the frame together and insulate them from any other contact.

If the frequency of the interference is a certain definite value, a band-stop filter may be used in the circuit. A type of interference generally to be encountered is standard 60 cycle. The filter is effective in eliminating this. If the interference is a sine wave of 60 cycle, or any other frequency a device may be built comprising an oscillator, variable transformer, and variable inductance and capacitance which will produce a variable voltage of variable phase. When this voltage is applied to the circuit it may be adjusted to give an opposite voltage as that of the interference and yield a net voltage of zero applied to the oscilloscope.

It is important to be able to locate the source of the interference in the circuit. Generally it is impossible to control the outside cause. A good procedure to follow is to disconnect all component parts of the circuit, and note

if the oscilloscope is "clean", that is free from any wave forms and the sweep is horizontal. If interference is noted at this point then the source is internal with the oscilloscope. Considering the screen to be normal, then component parts of the circuit are then connected in sequence, noting the effect of each connection on the screen. By this process of elimination the source may be located.

As may be presumed by the above discussion, considerable difficulty was encountered with this equipment. A few words of advice to future investigators might be in order. Once the interference has been eliminated, do not change the equipment in any respect. The effect of changing the length of a wire by an inch or two, or of soldering some connection may be enough to destroy the balance of the circuit. It was found that simply placing one cabinet on top of another instead of beside it was a definite factor. In conclusion it may be said that the process of interference elimination is a tedious one requiring a great deal of patient experimentation, and it seems the more novice is the worker, the better success will be enjoyed.

Circuit for Recording Contact of the Pendulum with the Model.-- It was necessary to have some means of measuring the length of time the pendulum was in contact with the model during impact. A simple circuit was used for this purpose. A small battery voltage was applied between the pendulum, and the input to the oscilloscope. As the pendulum came in contact with the model, which was grounded, the voltage was

registered on the screen and photographed similiarly to the other traces. In order to have an accurate record of the instant of impact, this circuit was such that this contact voltage could be superimposed on the strain gage output, clearly marking the instant of impact.

Calibration of Entire Apparatus.--The ideal type of calibration would be to make an investigation of the static strains in the model so that they would be known for a given loading. Then to apply this loading and measure the deflection on the oscilloscope screen for the strain at each gage, thereby effecting a calibration of the circuit as a whole. Unfortunately this was not done for several reasons. The particular oscilloscope, as has been mentioned previously, did not respond to static strains. Thus a different type of amplifier and oscilloscope would have been required. This could have been circumvented by using an AC power supply to the strain gage bridge. However due to the fixed resistors in this bridge circuit, the bridge was out of balance by perhaps 0.5 per cent. This resulted in a bridge output, under no strain of greater magnitude than the bridge output to be measured. The answer to this would have been to install variable resistors in the bridge as has been mentioned previously. This would also have necessitated the installation of variable capacitors in the bridge circuit to aid in an accurate initial balance of the bridge.

Instead of an overall calibration, the bridge power supply and the amplifier-oscilloscope circuit was calibrated

separately and the strain gage output was calculated by Eq. (4). This was thought to be sufficiently accurate, and the convenience of using the fixed resistors in the bridge circuit made this type of calibration worthwhile.

Accuracy to be Expected.--The model was fabricated with a tolerance of ±0.010 in. with respect to the arch axis. The thickness was 0.500 in., and the depth of section was accurate to 0.005 in. Possibly one per cent error should be expected in strains from the model. The frame as will be shown did not succeed in completely restraining the ends of the model. This one factor is responsible for the majority of the error encountered experimentally. The proving ring used in the static testing was accurate to ± one per cent. The strain gages are specified by the manufacturer to have an accuracy of ± two per cent. The bridge power supply was accurate to two per cent. The electronic equipment was believed to be calibrated to four per cent. Hence the experimental error should be certainly no more than 10 or 12 per cent should all the errors be additive. Unfortunately this was about the magnitude of the error encountered. The majority of the errors can be attributed to the frame stiffness, however, and the direction of the error may be seen.

CHAPTER III

EXPERIMENTAL PROCEDURE AND DESCRIPTION OF EXPERIMENTAL DATA

Static Data.--The moment and thrust strains were recorded by means of the Baldwin Strain Indicator as mentioned previously. The load was applied in increments of 300 pounds up to 900 pounds, the strain being recorded at each load step. The strain for each increment was averaged and then divided by the load increment to obtain the strain with respect to a one pound load. Knowing the dimensions of the model, the bending moments and the thrusts at the specific points on the model were calculated. Curves were plotted of these values being shown by Fig. 15(a), (b), and (c) respectively. The deflections were measured at the point of application of the load for the same load increments as above by means of the micrometer dial gage visible in Fig. 3. These values also are given in terms of a unit load.

Dynamic Data.--At the beginning of any test sequence, a pendulum distance was computed so as to give a maximum impact stress in the arch of 15,000 psi. The pendulum distance was then set at roughly this distance, and recorded to 0.01 in. The trigger lever was then adjusted so that the sweep would begin at the proper time for this pendulum distance. This was a rather sensitive adjustment as the mechanism would repeat itself only to about 0.001 sec and was difficult to

adjust to this same tolerance. For this reason the oscilloscope traces shown in the Appendix do not all begin at the same distance from the left hand vertical line. It would appear then that there is no accurate manner by which to locate the point of "zero time" or the instant of initial contact of the pendulum with the model; provision was made for this however, and will be discussed subsequently.

After the trigger mechanism was adjusted the proper sweep speed was selected by observing visually the type of trace produced. The speed used generally throughout these tests was 0.001 sec/cm (one centimeter on the screen being given by the distance between the gage lines visible on every trace).

The vertical sensitivity was then selected, it could be controlled by varying the strain gage voltage. Each trace to be recorded was run and inspected visually with respect to the maximum height. This was done by running the trace consecutively, on the second run a piece of black plastic tape was placed just under the maximum height and the trace observed to see if the first reading was correct. This was done because the trace was so fast, the entire sweep occurring in 0.01 sec, and it was difficult to note properly by eye the maximum height. With these recorded maximum ordinates the proper vertical sensitivity of each respective gage was selected in order to keep the entire trace within the linear portion of the oscilloscope screen which was plus or minus 2.2 cm from the base line. It might be well to note what

happens to the trace when the linear portion of the screen is exceeded. All of the trace within this linear portion remains undistorted, but the portion outside these limits becomes compressed toward the base line. This was used to an advantage on some of the traces when the smaller portions of the trace required magnification, and the larger portions were not being studied.

With the above adjustments made, the film was exposed to the illuminated grid on the screen in the positions which the trace would occur on the film. About five seconds were required for this for each grid. The procedure for photographing a trace was to release the pendulum, open the camera shutter just before contact, then close the shutter after the trace had occurred.

In order to record the contact of the pendulum with the model, the contact circuit as previously described was switched direct to the oscilloscope and the trace recorded as above. This resulted in a trace that appeared to be a series of broken lines above the base line. The length of these lines and their position indicates the time the pendulum was in contact with the arch. The amount of displacement from the base line had no significance, being proportional only to the voltage in the contact circuit.

As was mentioned above, the instant of contact referred to as the point of "zero time" is not recorded on the traces. In order to locate this point accurately, a second series of photographs were made placing the strain

gage circuit and the contact circuit in parallel. Thus this trace would exhibit an initial jump when contact occurred and a jump in the opposite direction when contact between the pendulum and the arch was broken. These traces could be compared with the normal traces and hence the point of zero time could be accurately located.

In studying the value of the maximum ordinate for each respective trace the pendulum distance was varied in order to give a variable equivalent static load as given by Eq. (7).

The traces were inspected visually as noted above for these several different dynamic loadings. A load-strain curve was then plotted for each gage point and the strain per unit load was found as the slope of the line. All of these curves were found to be straight lines and it was found sufficiently accurate to simply scale the peak strain from the traces for one pendulum distance.

CHAPTER IV

THEORETICAL CONSIDERATIONS

Maximum Possible Dynamic Stress

It is convenient to have a simple relation which will yield the maximum possible values of the stress in any elastic system subjected to the impact of a rigid mass moving at a velocity v_o at the time of impact. Such an expression may easily be derived by assuming:

(a) the elastic system has one degree of freedom; that of the static deflection curve

(b) the elastic system is weightless

Then the entire kinetic energy of the moving mass, M is transferred into the strain energy of the elastic system as the system stops the mass, at which instant the stress in the elastic system will be a maximum. Denoting P as the maximum force exerted on the system by the mass, and Δ_o as the maximum deflection of the system in the direction of P, then equating the energies

$$\frac{Mv_o^2}{2} = \frac{P\Delta_o}{2} \quad . \tag{5}$$

However

$$P = h\Delta \tag{6}$$

where h is the familiar spring constant in weight per length.

Thus $$\frac{P^2}{K} = Mv_o^2 \ ,$$

or $$P = \sqrt{hMv_o^2} \ .$$

If h is so chosen so that its numerical value is the weight W of the mass divided by the deflection Δ_s caused by W applied statically, then it may be shown that

$$P = W\sqrt{\frac{v_o^2}{g\Delta_s}} \ , \qquad (7)$$

where g is the acceleration of gravity. Once P has been determined by Eq. (7), a static analysis of the system may then be performed.

To show that the assumptions lead to the maximum possible value of P, Eq. (5) may be rewritten as

$$\frac{Mv_o^2}{2} = \frac{P\Delta_o}{2} + U_s$$

where U_s represents the kinetic energy of the elastic system. As U_s has a finite value, P as indicated by Eq. (7) must be larger than the actual value. Furthermore the assumption that P varies linearly with the deflection, Δ also represents the maximum condition, as is shown by these tests, as the motion during contact is a combination of the static deflection and the natural modes of vibration of the system allowing more energy to be absorbed by the system with a consequent reduction in the force P.

Equation (7) is well established and the reader is

referred to any standard textbook on the subject, especially to (Reference 1, p. 393).

Approximation Equation for Motion during Impact

The motion during impact may be approximately described by making the same assumptions used for Eq. (7). The force exerted by the mass on the system must equal $M\frac{d^2\Delta}{dt^2}$, where t is time. Similiarly the force exerted by the system on the mass is $h\Delta$. As the sum of the two forces must be zero, then

$$\frac{d^2\Delta}{dt^2} + \frac{h}{M}\Delta = 0 \ . \tag{8}$$

The general solution of Eq. (8) is given by

$$\Delta = C_1 \sin\sqrt{\frac{h}{M}}\, t + C_2 \cos\sqrt{\frac{h}{M}}\, t \ .$$

At $t = 0$, however, $\Delta = 0$, and thus $C_2 = 0$. Also at $t = t_o$, t_o representing the time of contact, $\Delta = 0$, hence,

$$\sin\sqrt{\frac{h}{M}}\, t_o = 0 \quad \text{and} \quad \sqrt{\frac{h}{M}}\, t_o = \pi \ .$$

From which

$$t_o = \pi\sqrt{\frac{M}{h}} \ . \tag{9}$$

It is noted here that the time the mass is in contact with the system is independent of the velocity of the mass, and depends only on the mass M and the spring constant h.

Now at $t = t_o/2$, $\Delta = \Delta_o$ which is the maximum deflection. It may then be shown that $C_1 = \Delta_o$. Thus:

$$\Delta = \Delta_o \sin \sqrt{\frac{h}{M}}\, t \quad . \tag{10}$$

This is the equation of motion which is seen to be sinusoidal with respect to time, such motion being known as simple harmonic motion.

It may be noted that Eqs. (9) and (10) are quite independent of the vibrations of the elastic system itself and of the ratio of the striking mass to that of the system which is quite important. These equations are also independent of the geometry of the contact surface and also of the vibrations of the mass which has been heretofore considered as a rigid body. Rigorous solutions are possible, but are extremely complex. Such solutions will not be made in this paper and the reader is referred to (References 2, 3, and 4) for specific information regarding such cases. It will be noted so long as the mass of the system is small with respect to the striking mass, the above analysis is approximately correct.

Free Vibrations of Curved Bars

After the mass has bounded away from the elastic system, free natural vibration is quickly established in the system and gradually is dampened out. The theory of free vibrations of curved bars is quite complicated. In fact at present there is no general solution to the problem available. For circular bars of constant cross section Lamb (5) has proposed a solution. Den Hartog (6 and 7) has

made a solution for the fundamental frequencies of circular bars based on the Rayleigh-Ritz method. Solutions are available for a full ring (8). There are no solutions available for modes of vibration higher than the first mode; for bars of non-uniform cross-section; or for other than circular bars at the present time.

In view of the above, it is obvious therefore, that an approximate solution to the problem is needed. Such an approximation is given below for circular rings of uniform section. Any approximation made in an analysis of this kind results in imposing artificial restraints upon the system thus implying greater stiffness, and with resulting higher frequencies than actually will exist. Thus frequencies yielded by this approximation should be expected to be somewhat high.

Assumptions.--The following assumptions will be made as well as those stated in following paragraph:

(a) steady-state, undamped, free vibration

(b) small deflections of thin bars

(c) validity of flexure formula

(d) bending of the bar in its own plane

(e) shear distortion may be neglected

(f) energy of rotation of a differential element in its own plane may be neglected

The complexities which arise in the exact analysis come from considering the tangential as well as radial deflections. In this approximation, only radial deflections are considered.

The effect of each of the above eliminated items increases with increasing central angle of the partial ring. For small central angles the approximation should then yield quite good values, with the maximum error occurring when applied to a full ring of central angle of 360 degrees.

In civil engineering structures, such as arch bridges, the central angles are generally less than 180°. For this application, the approximation was developed.

General Equation of Motion.--First the differential equation of the elastic curve of the circular arc must be written. Consider the differential element shown of original length ds, and deflected length ds + Δds.

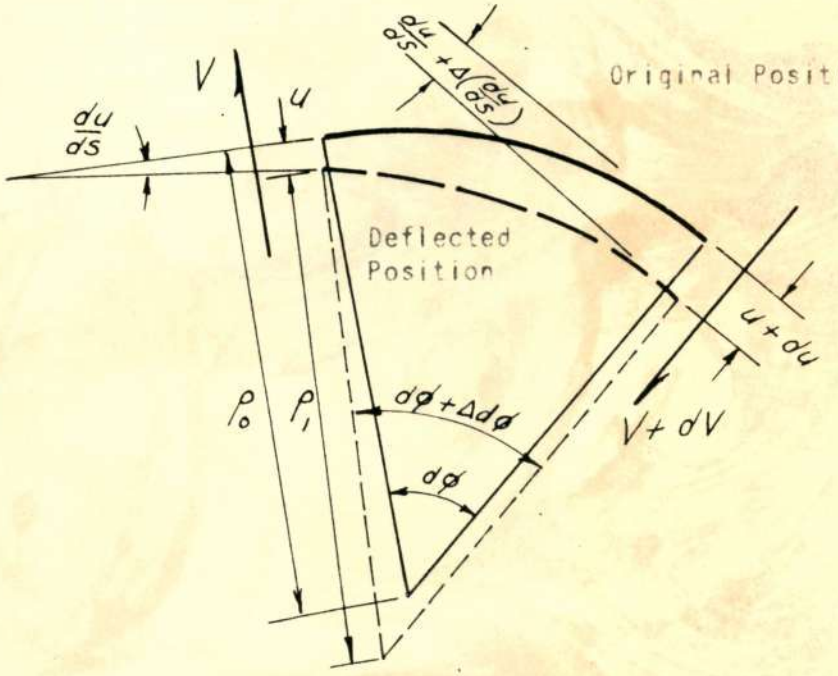

FIG. 10 DISPLACED ELEMENT OF ELASTIC CURVE OF A CIRCULAR ARC

$$\frac{du}{ds} + \Delta\left(\frac{du}{ds}\right) = \frac{du}{ds} + \frac{\partial}{\partial s}\left(\frac{du}{ds}\right)ds = \frac{du}{ds} + \frac{d^2u}{ds^2}ds$$

By similar Δ's it is noted that

$$\Delta d\phi = \frac{d^2u}{ds^2}\, ds \tag{11}$$

As; $\frac{d\phi}{ds} = \frac{1}{p_o}$ then $\frac{d\phi + \Delta d\phi}{ds + \Delta ds} = \frac{1}{p_1}$ (12)

Approximately:

$$ds + \Delta ds = (p_o - u)d\phi$$

therefore $$p_o d\phi + \Delta ds = p_o d\phi - u d\phi$$

hence $$\Delta ds = -u d\phi = -u\frac{ds}{p_o} \tag{13}$$

Substituting Eqs. (11) and (13) into (12)

$$\frac{1}{p_1} = \frac{d\phi + \frac{d^2u}{ds^2}\, ds}{\left(1 - \frac{u}{p_o}\right) ds}$$

Realizing u to be small compared to p_o, and

$$\frac{1}{1 - \frac{u}{p_o}} \approx 1\left(1 + \frac{u}{p_o}\right) \quad \text{for} \quad \frac{u}{p_o} << 1$$

$$\frac{1}{p_1} = \left(1 + \frac{u}{p_o}\right)\left[\frac{d\phi}{ds} + \frac{d^2u}{ds^2}\right]$$

$$\text{but} \quad \frac{d\phi}{ds} = \frac{1}{p_o}$$

thus

$$\frac{1}{p_1} = \left(1 + \frac{u}{p_o}\right)\left[\frac{1}{p_o} + \frac{d^2u}{ds^2}\right]$$

Realizing $\frac{d^2u}{ds^2}$ is small, multiplying and simplifying:

$$\frac{1}{p_1} - \frac{1}{p_o} = \frac{u}{R^2} + \frac{d^2u}{ds^2}$$

but $$\frac{1}{p_1} - \frac{1}{p_o} = \frac{M}{EI}$$

$$\frac{d^2u}{ds^2} + \frac{u}{R^2} = \frac{M}{EI} \qquad (14)$$

or $$\frac{d^2u}{d\phi^2} + u = \frac{R^2M}{EI} \qquad (14a)$$

This differential equation is well known and the reader is referred to any textbook on advanced mechanics. It gives a relation between the bending moments, central angle, and radial deflections in a circular arch.

Considering now the radial movement of the differential element, let c be the weight of the beam per unit of length. The mass of the element, dM is:

$$dM = \frac{cds}{g}$$

The resultant force must at all times be this mass times its acceleration, $\frac{d^2u}{dt^2}$. Assuming harmonic motion, it is known that:

$$\frac{d^2u}{dt^2} = -u\omega^2$$

Where ω equal the angular frequency of vibration, in radians per second and is equal to $2\pi f$ (f being the frequency in cycles per second). Hence the resultant force = $-\frac{cds}{g} u\omega^2$.

If $ds \to 0$, the net radial force acting on the element is $-dV$.

Hence $$-dV = -\frac{c\,ds}{g}\, u\omega^2$$

Remembering that in the limit,

$$\frac{dM}{ds} = V \quad \text{and} \quad \frac{d^2M}{ds^2} = \frac{dV}{ds}$$

thus $$-\frac{c}{g}\,\omega^2 u = -\frac{d^2M}{ds^2}$$

or from Eq. (10a)

$$\frac{c}{g}\,\omega^2 u = \frac{d^2}{R^2 d\phi^2}\left[\frac{EI}{R^2}\left(\frac{d^2u}{d\phi^2} + u\right)\right]$$

Now if EI is constant

$$\frac{d^4u}{d\phi^4} + \frac{d^2u}{d\phi^2} - \frac{R^4 c\omega^2}{EIg}\, u = 0 \qquad (15)$$

This is the general equation governing radial motion if the motion may be assumed harmonic. Letting $K^2 = \frac{R^4 c\omega^2}{EIg}$, and denoting $\frac{d}{d\phi} = D$, $\frac{d^2}{d\phi^2} = D^2$, etc., Eq. (15) may be expressed as $(D^4 + D^2 - K^2)u = 0$ (which is in 'operator' form) solution may be made by 'completing the square' and letting $m = D^2$.

$$m^2 + m + 1/4 = K^2 + 1/4$$

$$(m + 1/2)^2 = (K^2 + 1/4)$$

therefore $$m = -1/2 \pm \sqrt{K^2 + 1/4} = D^2$$

thus $$D = \pm [-1/2 \pm \sqrt{K^2 + 1/4}\,]^{1/2}$$

$$\begin{aligned} D &= + [-1/2 + \sqrt{K^2 + 1/4}\,]^{1/2} = +a \\ &= - [-1/2 + \sqrt{K^2 + 1/4}\,]^{1/2} = -a \\ &= +i[+1/2 + \sqrt{K^2 + 1/4}\,]^{1/2} = +ib \\ &= -i[+1/2 + \sqrt{K^2 + 1/4}\,]^{1/2} = -ib \end{aligned} \qquad (16)$$

Hence the solution to Eq. (11) is:

$$u = C_1 e^{a\phi} + C_2 e^{-a\phi} + C_3 e^{+ib\phi} + C_4 e^{-ib\phi}$$

From MacLaurin's Series it may be proved that:

$$C_3 e^{ib\phi} + C_4 e^{-ib\phi} = A\cos b\phi + B\sin b\phi$$

It may also be shown that:

$$C_1 e^{a\phi} + C_2 e^{-a\phi} = C\cosh a\phi + D\sinh a\phi$$

Hence the general solution to Eq. (5) may be expressed as:

$$u = A\cos b\phi + B\sin b\phi + C\cosh a\phi + D\sinh a\phi \qquad (17)$$

Where A, B, C, and D are constants such that

$$A = (C_3 + C_4) \qquad C = (C_1 + C_2)$$

$$B = (C_3 - C_4) \qquad D = (C_1 - C_2)$$

Specific Solutions of General Equation of Motion

In order to obtain some idea of the accuracy of Eq. (17) solutions will now be made for examples for which numerical answers are known. Three cases will be considered:

(1) Full Ring with No Restraint

(2) Hinged-end Partial Ring

(3) Fixed-end Partial Ring

Case (3) is the solution for the model studied experimentally in this paper.

Full Free Ring.--Equation (17) will be repeated here. Then

$$u = A\cos b\phi + B\sin b\phi + C\cosh a\phi + D\sinh a\phi \qquad (17)$$

$$\frac{du}{d\phi} = -Ab\sin b\phi + Bb\cos b\phi + Ca\sinh a\phi + Da\cosh a\phi \qquad (18)$$

$$\frac{d^2u}{d\phi^2} = -Ab^2\cos b\phi - Bb^2\sin b\phi + Ca^2\cosh a\phi + Da^2\sinh a\phi \qquad (19)$$

$$\frac{d^3u}{d\phi^3} = +Ab^3\sin b\phi - Bb^3\cos b\phi + Ca^3\sinh a\phi + Da^3\cosh a\phi \qquad (20)$$

Denoting ϕ_t as the total central angle of the ring, which in this case is 2π; due to complete symmetry of the deflection curve Eq. (17) must yield the same value when $\phi = 0$, as when $\phi = \phi_t = 2\pi$; similiarly with Eqs. (18), (19), and (20).

Then

$$A = B\,\frac{1 - \cos(2\pi b)}{\sin 2\pi b}$$

and $$A = B \frac{\sin 2\pi b}{\cos(2\pi b) - 1}$$

Equating the multipliers of B, the frequency equation may be obtained:

$$\cos 2\pi b = +1 \qquad (21)$$

thus $2\pi b = 0, 2\pi, 4\pi, 6\pi$, etc.

or $b = 0, 1, 2, 3, 4$, etc.

The modes correspond to:

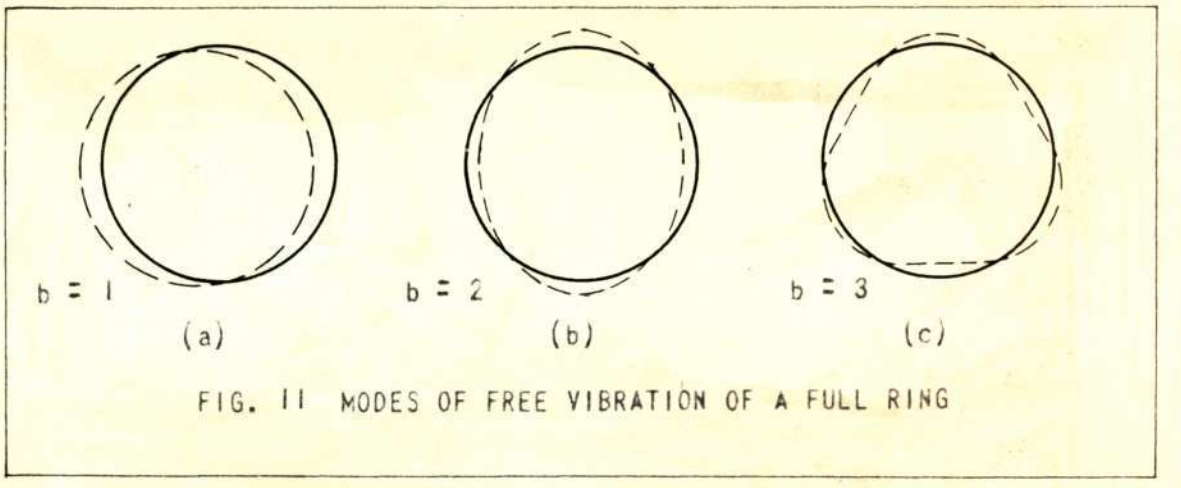

FIG. 11 MODES OF FREE VIBRATION OF A FULL RING

From Eq. (16)

$$b = \sqrt{1/2 + \sqrt{K^2 + 1/4}} \text{ or } K = \sqrt{(b^2 - 1/2)^2 - 1/4}$$

also

$$K^2 = \frac{R^4 c \omega^2}{EIg} \quad \text{or} \quad \omega = \frac{K}{R^2} \frac{EIg}{c}$$

Thus when $b = 0$, K is imaginary and no vibration is possible. Also when $b = 1$, the angular frequency $\omega = 0$, and no vibration takes place as the ring moves as shown in

Fig. 11a above. Thus $b = 2$ corresponds to the fundamental mode of vibration, $b = 3$ to the second mode, and etc.

Deflection curves and frequencies will be discussed more fully in connection with the following case of the hinged-end partial ring. The deflection curve will be shown to be a sine curve on the projected length of the arc.

Hinged-end Partial Ring.--In order to derive a frequency equation for this case, Eq. (17) must be taken as:

$$u = C_1(\sin b\phi + \sinh a\phi) + C_2(\sin b\phi - \sinh a\phi) + C_3(\cos b\phi + \cosh a\phi) + C_4(\cos b\phi - \cosh a\phi) \quad (22)$$

where C_1, C_2, C_3, C_4, are new arbitrary constants.

Now

$$\frac{d^2u}{d\phi^2} = C_1(-b^2\sin b\phi + a^2\sinh a\phi) + C_2(-b^2\sin b\phi - a^2\sinh a\phi) + C_3(+a^2\cosh a\phi) + C_4(-b^2\cos b\phi - a^2\cosh a\phi) - C_3(b^2\cos b\phi) \quad (23)$$

When $\phi = 0$, $u = 0$. Therefore $C_3 = 0$.

When $\phi = 0$, the moment must be zero, hence:

$$-C_4(+b^2 + a^2) = 0$$

If vibration exists $(a^2 + b^2) \neq 0$, therefore $C_4 = 0$.

When $\phi = \phi_t$, $u = 0$, therefore

$$C_1 = -C_2 \frac{\sin b\phi_t - \sinh a\phi_t}{\sin b\phi_t + \sinh a\phi_t} . \quad (24)$$

When $\phi = \phi_t$, $\frac{d^2u}{d\phi^2} = 0$,

therefore $$C_1 = -C_2 \frac{-b^2 \sin b\phi_t - a^2 \sinh a\phi_t}{-b^2 \sin b\phi_t + a^2 \sinh a\phi_t} . \qquad (24)$$

Remembering that $a^2 = -b^2$, and equating the multipliers of C_2 above, it may be shown that:

$$\sin b\phi_t = 0 \qquad (25)$$

or $b\phi_t = 0, \pi, 2\pi, 3\pi, 4\pi, 5\pi$, etc.

Equation (25) will now give the natural frequencies of such a arc. Solution for the first seven modes are given with respect to central angles from 45 degrees to 270 degrees on Fig. 12.

To find the shape of the deflection curve, Eqs. (22) and (24) will be used.

$$u = C_1(\sin b\phi + \sinh a\phi) - C_1\left(\frac{\sin b\phi_t + \sinh a\phi_t}{-\sin b\phi_t + \sinh a\phi_t}\right)$$
$$(\sin b\phi - \sinh a\phi)$$

Multiplying through by the denominator:

$$\left[\frac{(-\sin b\phi_t + \sinh a\phi_t)}{C_1}\right]u = (\sin b\phi + \sinh a\phi)(-\sin b\phi_t + \sinh a\phi_t) + (\sin b\phi_t + \sinh a\phi_t)(\sin b\phi - \sinh a\phi)$$

Denoting the term in brackets as C_5, and simplifying

$$C_5 u = \sin b\phi \sinh a\phi_t - \sin b\phi_t \sinh a\phi \qquad (26)$$

which is the expression for the deflection curve.

It may be noted when $\phi_t = \pi, 2\pi$, i.e., a semi-circle or a full ring, then Eq. (26) reduces to

$$u \approx \sin b\phi \qquad (26a)$$

For other central angles, the deflection curve is more complicated. The general shape of the deflection curves for the various modes of vibration are given on Fig. 12.

The identity of the solutions for Eq. (25) for the hinged ring and Eq. (21) for the full free ring show the deflection curve for the full ring to be sinusoidal as given by Eq. (26a). Inspection of the deflection curves, Figs. 11 and 12, show that the fourth mode for the hinged-end case is the fundamental mode for the full free ring, and that the sixth mode for the hinged case is the second mode for the full ring, and so on.

Inspection of Fig. 12 will show that the first mode has negative values for values of ϕ_t greater than 180 degrees. It will be noted that this mode gives deflections in one direction throughout the projected length of the ring. This will not happen for a ring with a central angle greater than 180 degrees, and is hence a fictitous mode.

Fixed-end partial Ring.--Equations (17), (18), and (19) are used for this case. The end conditions are that:

When $\phi = 0$ and $\phi = \phi_t$ $u = 0$,

and when $\phi = 0$ and $\phi = \phi_t$ $\frac{du}{d\phi} = 0$.

It may then be shown that:

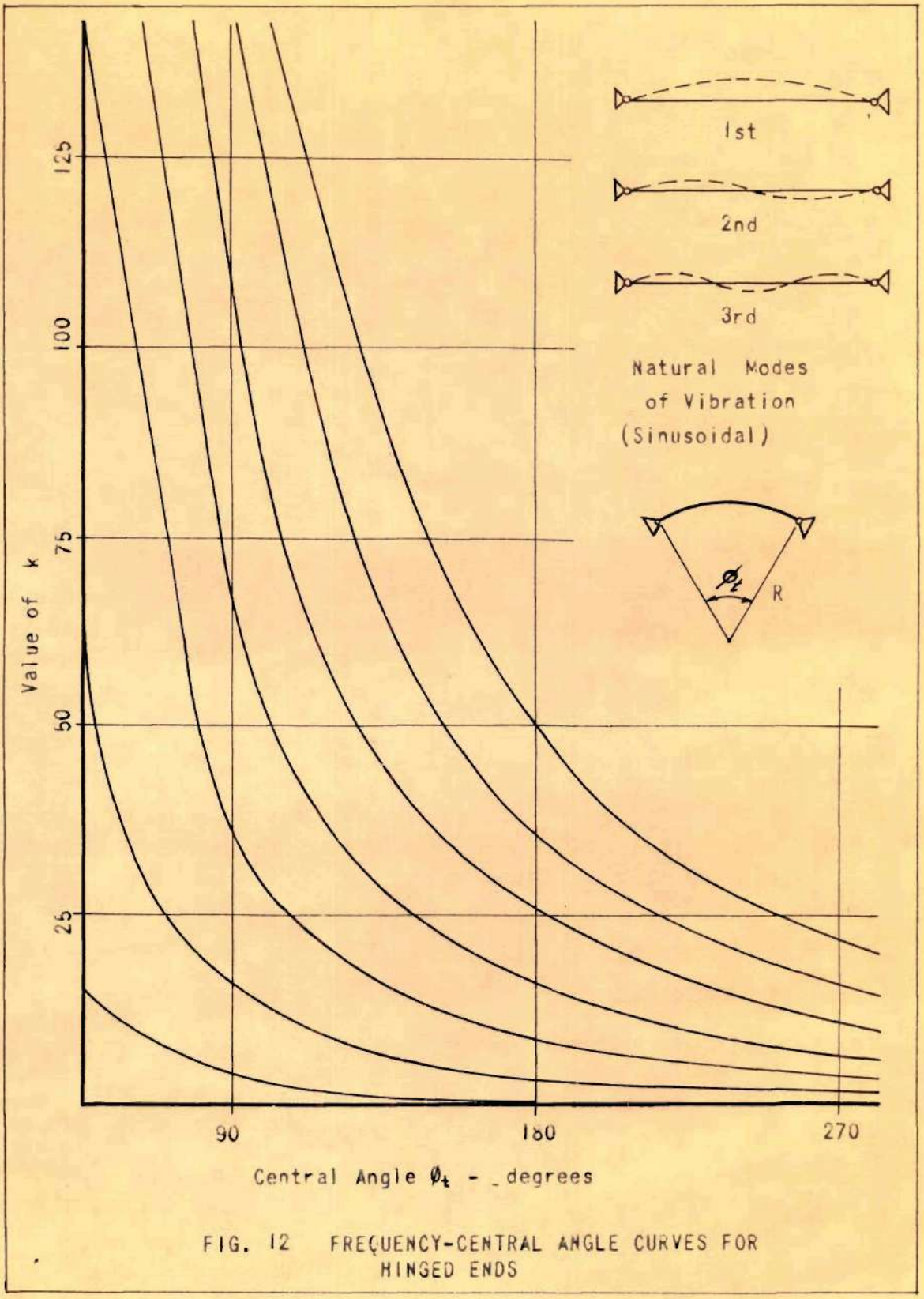

FIG. 12 FREQUENCY-CENTRAL ANGLE CURVES FOR HINGED ENDS

$$A = -C \quad \text{and} \quad D = -\frac{Bb}{a}$$

and
$$A = B\left(\frac{\sin b\phi_t - b/a \sinh a\phi_t}{\cosh a\phi_t - \cos b\phi_t}\right) \qquad (27)$$

and
$$A = B\left(\frac{b\cos b\phi_t - b\cosh a\phi_t}{a\sinh a\phi_t + b\sin b\phi_t}\right) \qquad (27)$$

Equating the multipliers of B and simplifying, remembering that $\left[\frac{b}{a} - \frac{a}{b}\right] = \frac{1}{K}$, Eq. (28) is obtained:

$$\cos b\phi_t \cosh a\phi_t + \frac{1}{2K} \sin b\phi_t \sinh a\phi_t = 1 \qquad (28)$$

where
$$a = \left[-1/2 + \sqrt{(K^2 + 1/4)}\right]^{1/2}$$

$$b = \left[1/2 + \sqrt{(K^2 + 1/4)}\right]^{1/2}$$

Solution for the first eight modes of this equation with respect to the central angle ϕ_t is given by Fig. 13. It will be noted that the equation is quite a formidable one; the solution is believed to be correct to three significant digits, many pages of paper being expended in its solution. It is interesting to compare the solutions of the frequency Eqs. (25) and (28) for the hinged-end case and for the fixed end case respectively. It would be expected that the former, being less stiff than the latter, would have somewhat lower frequencies. This is exactly what is found when the solutions with respect to central angle are presented graphically as shown on Fig. 14. It will be noted that the curves are approximately hyperbolic with the hinged end curves being "stepped down" from the fixed end curves.

The shapes of the modes of vibration of the fixed

end case may be evaluated once the frequencies have been determined. Denoting F as the reciprocal of the constant within the brackets in Eq. (27) then

$$u \approx \cos b\phi - \cosh a\phi + F \sin b\phi - \frac{b}{a}F \sinh a\phi \qquad (29)$$

$$\frac{d^2u}{d\phi^2} \approx -b^2\cos b\phi - a^2\cosh a\phi - Fb^2\sin b\phi - FK\sinh a\phi \qquad (30)$$

noting that $ab = K$.

From Eq. (14), it may be seen that the bending moments M vary as the sum of Eqs. (29) and (30). Simplifying

$$M \approx a^2\cos b\phi + a^2F \sin b\phi + b^2 \cosh a\phi + F(K + \frac{b}{a})\sinh a\phi \qquad (31)$$

Equations (29) and (31) give the shape of the deflection curve and the shape of the moment diagram, and are dimensionless equations in themselves. This is typical of the solution; the amplitude of the vibration at some point must be specified from some other initial condition.

Numerical Comparison with Existing Solutions.--From the foregoing it may be seen that the angular frequency ω is given by:

$$\omega = K/R^2 \quad \frac{EIg}{c}$$

where R = radius

EI = flexural rigidity

g = acceleration of gravity

c = weight per unit length

K = a constant

ω = radians per second

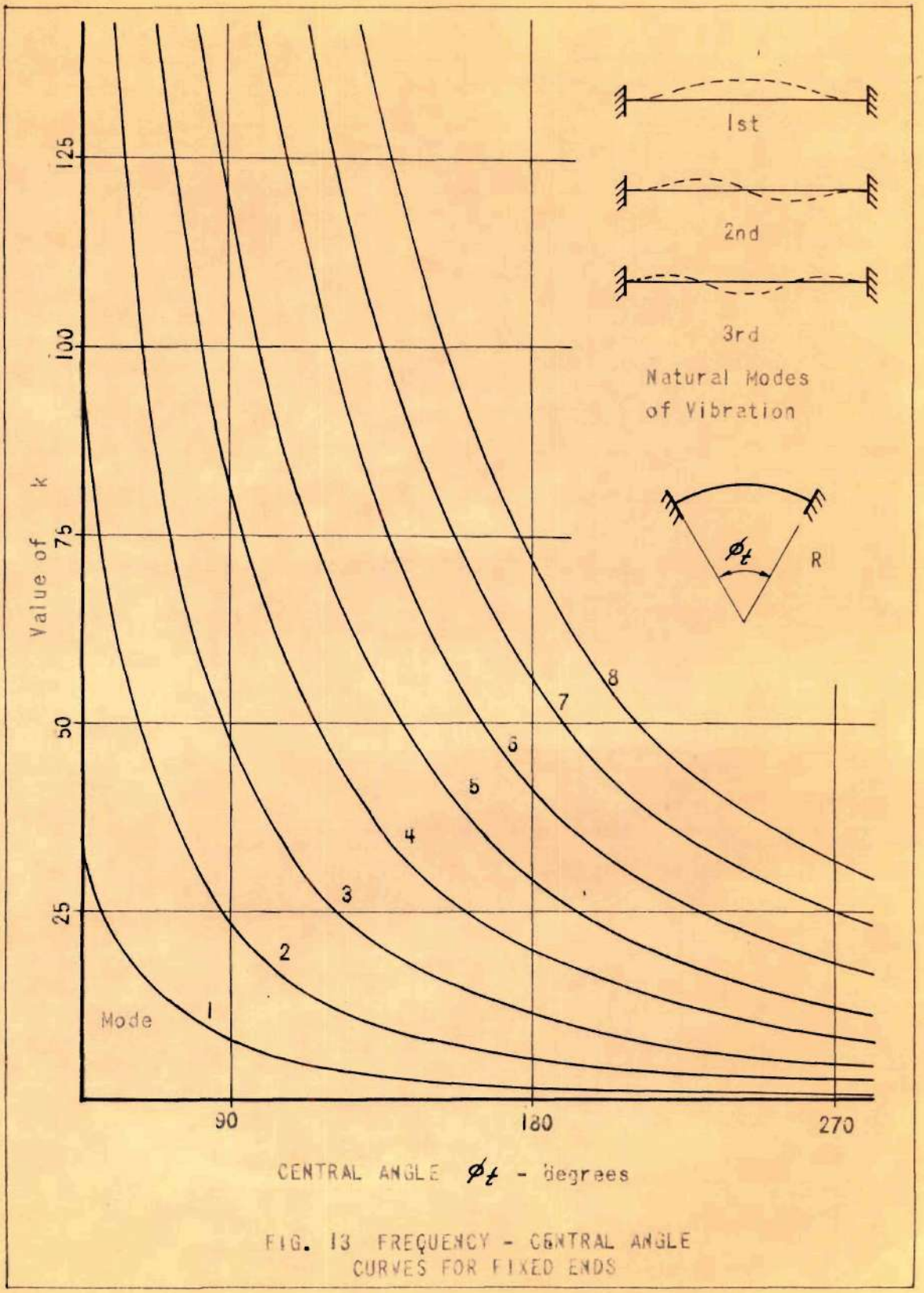

FIG. 13 FREQUENCY - CENTRAL ANGLE CURVES FOR FIXED ENDS

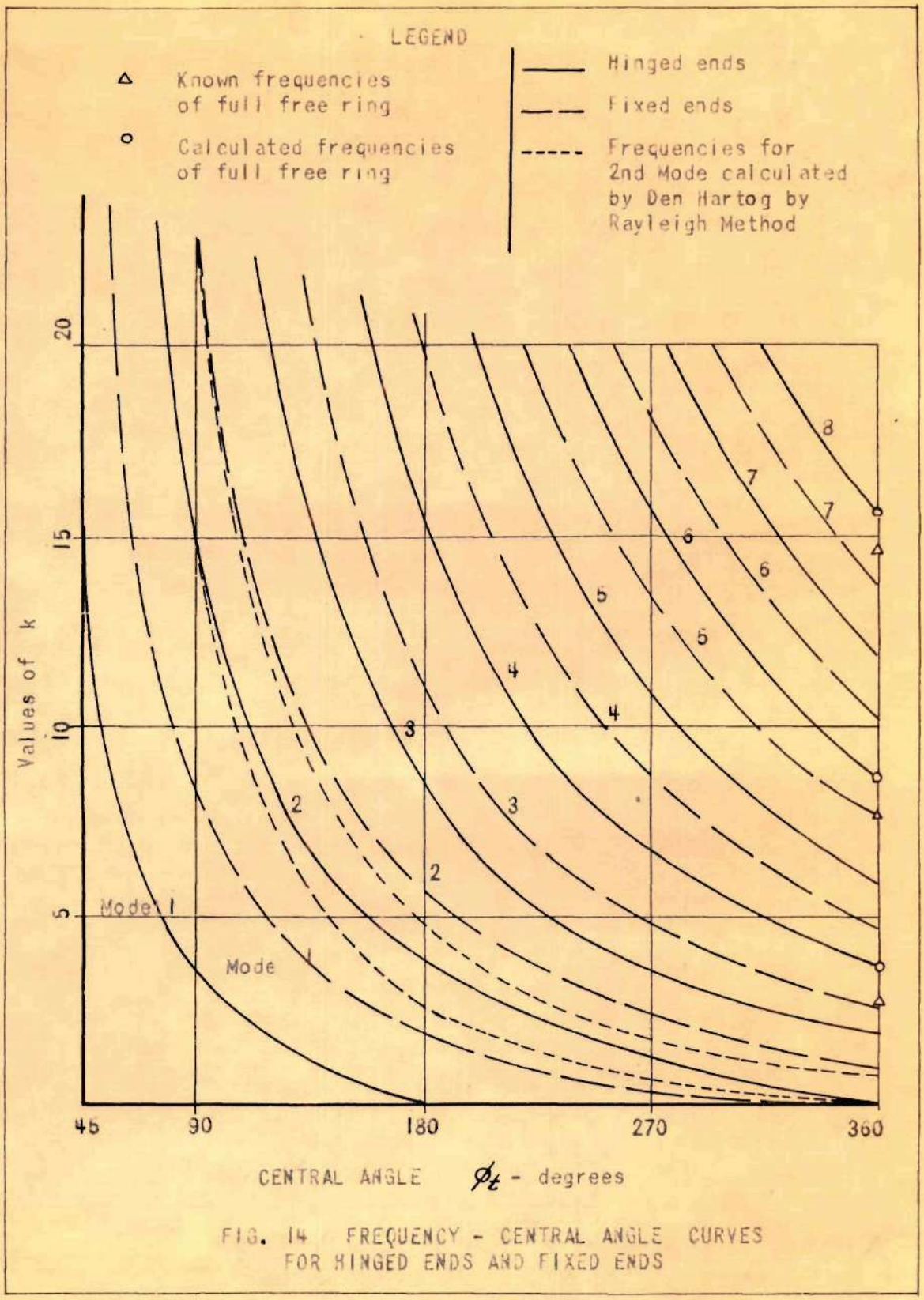

FIG. 14 FREQUENCY - CENTRAL ANGLE CURVES FOR HINGED ENDS AND FIXED ENDS

In the table below the values of K as given by Eq. (21) are compared with the values of K obtained by the exact solution for the full unrestrained ring.

Table 1. Comparison of K-Values Given by Eq. (21) with those Given by Exact Analysis

Mode	K (Eq. 17)	K (Exact)
Fundamental	3.46	2.68
Second	8.50	7.59
Third	15.50	14.6
Fourth	24.5	23.5

It is to be noted that the higher the mode considered, the percentage error becomes less.

Comparison can also be made for the frequencies of the hinged end and the fixed end partial ring as given by Eqs. (25) and (28) respectively, with the values given by Den Hartog (7) computed by the Rayleigh-Ritz method. This is expressed graphically on Fig. 14. It will be noted that the Rayleigh-Ritz method yields values only for the second mode of vibration.

Inspection of these curves will show that for central angles below 90 degrees the approximate curves are virtually identical with those by the Rayleigh method, and that reasonable accuracies are obtained up to central angles of 135 degrees. These central angles embrace most civil engineering structures. It will also be noted that the

higher the mode considered, the less is the percentage error, as previously mentioned. It is believed by the writer that this approximation is the only available method for calculating the frequencies of the higher modes.

It is seen that the error is always on the high side, in other words the actual frequencies will always be somewhat less than those calculated by this approximation. Indeed it is noted that if the values of K are reduced by 1.0, good agreement with existing solutions is found in virtually all cases, excepting those values of K which are quite small (less than 1.5). This correction is not applied to any of the calculations in this paper. This line of thought leads to the possibility that the original differential equation of motion (Eq. (15) might be modified to such a form as

$$\frac{d^4u}{d\phi^4} + \alpha \frac{d^3u}{d\phi^2} + \left(\frac{R^4 c\omega^2}{EIg}\right)u = 0$$

where α is a constant established by experimental evidence and by comparison with exact solution. It is believed that α would have a value of about 3/2.

In concluding this study of the approximation, it may be said that values of the natural frequencies are given to 10 per cent for central angles of less than 120 degrees, the error decreasing as the central angle is decreased. The errors are on the high side. This is exactly what was expected as previously mentioned.

CHAPTER V

COMPARISON OF THE THEORETICAL CALCULATIONS WITH EXPERIMENTAL DATA

Static Strains and Deflections

Strains.--The column analogy was used in calculating the reactions and bending moments of the model for the two static loadings. No correction was made for rib shortening or for shear deformation. The ordinary flexure formula was used in computing the strains. Typical strains were also computed by the "curved-beam" theory, the difference between these results and those given by the flexure formula was less than one per cent. These methods of calculation are routine, therefore the numerical calculations are not given.

The experimental static strains were measured with the SR-4 Strain Indicator as mentioned previously. A comparison between the analytical and the experimental strains is given by Figs. 15a, b, and c. The stresses resulting from a one pound load are plotted on the projected length of the arch axis. The solid line represents the theoretical stress; the dashed line with circular points representing the measured experimental values. Fig. 15a is for load Series II referred to in the Appendix. Fig. 15b is for Series I and III. These figures show the stresses due to bending moment only. Fig. 15c shows the theoretical static thrust stresses due to a unit load. The experimental values for

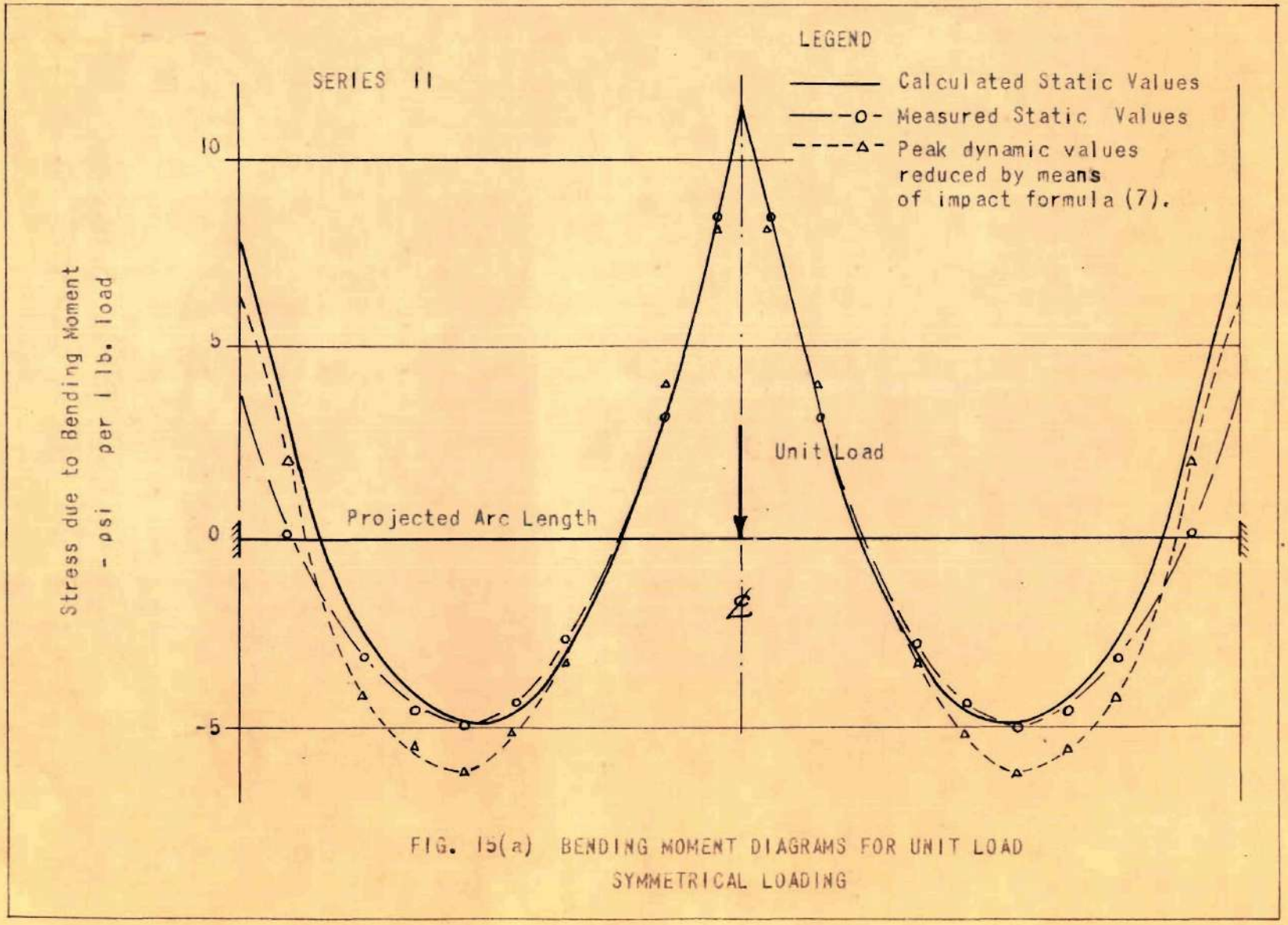

FIG. 15(a) BENDING MOMENT DIAGRAMS FOR UNIT LOAD SYMMETRICAL LOADING

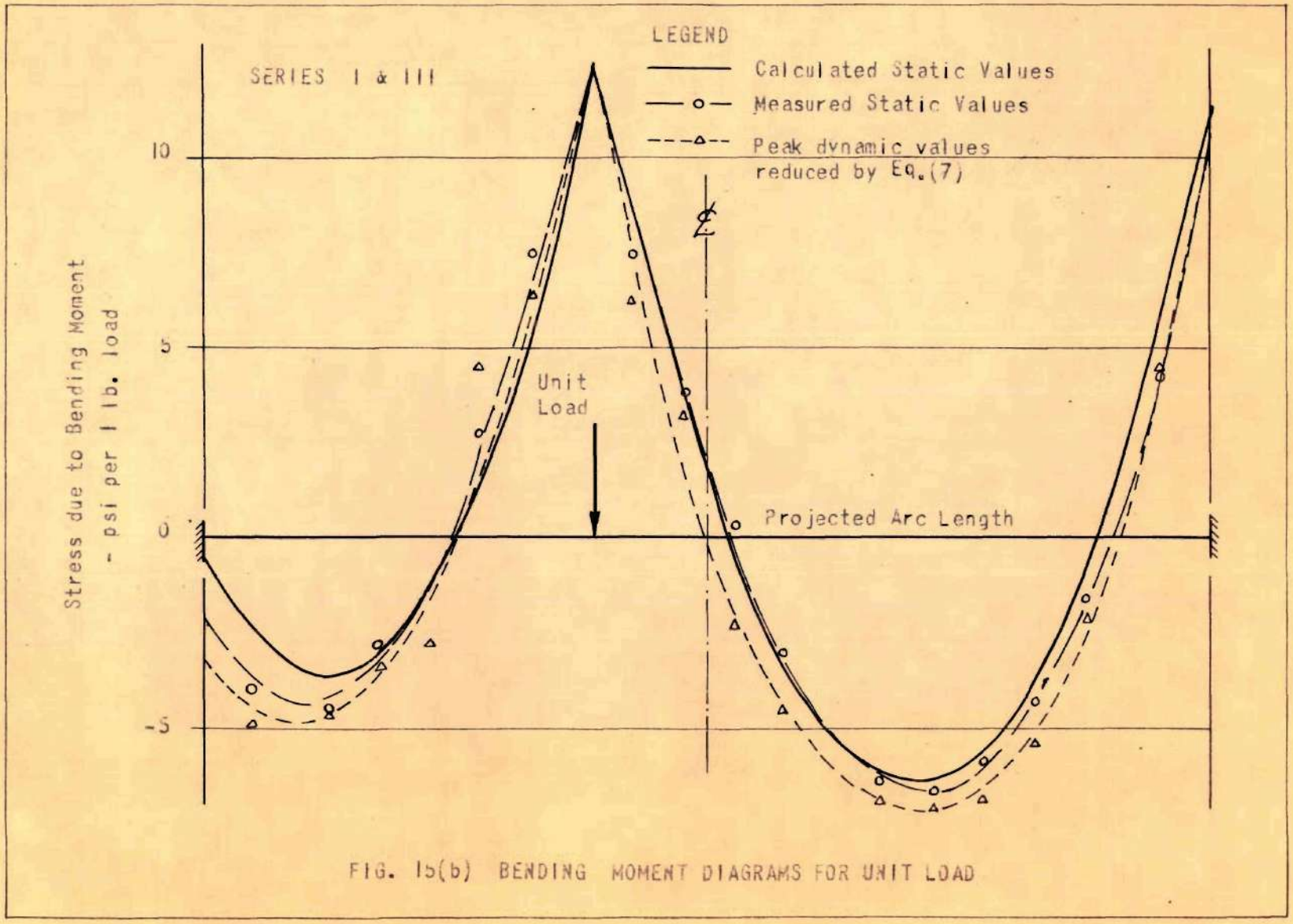

FIG. 15(b) BENDING MOMENT DIAGRAMS FOR UNIT LOAD

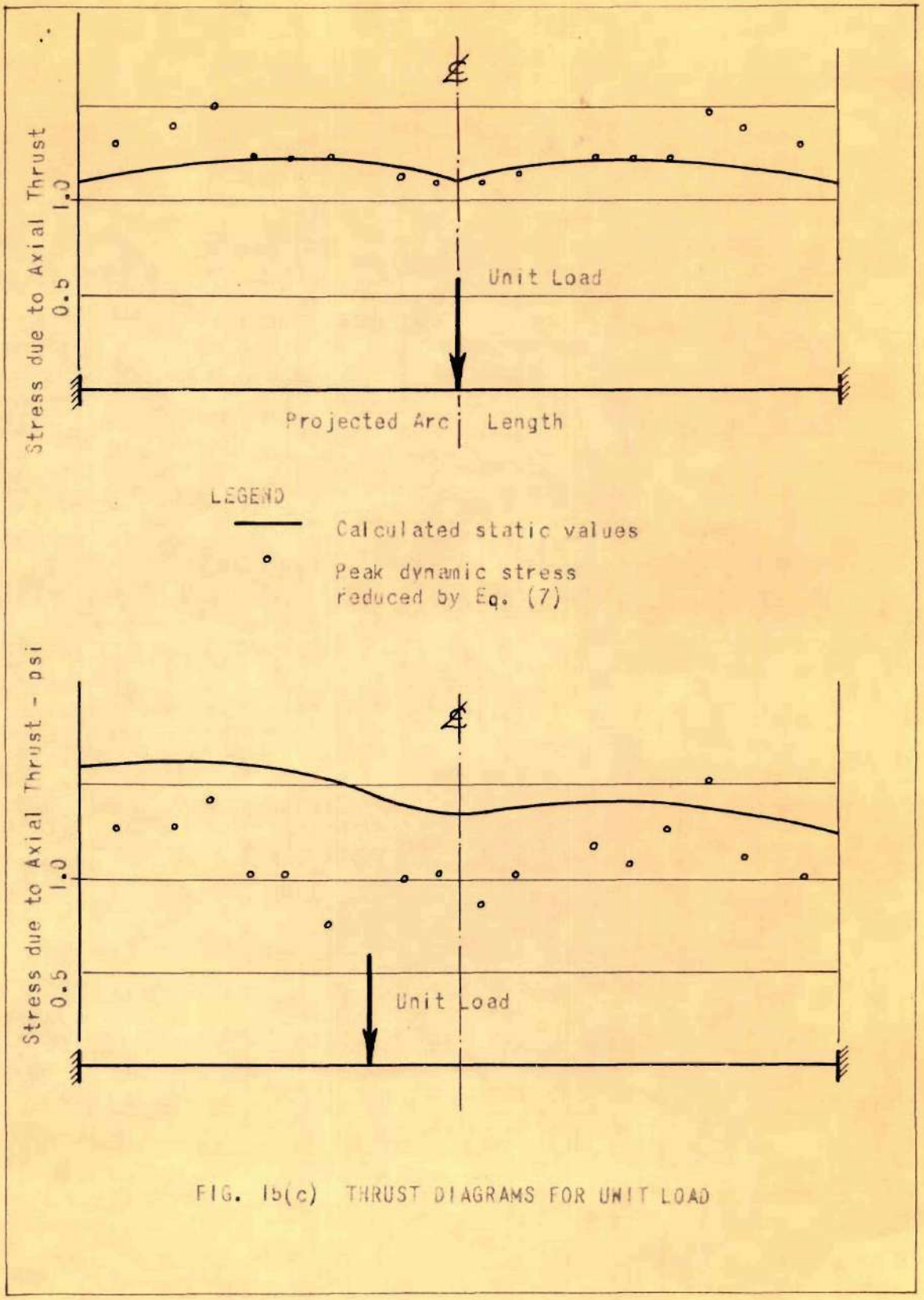

FIG. 15(c) THRUST DIAGRAMS FOR UNIT LOAD

this are not shown, as the measurement of these values could not be made with sufficient accuracy to warrant presentation.

In Fig. 15a, for central loading, good agreement is shown between the two curves except at the supports. A theoretical stress of about 8 psi is shown here, but the experimental stress is only about half this value. This indicates a rotation of the supports, which indicated that the end conditions at the springing points lay somewhere between complete fixity and simple pinned-end conditions. The base frame was extremely stiff, yet this rotation of the supports presented a major source of error in the study.

For the eccentric loading of the model, shown by Fig. 15b the agreement is not so close as with the first load condition. At the left support the stress is larger than theoretical calculations would predict, at the right support the experimental values and the theoretical values agree quite closely. Also the experimental values are larger than the theoretical values for the area of negative bending moment in the right portion of the span.

The explanation of this lies in the method of applying the load. In Fig. 3 it is evident that the load is applied from a fixed point, instead of a gravity loading on the model. When this eccentric vertical load is applied horizontal deformation of the model is prevented to some extent resulting in the application of a horizontal load as well as a vertical load. It is seen in Fig. 16 that the

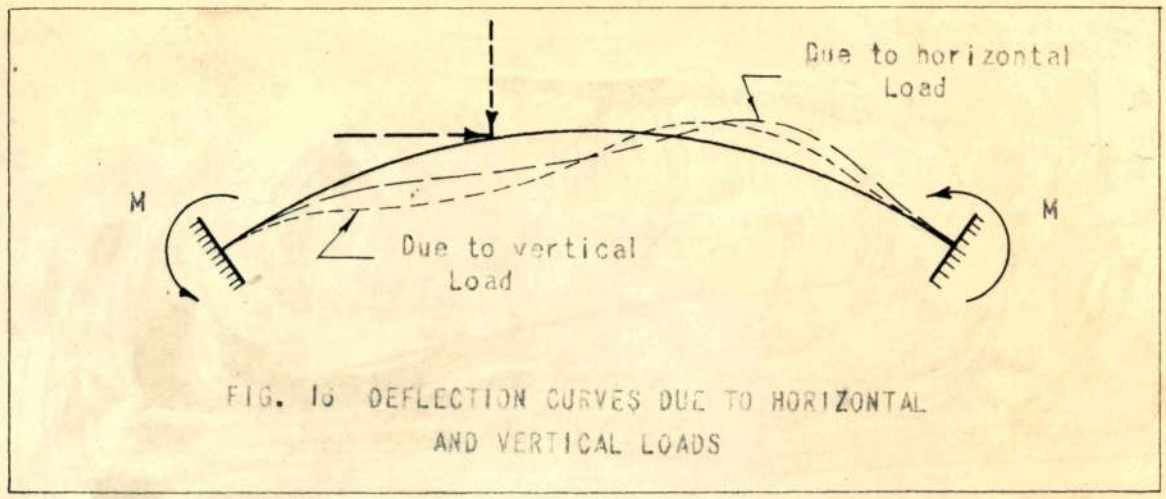

FIG. 16 DEFLECTION CURVES DUE TO HORIZONTAL AND VERTICAL LOADS

action of the horizontal load is to increase the bending moments at both ends of the model. The value of this horizontal load cannot be easily determined as it is dependent upon the rigidity of the loading frame, the stiffness of the base frame, etc.

This error is not present in Series II, (symmetrical loading) and would not be present had loading been made by using dead weights.

Deflections.--The analytical deflections were calculated by routine application of the energy methods for each load condition. The experimental values were measured under the load for the two loading conditions. Results of this are tabulated below.

Table 2. Static Deflections under the Load

Load Series	Theoretical Deflection in in. due to one lb load	Experimental Deflection in in. due to one lb load
II - Center	0.0000179	0.0000350
I - Eccentric	0.0000276	0.0000425

By inspection of the above table it becomes quite evident that the rotation of the supports has profound effect upon the value of the deflections, the experimental values being almost twice the analytical ones.

Maximum Stress during Impact

The third set of curves shown on Fig. 15 represent the maximum stresses in the model during impact. These curves were obtained by scaling the peak strains at the various gage points from the strain-time traces given in the Appendix. These strains were multiplied by the static modulus of elasticity to obtain the peak stress. The peak stresses were then divided by the equivalent static load given by Eq. (7) to give the peak dynamic stresses in pounds per square inch per one pound load.

The equivalent static load given by Eq. (7) depends on the deflection at the point of impact. This dynamic deflection was not measured experimentally. Instead the value of the experimental static deflection was used in the calculations

for the curves in Fig. 15. As was previously mentioned there was a considerable difference between the theoretical calculated deflection and the measured static deflection under the load. This calculated deflection was based upon the assumption of perfect fixity at the springing. This perfect fixity was not actually obtained; hence, it was more reasonable to use the experimental value of the deflection. In the dynamic case, however, the large mass of the base with its corresponding low natural frequency contributed a greater degree of fixity to the model than was indicated by the experimental static data. Therefore the curves of peak dynamic stress of Fig. 15 should lie between the calculated and the experimental static curve. Inspection of Fig. 15 will show this to be true in the regions near the supports.

Plastic Action of the Model

All of the discussion in this report deals with the elastic behavior of the model. At the end of the test the dynamic load was increased by increments until the first sign of permanent set was detected by means of a deflection gage under the point of application of the load. The equivalent static load calculated by means of Eq. (7) for Series III gave a load of 1530 lbs, which gave a maximum theoretical stress in the model of about 20,000 psi. This compares precisely with the stress strain curve of Fig. 4 which gives the elastic limit of the material as 20,000 psi.

Time of Contact

From the discussion with respect to the derivation of Eqs. (9) and (10), simple sinusoidal motion would be expected during the impact cycle from an ideal elastic system of no mass. The length of time of this cycle, or rather half-wave, is given by Eq. (9). The time of contact, in this length of time, is given in the table below in which the experimental values scaled from the traces in the Appendix are compared with these analytical ones. The analytical values are based upon the static experimental deflections in determining the constant h in Eq. (9).

Table 3. Time of Contact of Pendulum with the Model

Load Series	Analytical Time in Seconds (by Eq. 9)	Experimental Time in Seconds
I	0.00297	0.00327
II	0.00324	0.00360

It is seen that very good agreement is attained. The experimental values should be somewhat larger than the theoretical values due to the "following" of the model as the pendulum tries to leave it at the end of the impact cycle.

Natural Frequencies of the Model

Each trace was analyzed graphically for indications

of natural frequencies. The results were tabulated, grouped, and averaged to give those values listed below. Table 4 shows the comparisons between the observed values and the values computed by the approximate theory for free vibrations given in Chapter IV. The observed frequencies are expected to be somewhere between the theoretical frequency for a pinned-end condition and the fixed-end condition due to the rotation as discussed above.

Table 4. Natural Frequencies

Mode	Theoretical Freq. for Fixed-end Condition cps	Observed Frequency cps	Theoretical Freq. for Pinned-end Condition cps
1	151	none observed	61
2	428	320	270
3	846	665	605
4	1401	none observed	1105
5	2100	1710	1730
6	2939	3100	2090
7	3890	3800	3390

As is seen the lower modes more nearly correspond to the pinned-end condition, and the higher modes correspond to the fixed-end condition. This is to be expected as the natural frequency of the heavy frame would be low and would affect the lower modes to a greater extent with respect to rotation of the ends of the model than the higher modes. There was a considerable scattering of the data in this analysis, and the accuracy could be questioned. However, the results

expressed in Table 4 may be taken as a fairly good indication of the response of the model. In the derivation of the approximate theory in Chapter IV, it is stated that the computed frequencies would be too high. This seems to be the case.

Natural Modes of Vibration

The modes of vibration studied experimentally are the shapes of the bending moment modes and not the deflections as normally considered. For the two modes most prominently observed in the experimental data, the theoretical bending moment diagrams were calculated by Eq. (31). These are plotted on Figs. 17a and b. The amplitudes of each respective mode was then scaled by inspection from the traces in the Appendix. This could not be done very accurately. Where data was available, several readings were averaged. A curve was then plotted after the modes had been examined as to time to tell whether the amplitude was positive or negative at that particular instant. The curve was then adjusted to have a maximum ordinate of unity. The points from this adjusted curve are plotted in Figs. 17a and b for comparison with the theoretical shape of the curves. As may be seen the agreement is quite good.

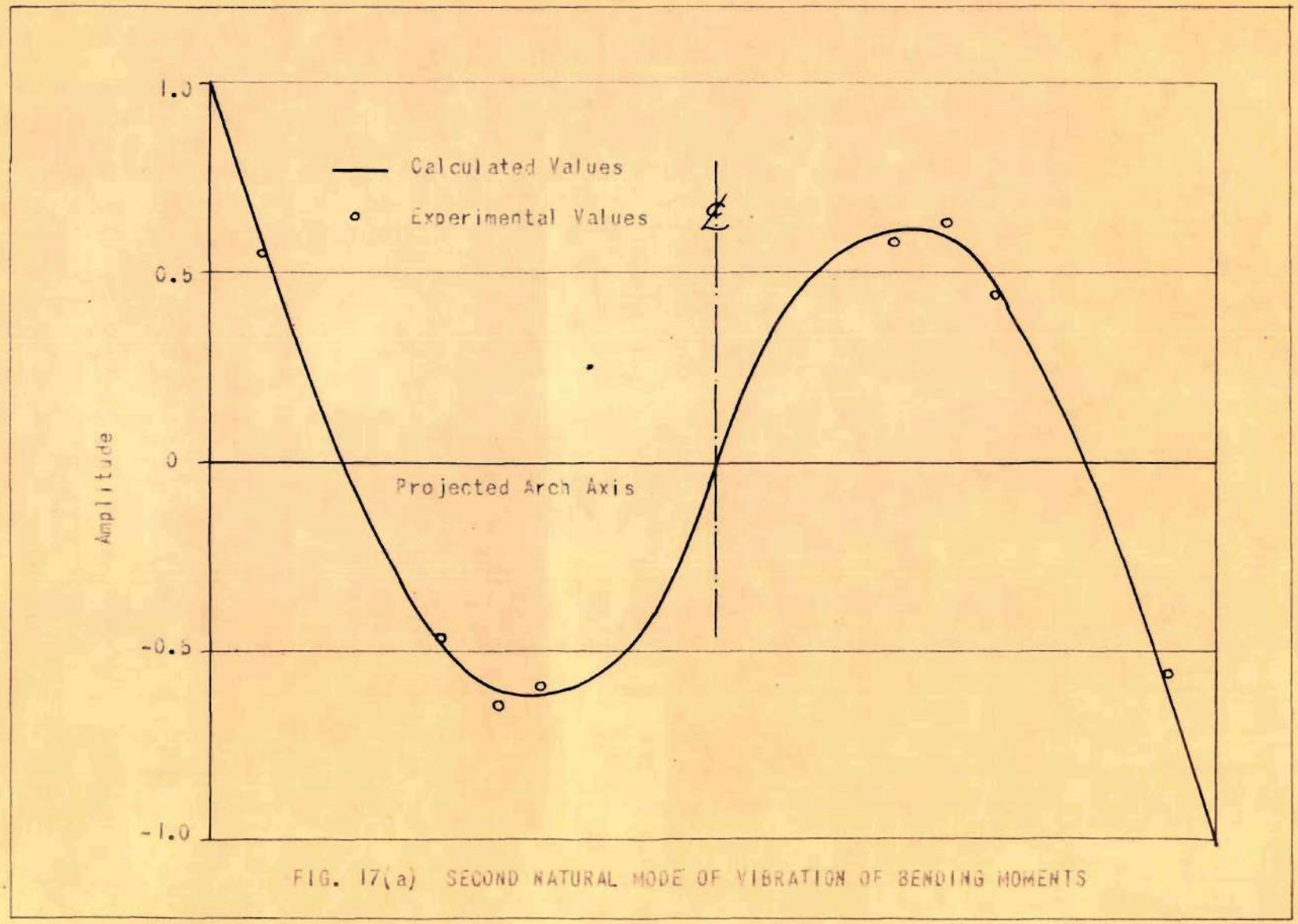

FIG. 17(a) SECOND NATURAL MODE OF VIBRATION OF BENDING MOMENTS

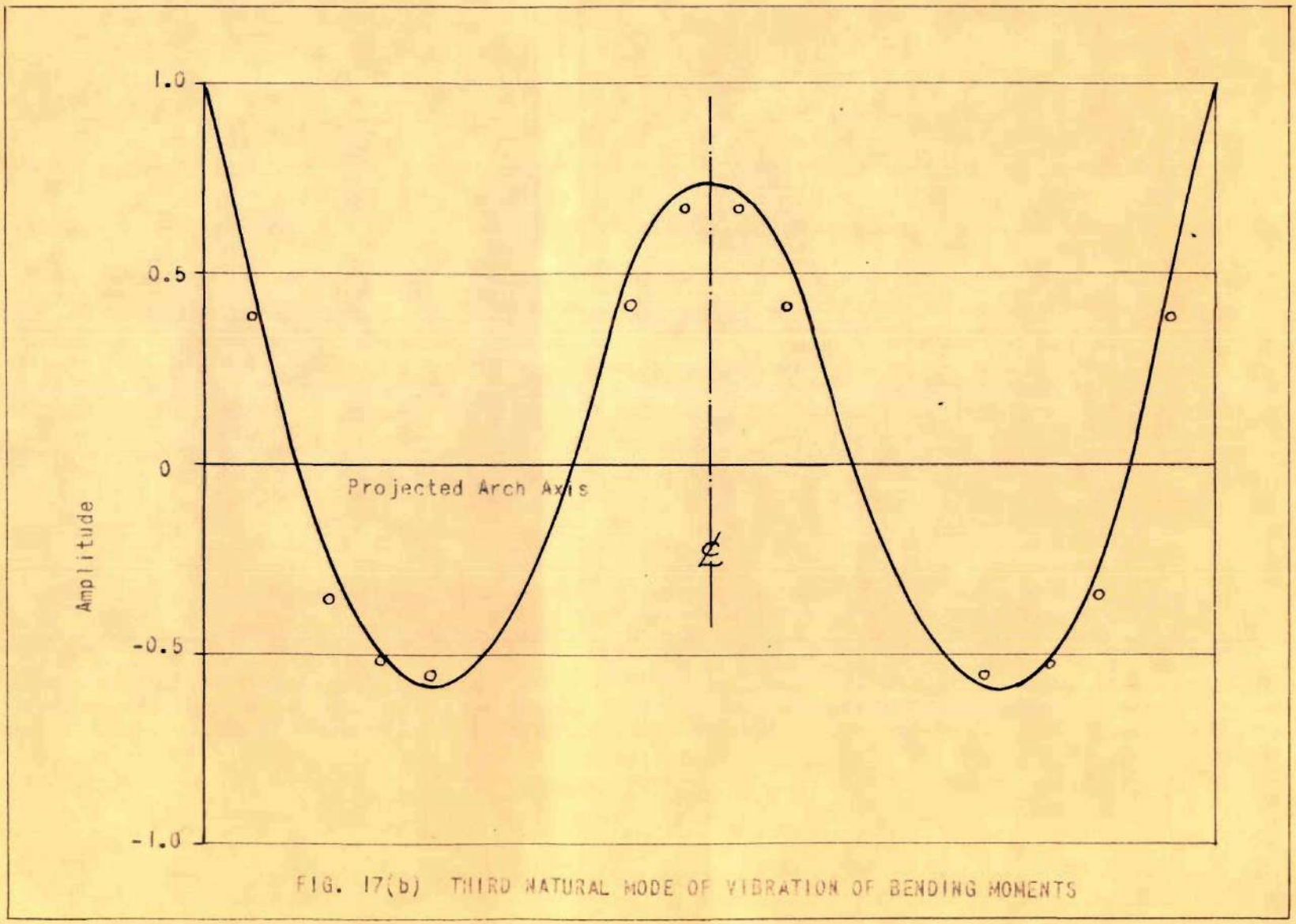

FIG. 17(b) THIRD NATURAL MODE OF VIBRATION OF BENDING MOMENTS

CHAPTER VI

CONCLUSIONS

In light of the preceding chapter and by inspection of the various traces in the Appendix, several conclusions may be made with regard to the theoretical discussion of Chapter IV.

(1) Equation (7) which predicts the maximum dynamic stress, is found to yield good accuracy for the case studied.

(2) Equation (9) which gives the time of contact yields results which are quite good for this same case.

(3) Equation (10) which describes the motion during the time of impact is quite reliable. The validity of this equation is borne out by an inspection of the traces which show sinusoidal motion during this period except for the superimposed vibrations of the model itself.

(4) The approximate theory of free vibrations developed in this thesis indicates good agreement with the experimental results in the case studied. This agreement appears to be better, however, when com-

paring the shapes of the modes of vibration, than it does when predicting the natural frequencies. In the latter case the approximate theoretical relationship predicts values that are somewhat higher than actual.

CHAPTER VII

RECOMMENDATIONS FOR FURTHER STUDY

Throughout the study a number of changes in apparatus suggested themselves. These are listed below.

(1) A more rigid frame should be used to prevent rotation of the ends of the model. The hinged-end condition probably could be fabricated more conveniently.

(2) It would be convenient to have a pressure measuring device between the pendulum and the model.

(3) The electronic equipment should be modified so as to permit an overall calibration of the apparatus.

(4) It would be desirable to measure the deflections of the model during its motion. This could be done by means of a linear differential transformer or a linear variable potentiometer. A more accurate method would be to use a thin cantilever leaf to which an SR-4 gage is attached. It would be necessary to so design the leaf that its fundamental frequency would be higher than any frequency measured.

Further theoretical development is needed. A few of the factors needing study are listed below.

(1) No solution exists for structures having a variable cross-section.

(2) A solution is needed for arches having an axis other than circular.

(3) The effect of damping has not been studied.

(4) The exact analysis of motion during the impact cycle is possible and the reader is referred to (Reference 1, 2 and 3). Such an analysis in the light of this experimental data should prove interesting.

(5) More data should be taken with regard to the effect of the ratio of the striking mass to the mass of the elastic system.

(6) Some criterian should be developed which would permit a prediction as to which natural modes of vibration would be excited as the blow is applied at various points.

(7) The plastic action and actual failure of the model should certainly receive some attention. The scope of the present investigation did not include the plastic action or the destruction of the model. It is believed that had the model been

tested to failure it would have proved somewhat stronger than a simple ultimate stress theory would indicate.

APPENDIX

STRAIN - TIME TRACES

The following traces were obtained by means of the Polaroid camera attached to the oscilloscope. It was then necessary to reproduce and enlarge these for presentation here. Images of each trace were projected upon a screen, photographed with a 35 mm camera and printed for reproduction. The process resulted in an enlargement of the original photographs of approximately three times.

In each case time is represented on the horizontal axis, with the variable under consideration represented on the vertical axis. The grid lines visible on each photograph are the grid markings on the oscilloscope screen, the grid being a one centimeter grid. Hence measurements made on the photographs must be correlated to the grid lines. All calibration factors are given with respect to centimeters, a centimeter on the photograph being the distance between adjacent pairs of the grid lines.

A typical trace consists of a burned spot to the left of the screen due to the camera shutter being open before the sweep was set in motion. Then a heavy line appears moving from left to right, this being the undeflected sweep just before impact. The sweep is deflected at impact, one large cycle becoming apparent, this being the cycle of contact of the pendulum with the model. From this point on,

the sweep records the free vibrations of the model. In some cases the sweep travels from right to left instead of from left to right. This was done to maintain the sign convention noted below.

The traces are catalogued in the following manner. For each series, representing a load condition of an identical load at the same point for each trace, the photographs are presented in the following order:

(1) The bending strains at each gage point at a small time scale to permit detailed inspection of the trace under the impact cycle.

(2) The bending strains at a large time scale to show a large number of cycles of free vibration.

(3) The bending strains plus the contact voltage to give an indication of the instant of impact, or "zero time".

(4) The strains due to axial thrust at each gage point.

(5) The contact traces indicating the length of time of contact of the pendulum with the model.

A serial number has been given to each trace, the details of this coding system are outlined below:

Series:

Series I: load point 5 in. away from the centerline of the model

in a direction away from the strain gages. Pendulum distance (see p. 10) equals 15.00 in.

Series II: load point at the centerline of the model. Pendulum distance equals 12.94 in.

Series III: load point 5 in. from centerline on the side of the gages. Pendulum distance equals 15.00 in.

Position of Strain Gages:

The gages were numbered consecutively from the springing toward the crown. For precise gage positions see Fig. 5.

Type of Strain:

M.....strain due to bending moment

T.....strain due to axial thrust

C.....contact voltage

(this has been superimposed upon the moment strains as previously mentioned)

Strain Sensitivity:

Noted as the vertical scale of the traces in micro-inches per inch of strain per centimeter.

Time Scale:

Time in thousandths of one second for the 10 cm sweep.

Strains Sign Convention:

Toward the top of the page on each trace is considered positive. A positive bending strain corresponds to an increase in curvature of the arch. A positive thrust strain corresponds to tension at that gage point. The sign of the contact voltage is insignificant.

As an example of how the coding system is applied, consider the serial number II M4 C 200 10. This represents center loading, pendulum distance 12.94 in., bending strain and gage point four plus contact voltage, 1 cm equals 200 micro-inches strain, sweep speed equals 0.01 sec for 10 cm, or 0.001 sec per cm.

SERIES II

Load Applied: Centerline

Pendulum Distance: 12.94 in.

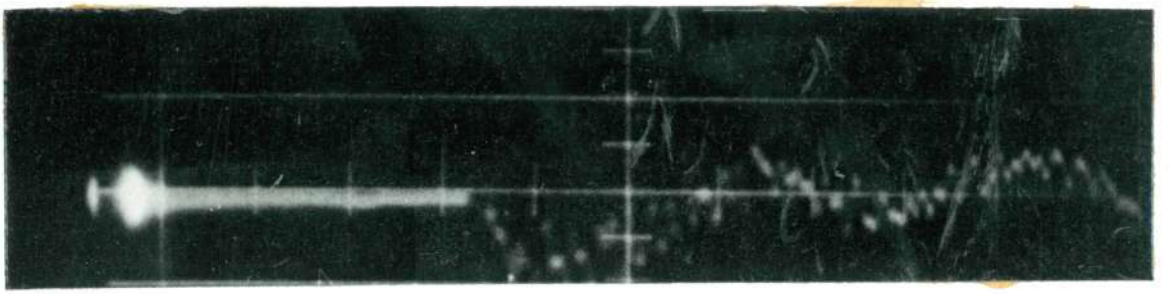

II M1 200 10

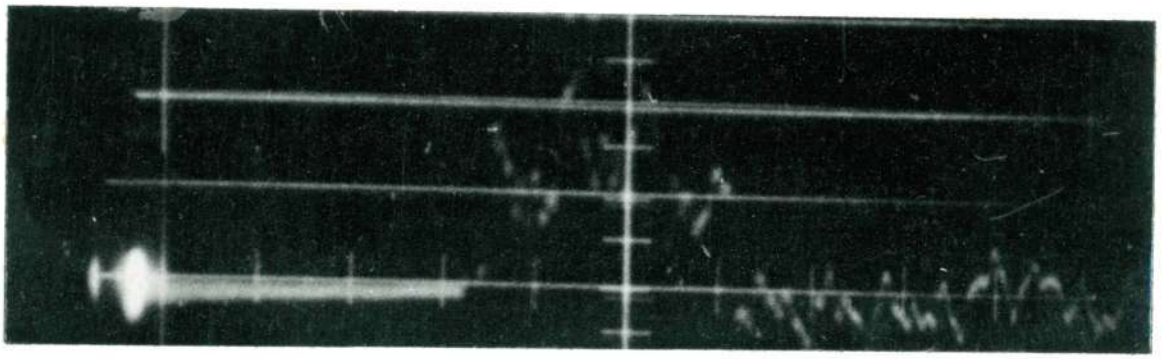

II M2 200 10

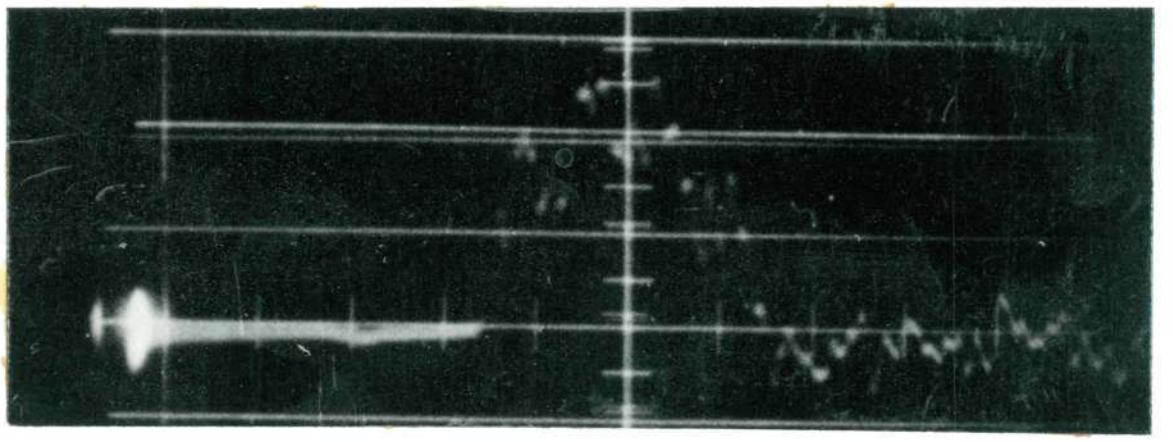

II M3 200 10

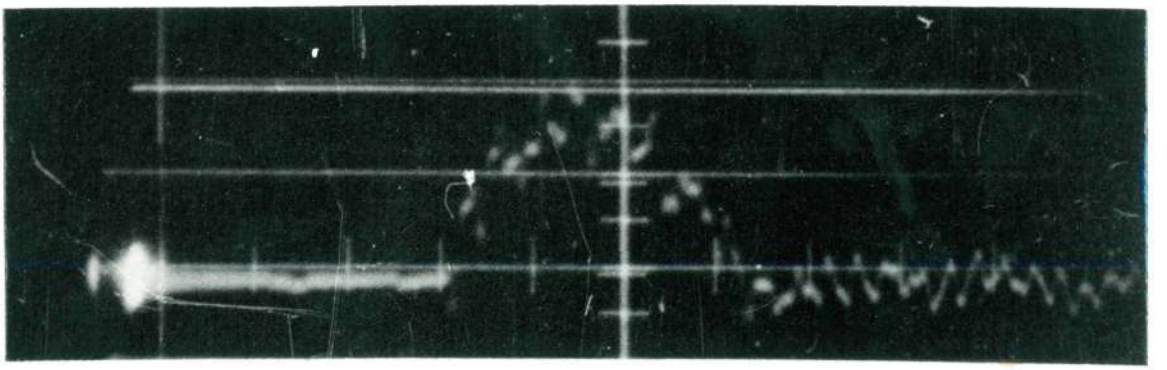

II M4 300 10

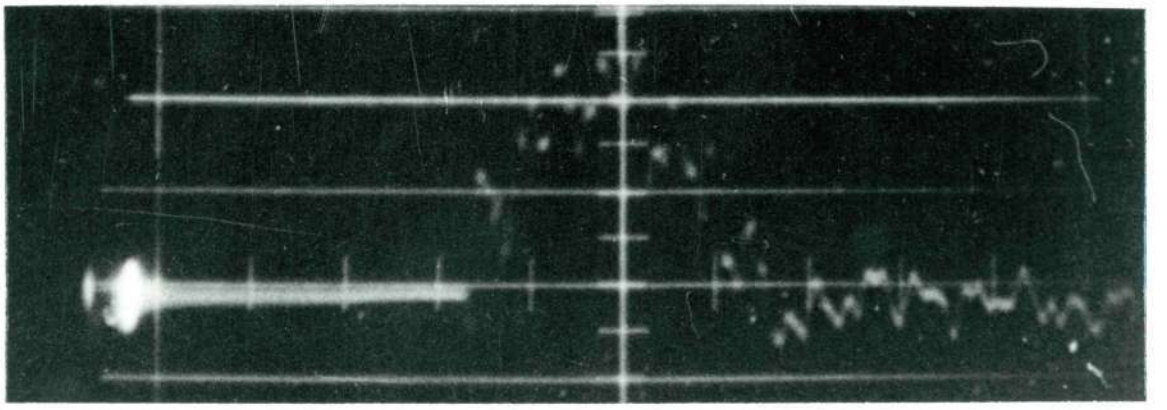

II M5 200 10

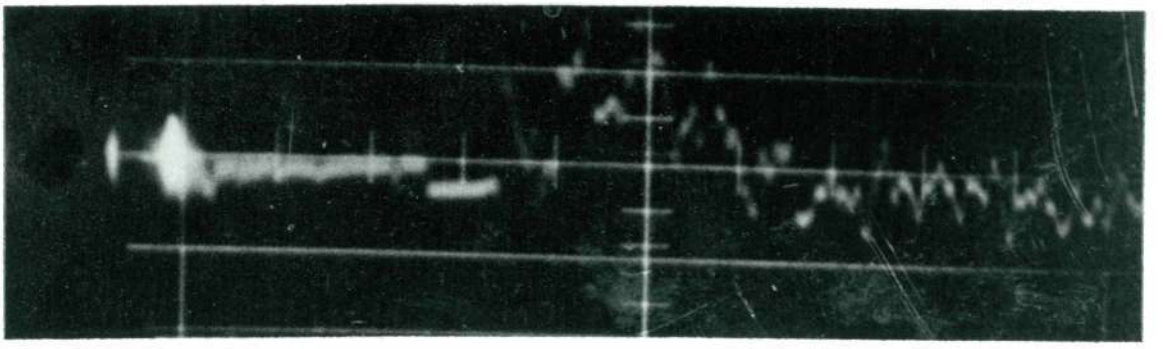

II M6 200 10

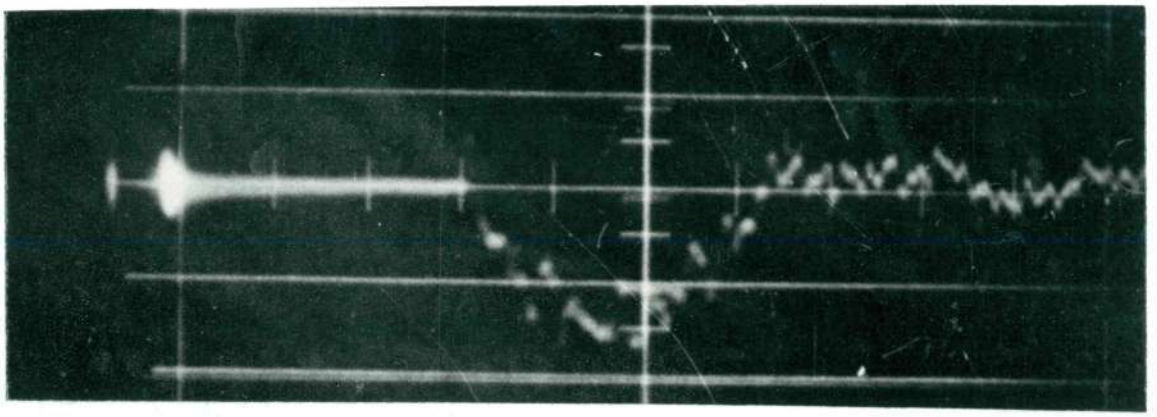

II M7 250 10

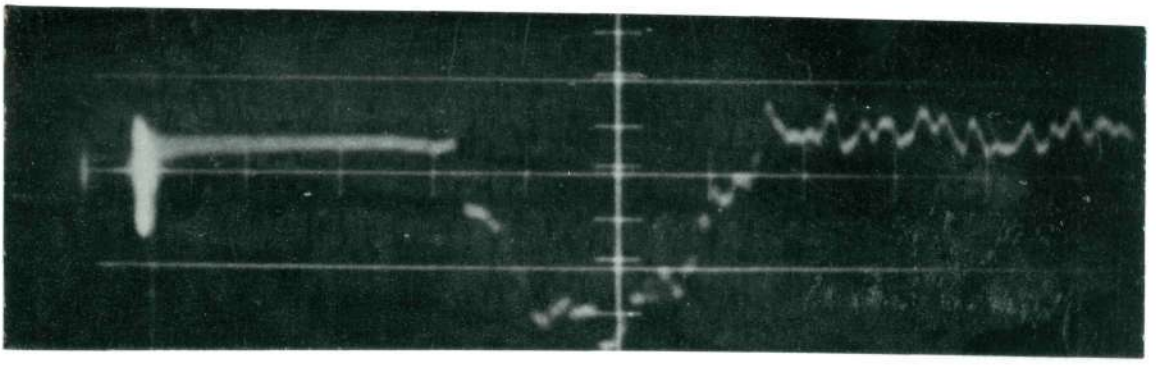

II M8 378 10

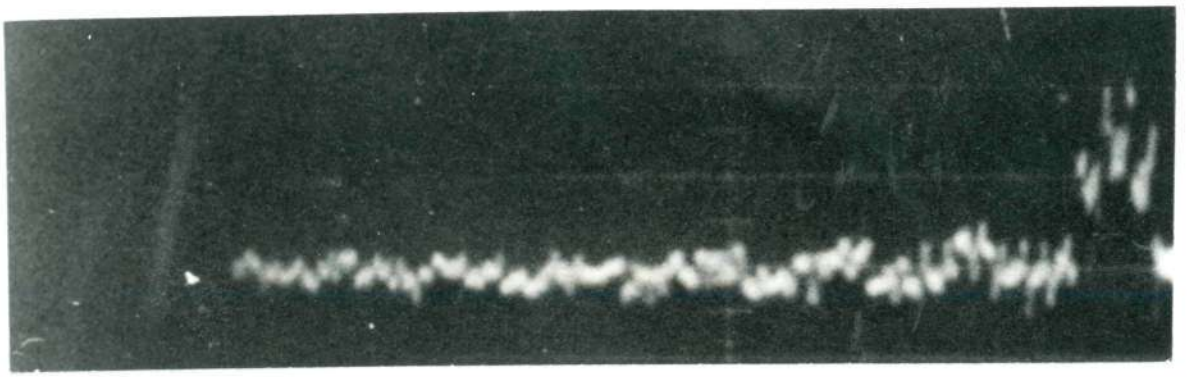

II M2 200 25

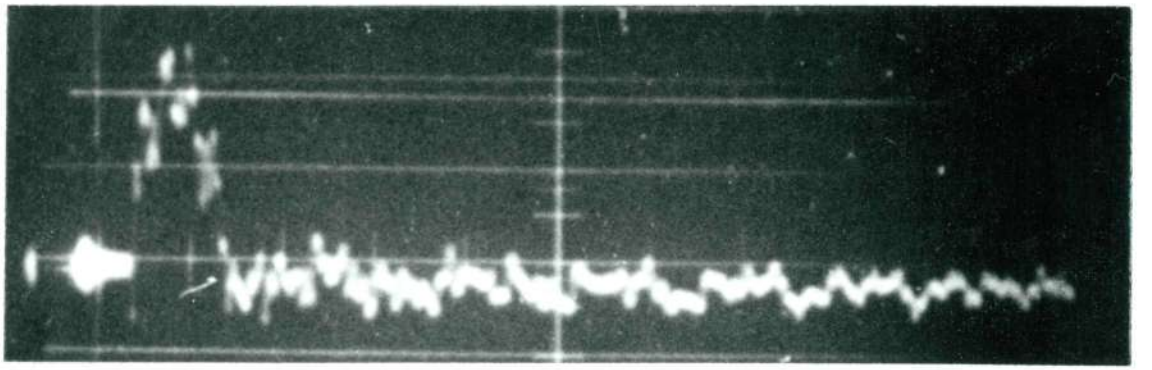

II M3 200 25

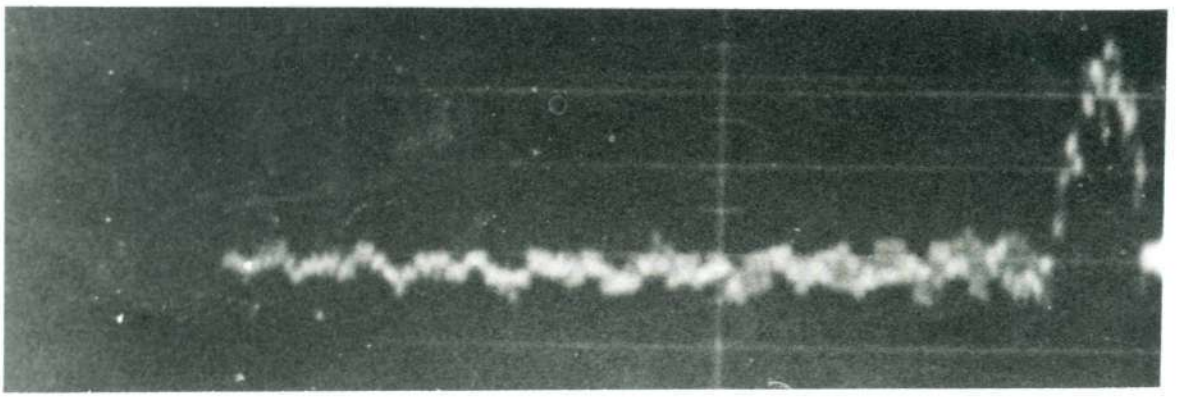

II M4 200 25

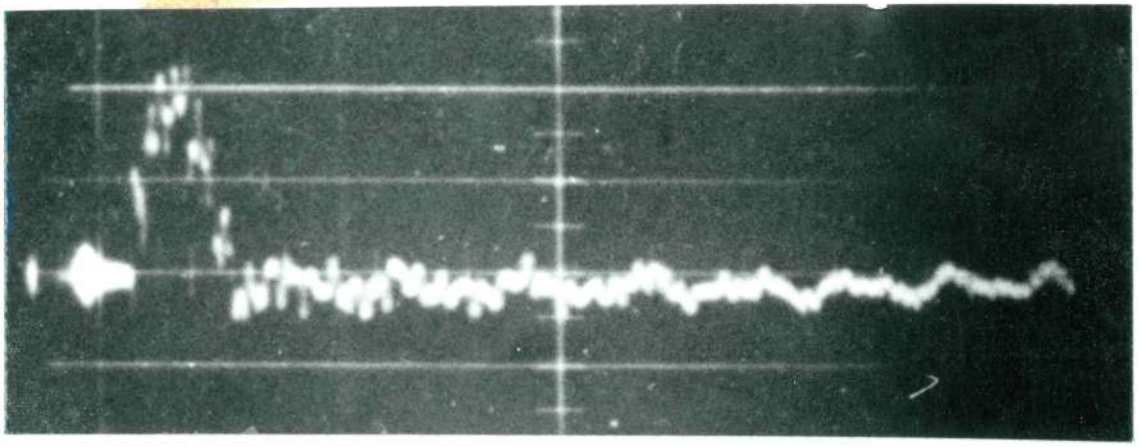

II M5 200 25

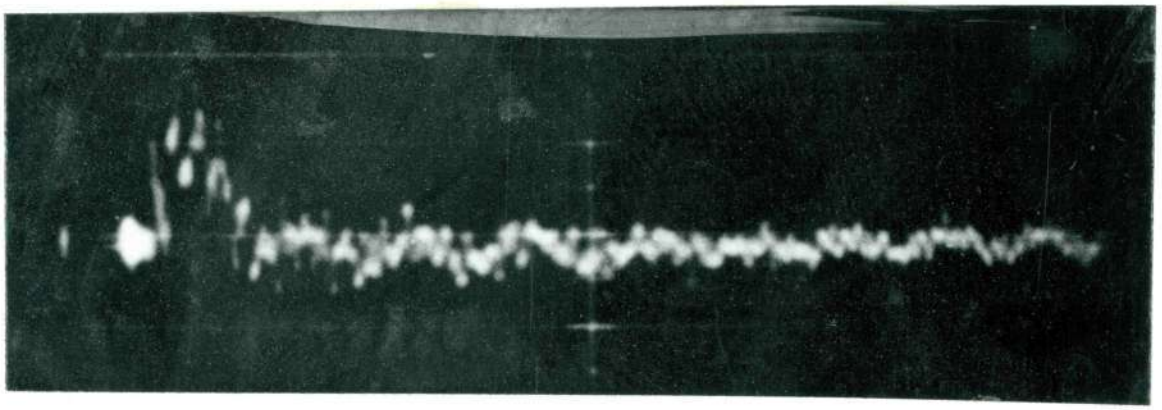

II M6 200 25

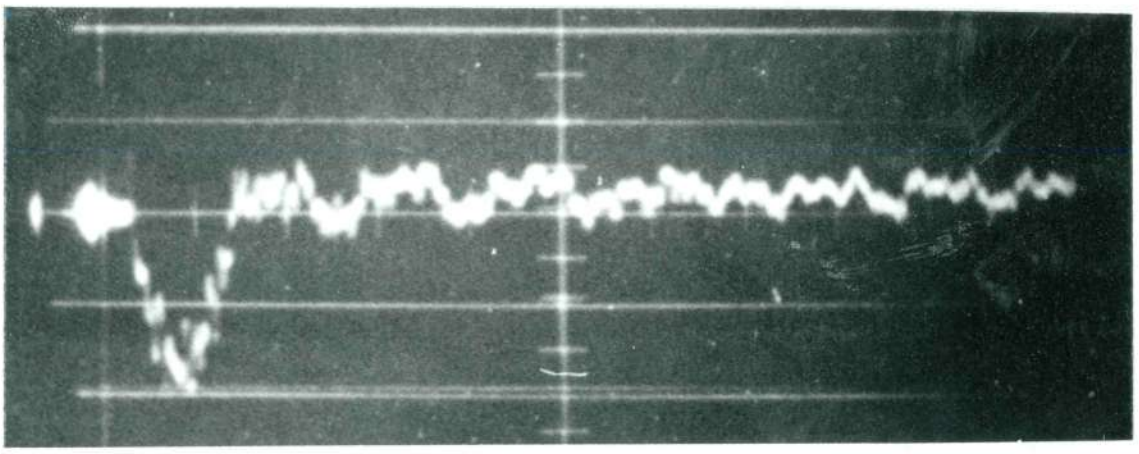

II M7 200 25

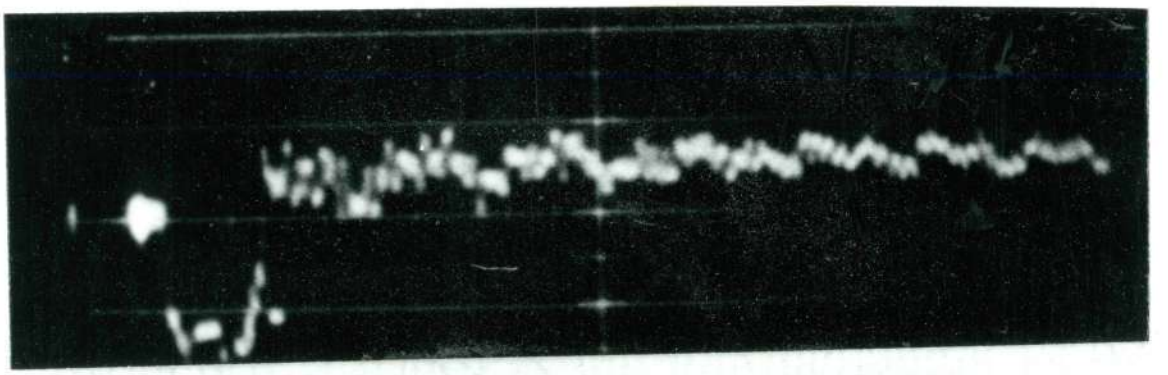

II M8 200 25

II M1 C 200 10

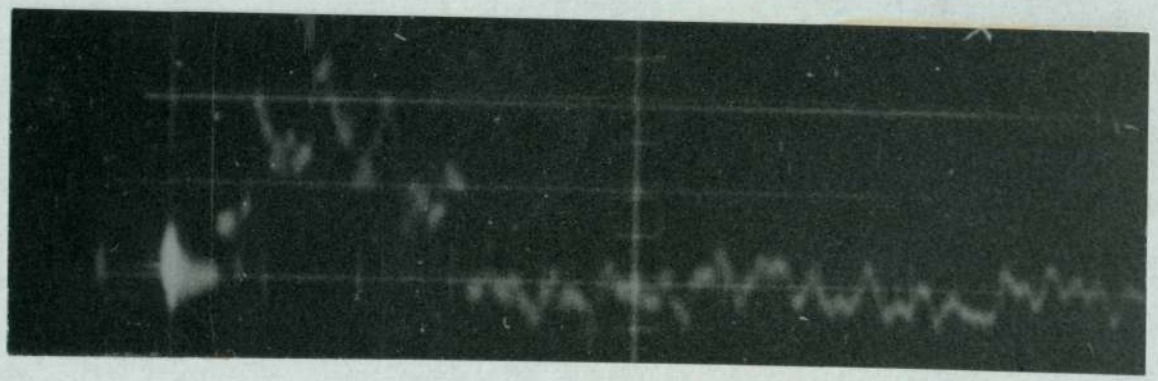

II M2 C 200 10

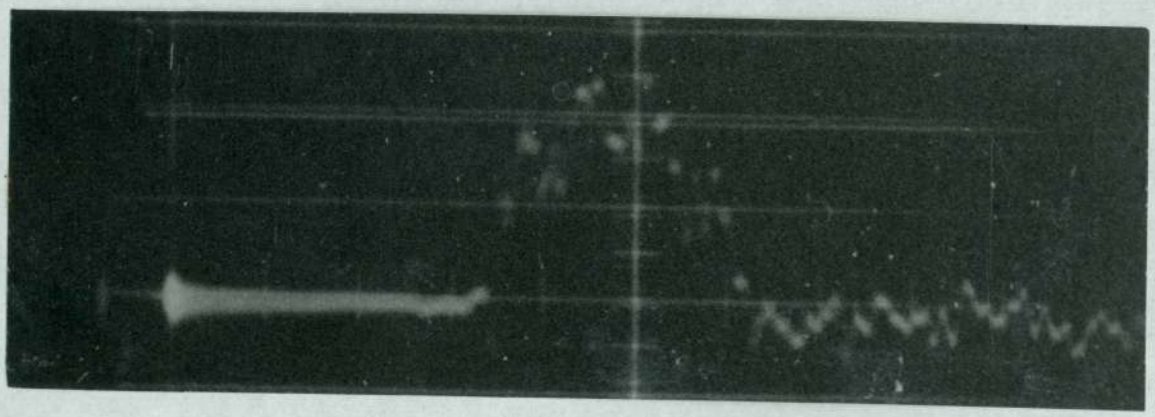

II M3 C 200 10

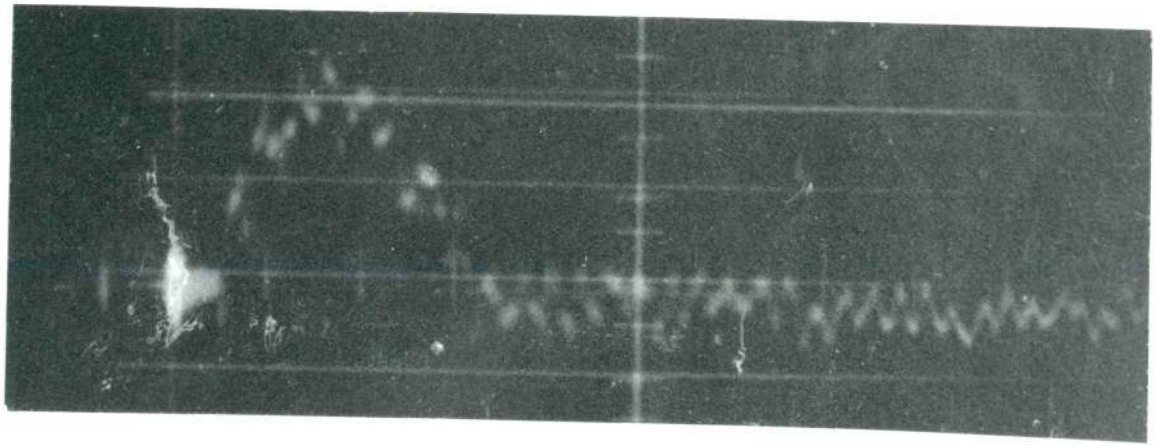

II M4 C 300 10

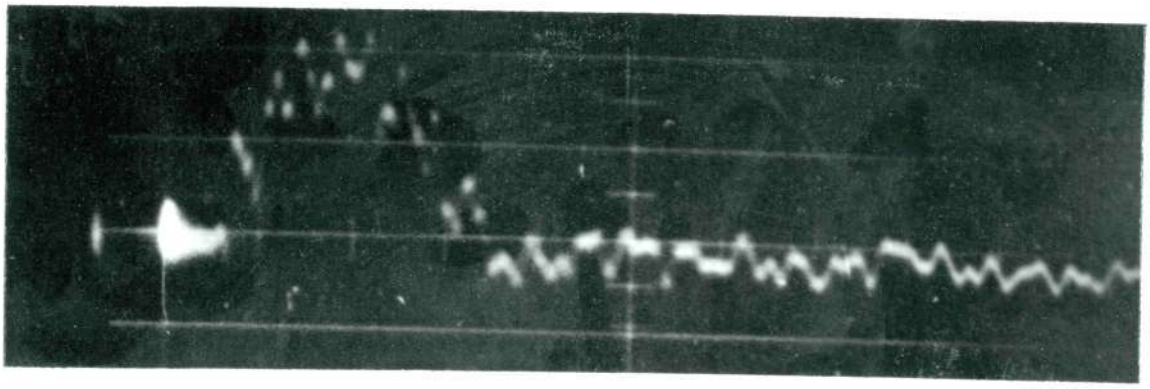

II M5 C 200 10

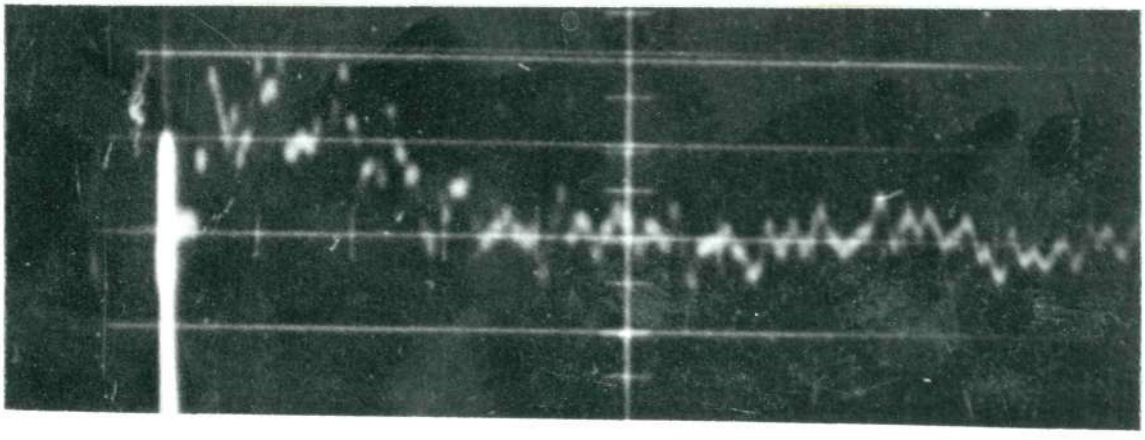

II M6 C 200 10

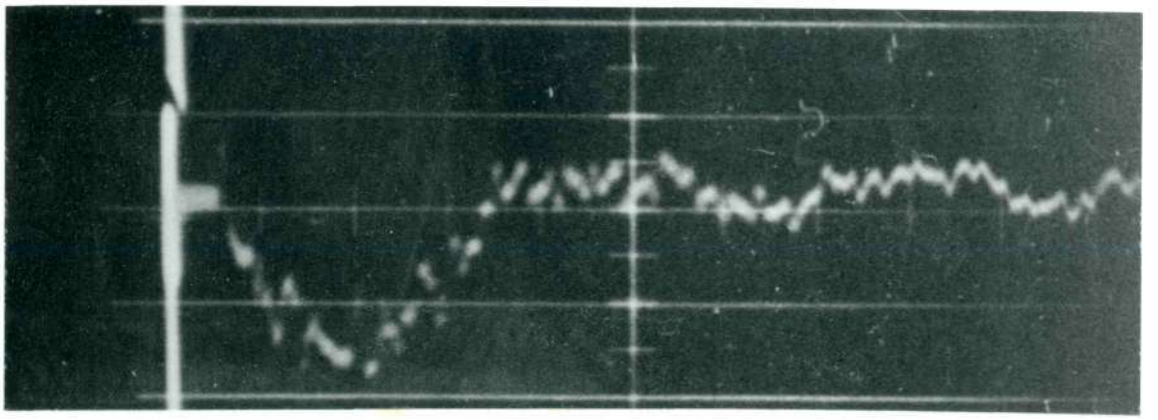

II M7 C 200 10

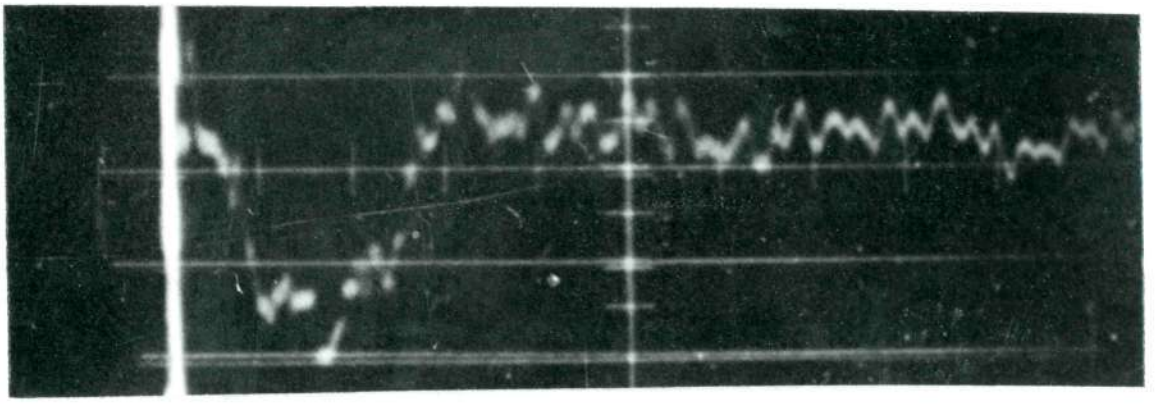

II M8 C 200 10

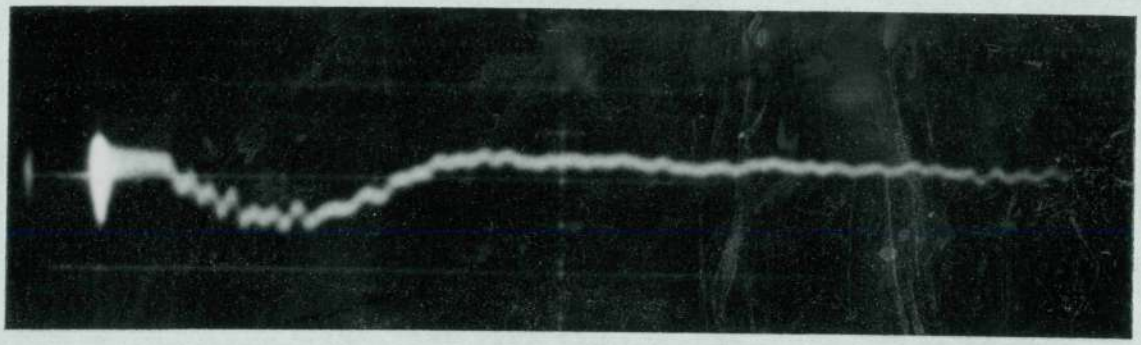

II T1 200 10

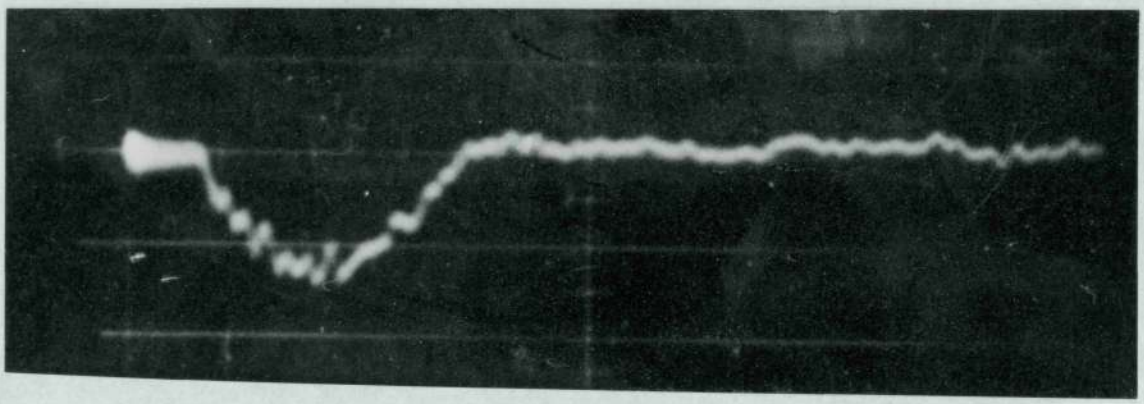

II T2 100 10

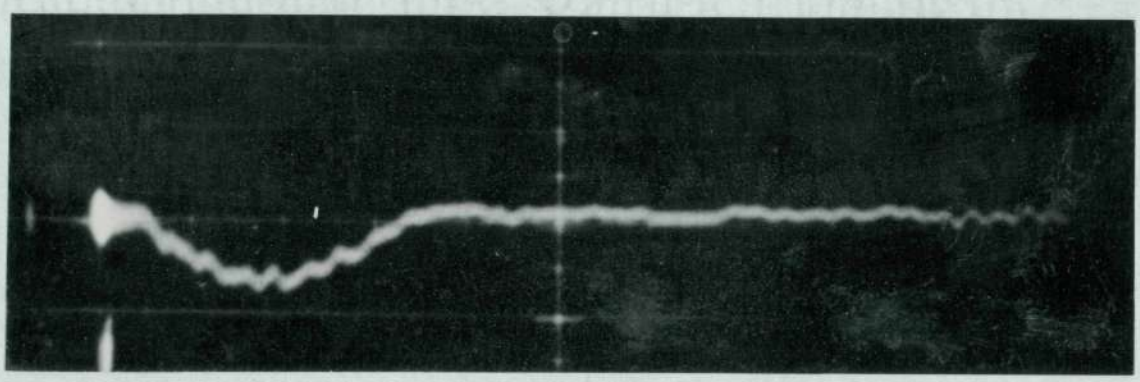

II T3 200 10

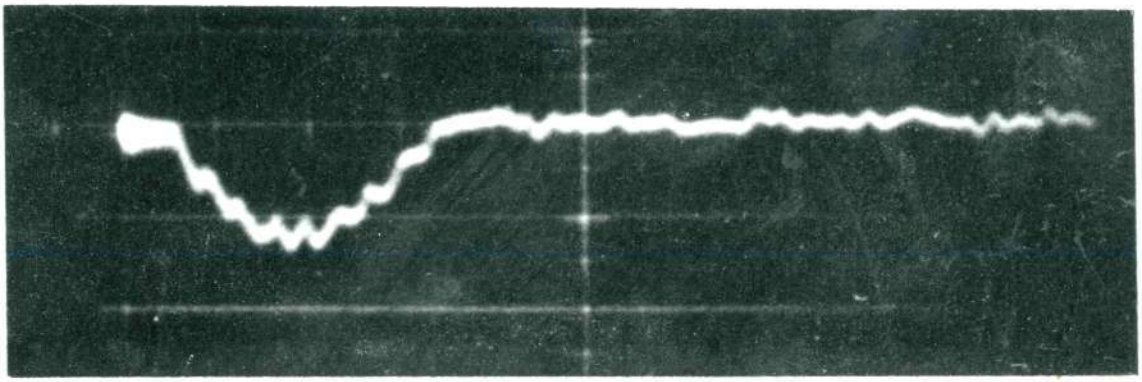

II T4 100 10

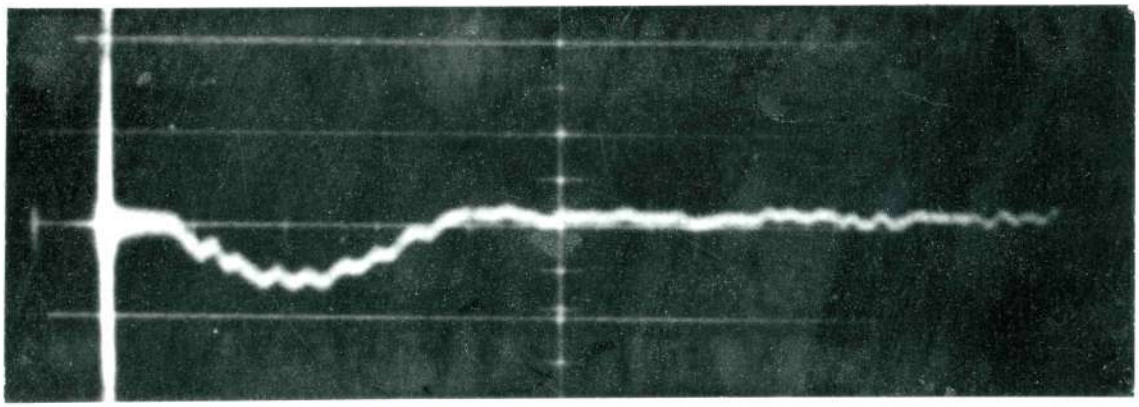

II T5 200 10

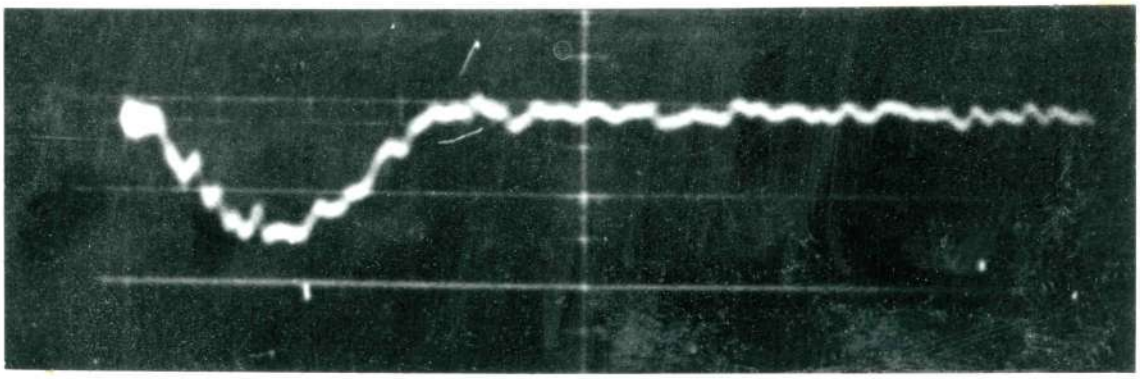

II T6 100 10

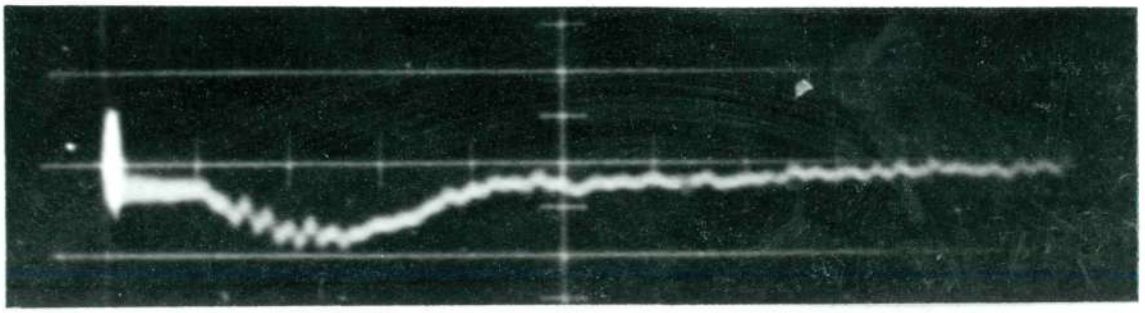

II T7 200 10

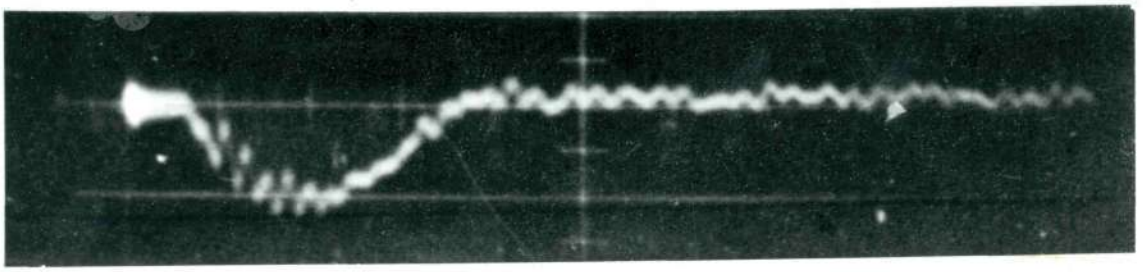

II T8 100 10

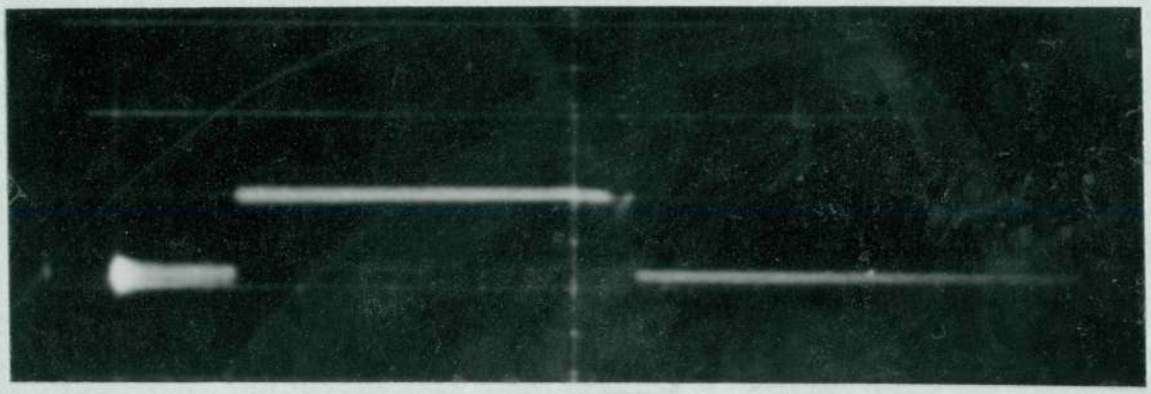

II C 7.5

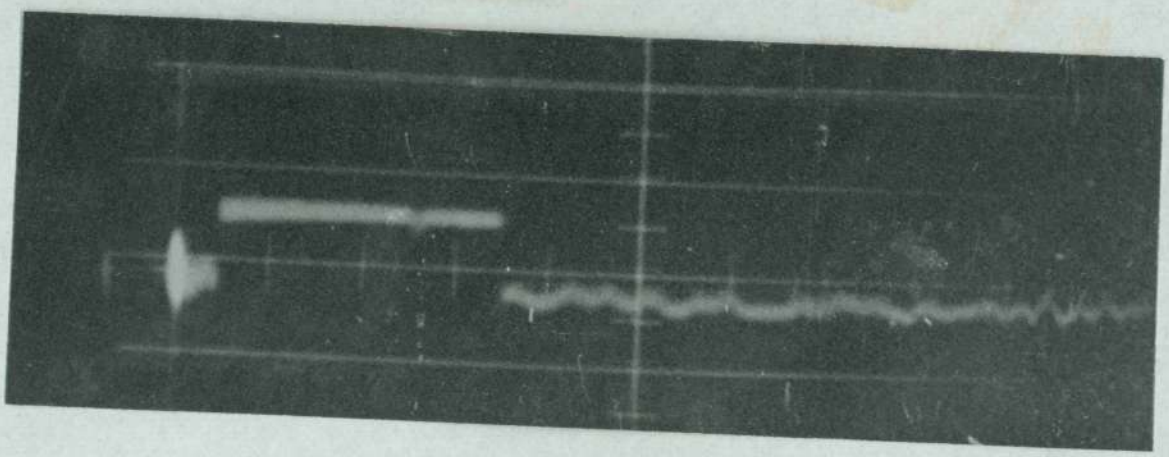

SERIES I

Load Applied: 5.0 in. from centerline away from gages

Pendulum Distance: 15.00 in.

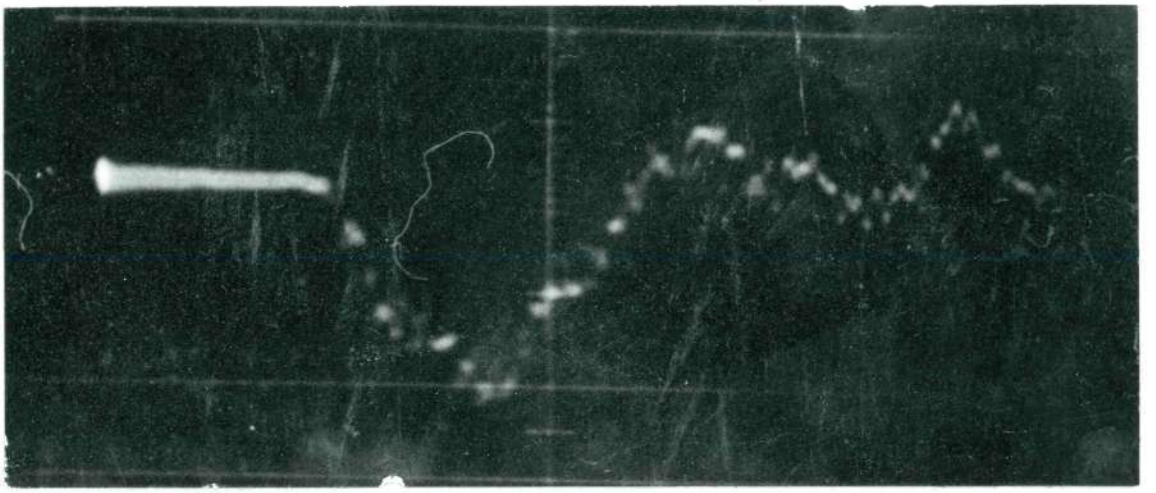

I M1 200 10

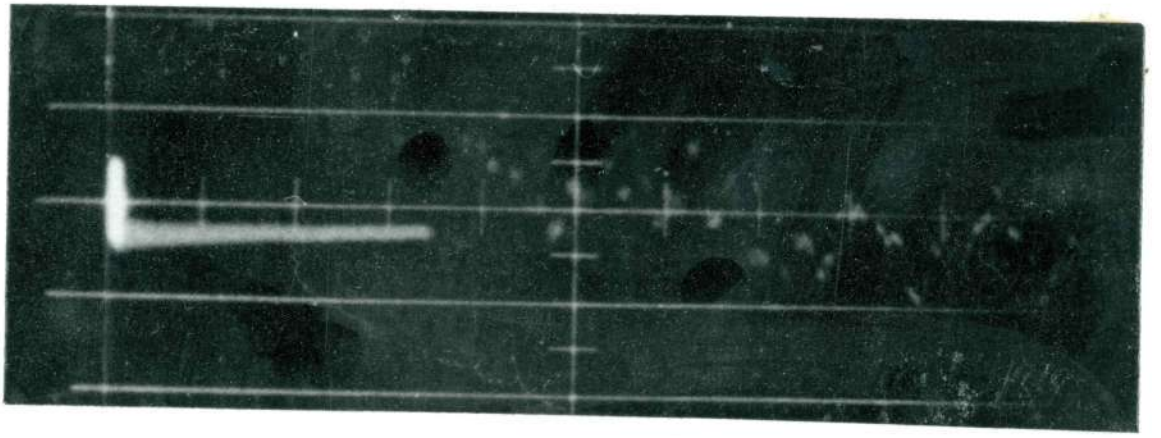

I M2 200 10

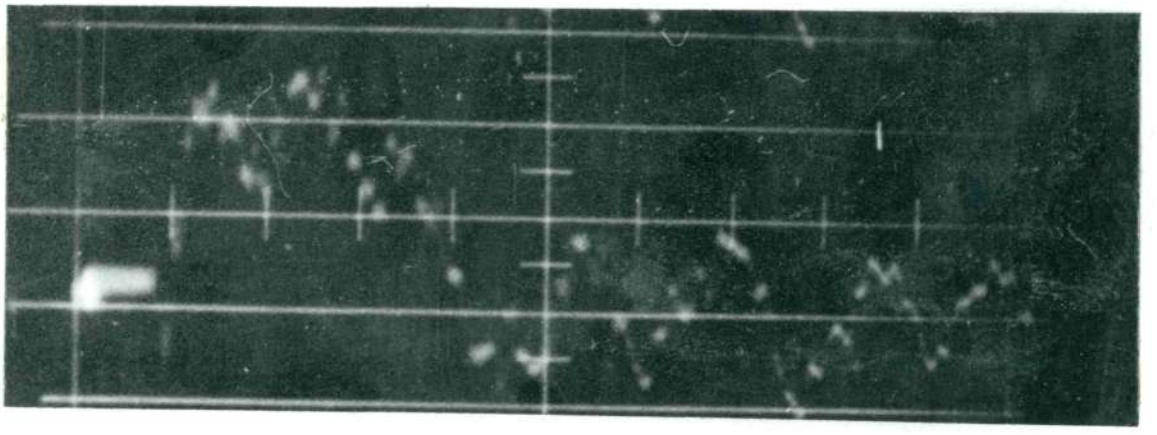

I M3 200 10

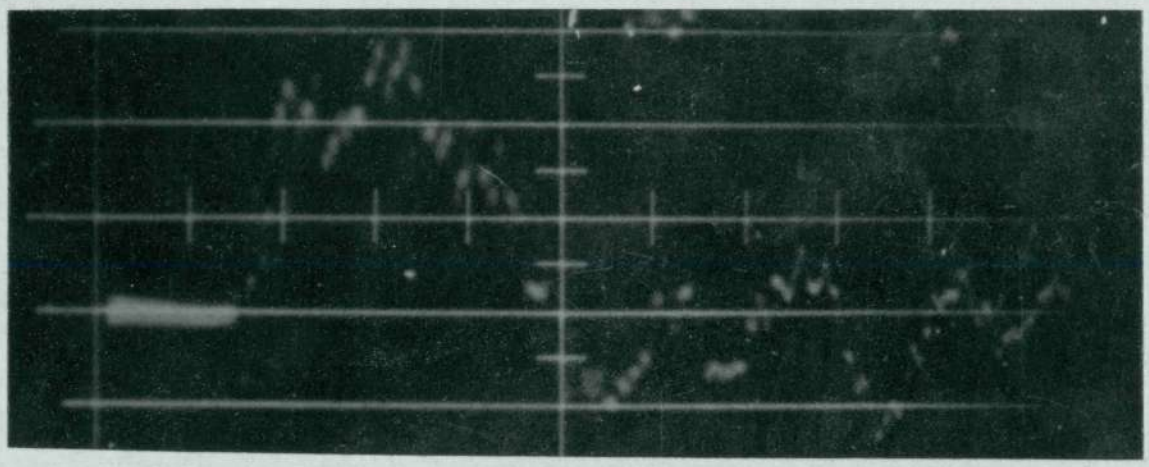

I M4 200 10

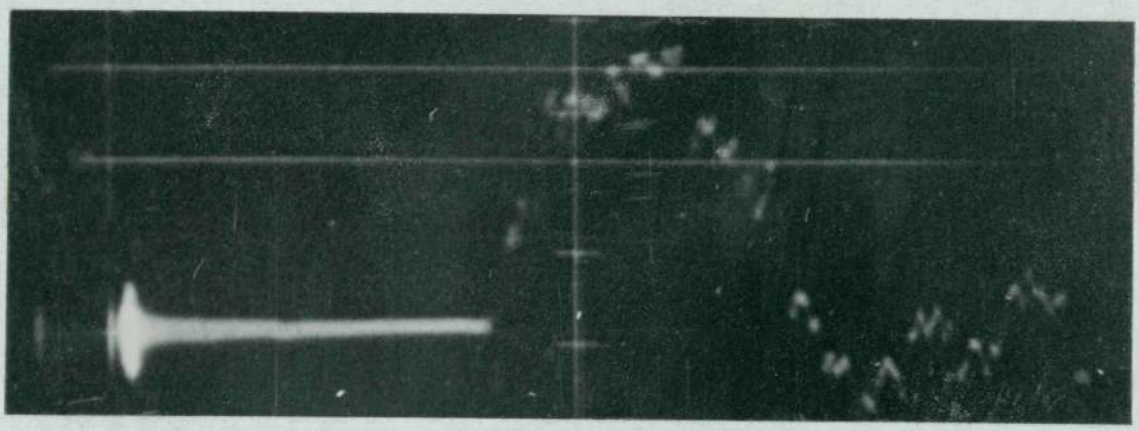

I M5 200 10

I M6 200 10

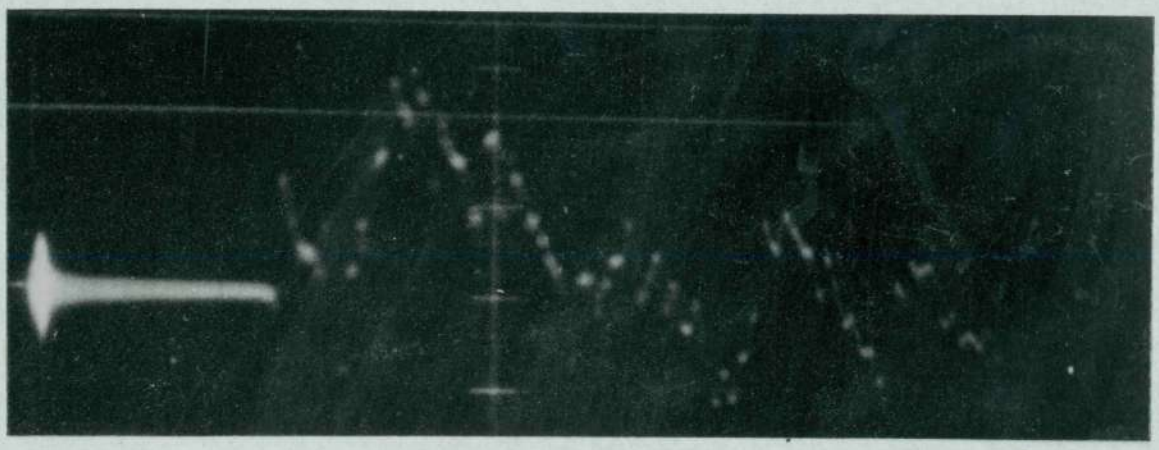

I M7 200 10

I M8 200 10

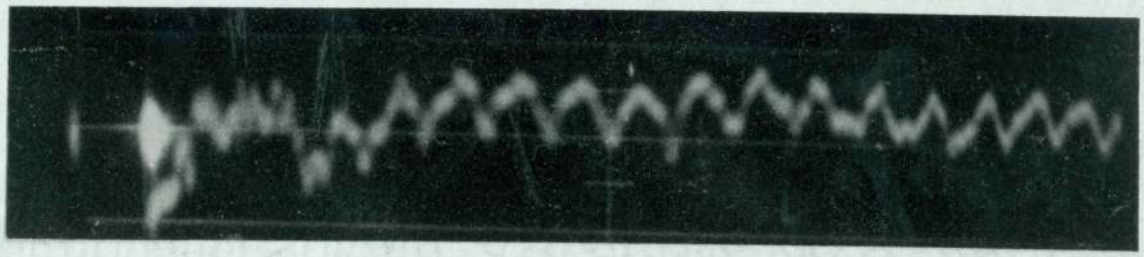

I M2 200 25

I M4 200 25

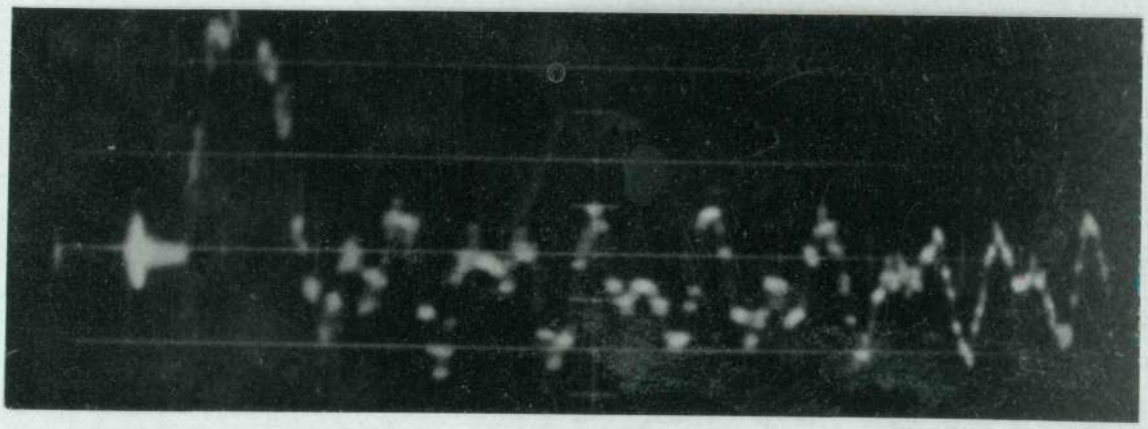

I M5 200 25

I M6 200 25

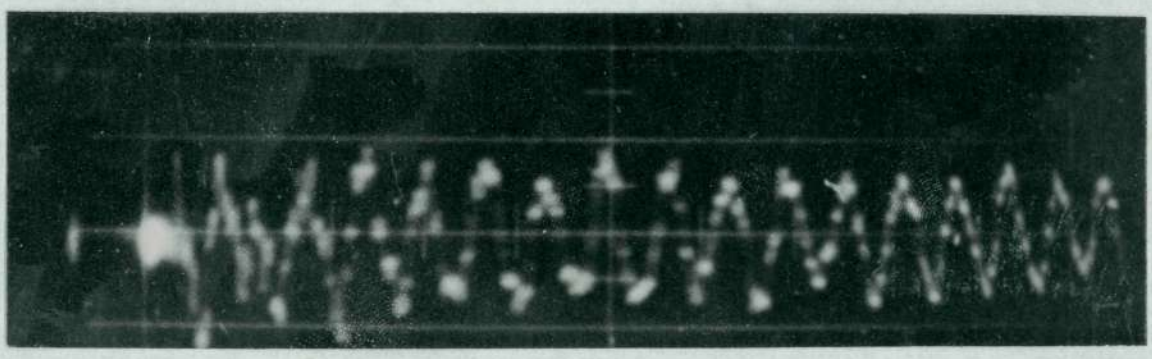

I M8 200 25

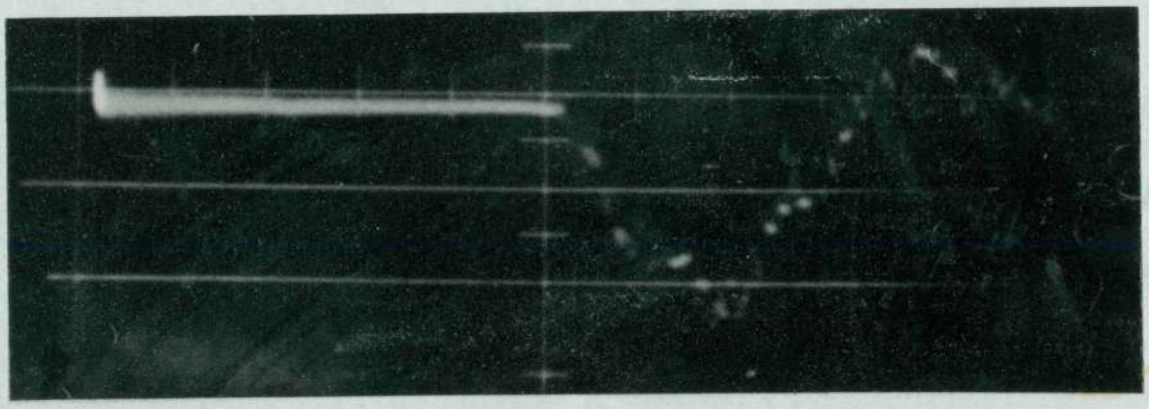

I M1 C 200 10

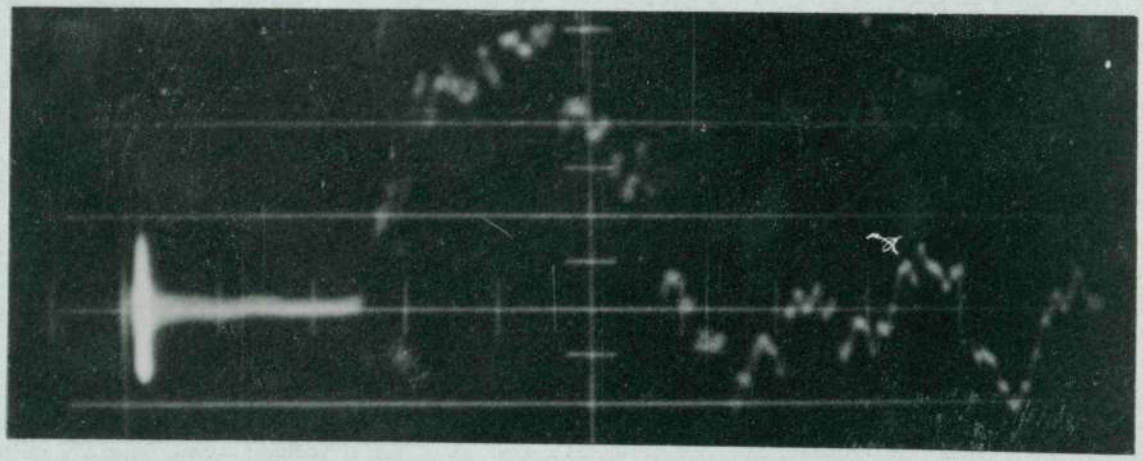

I M5 C 200 10

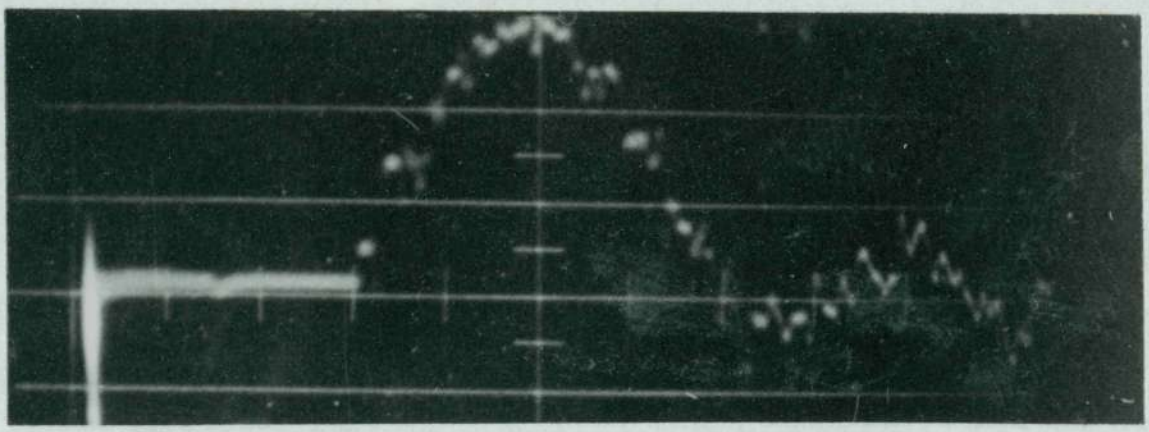

I M6 C 200 10

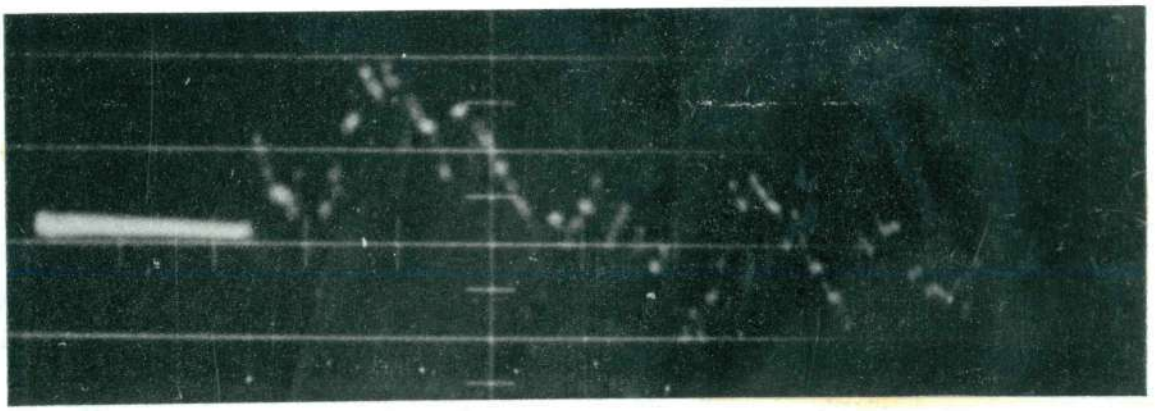

I M7 C 200 10

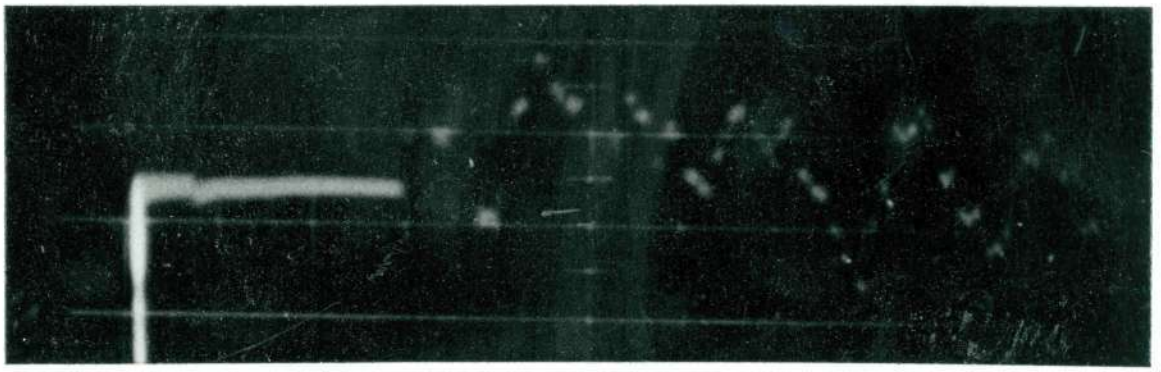

I M8 C 200 10

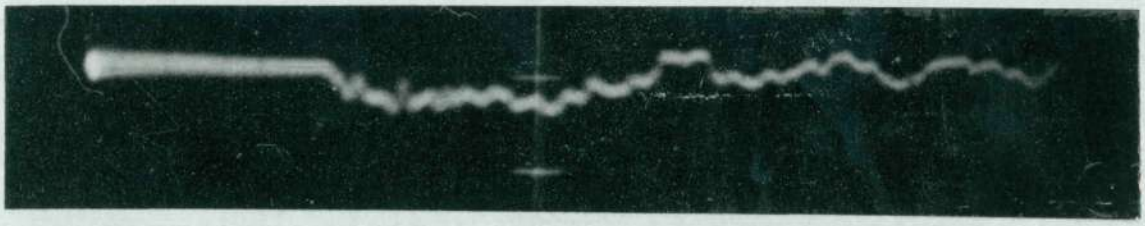

I T1 260 10

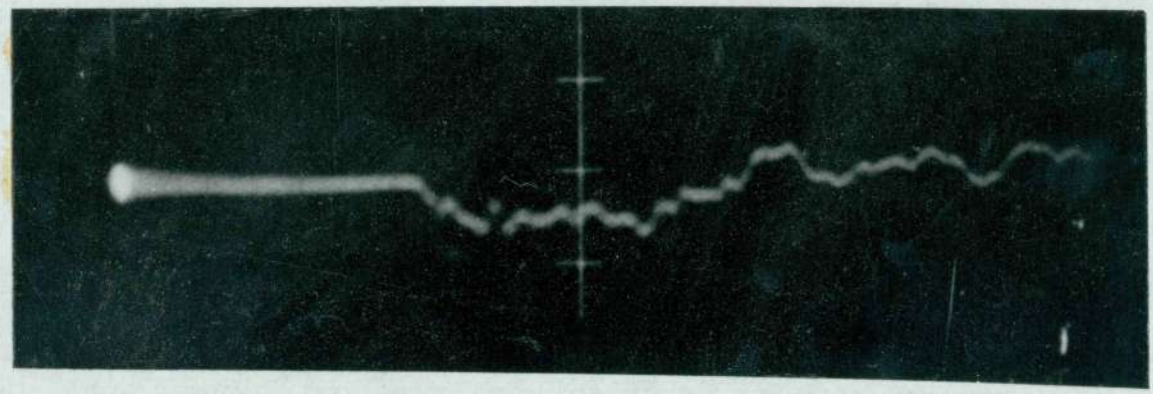

I T2 200 10

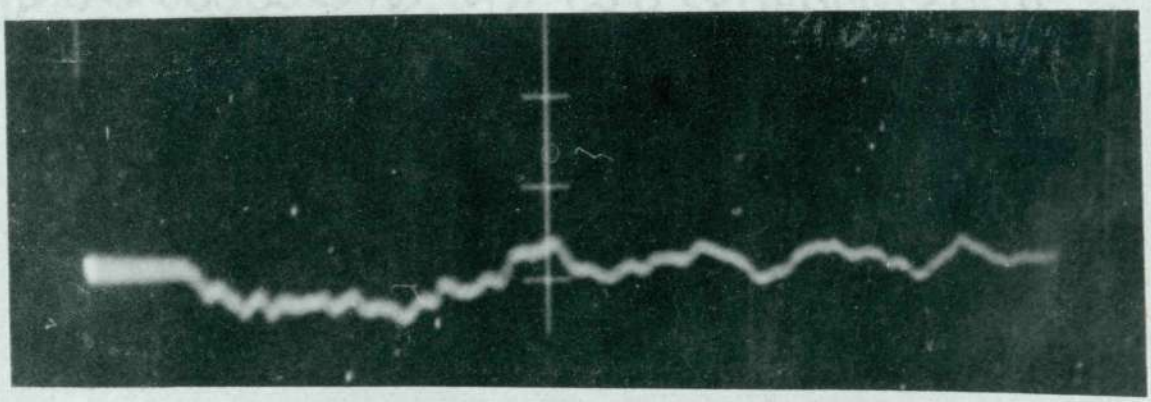

I T3 260 10

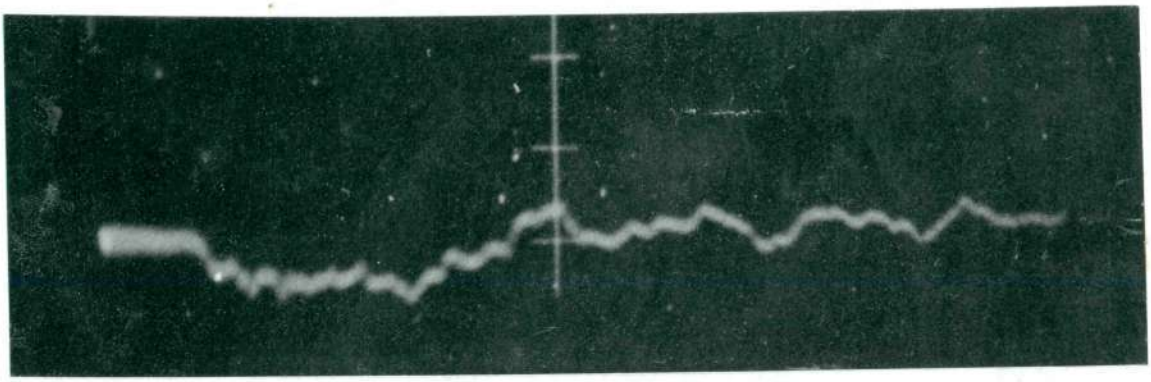

I T4 200 10

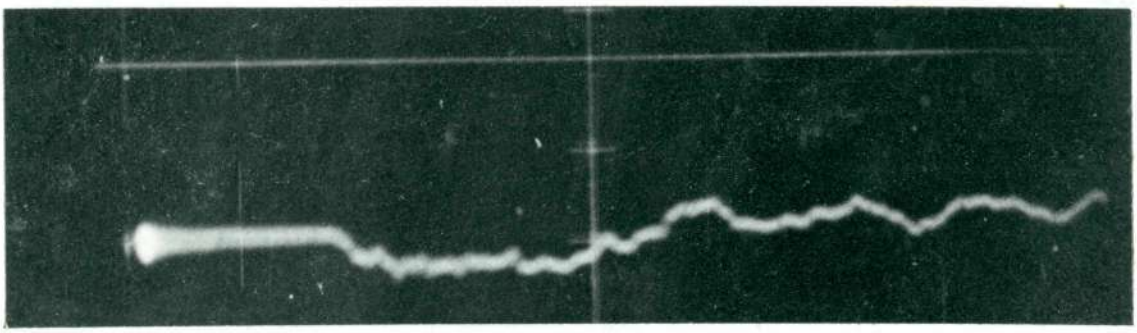

I T5 260 10

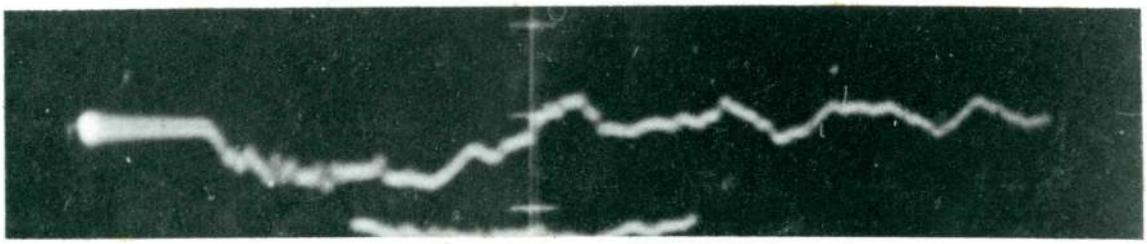

I T6 200 10

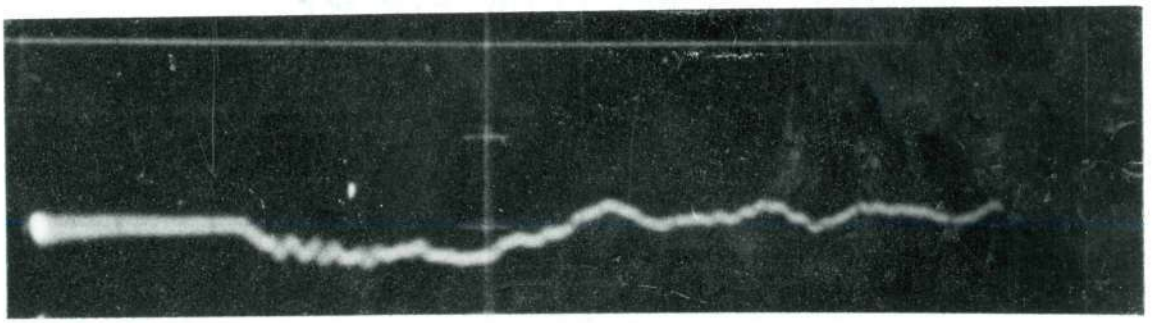

I T7 260 10

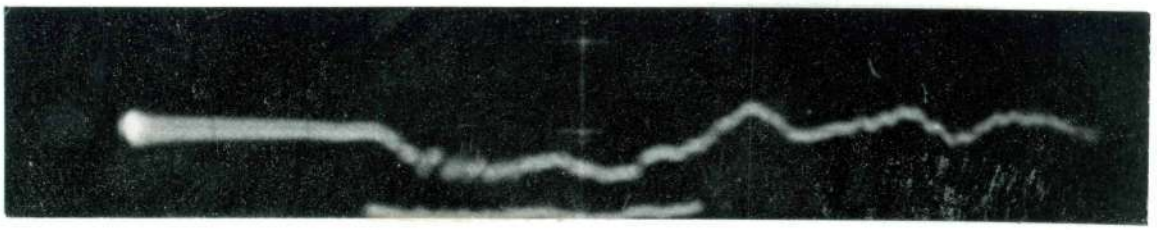

I T8 200 10

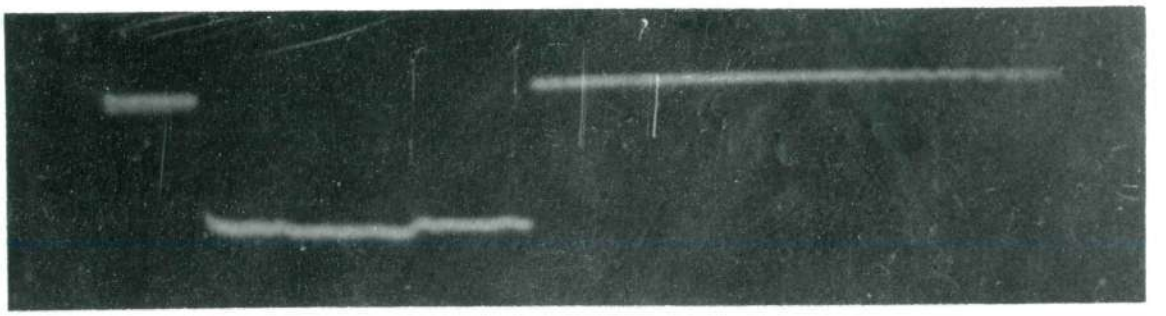

I C 10

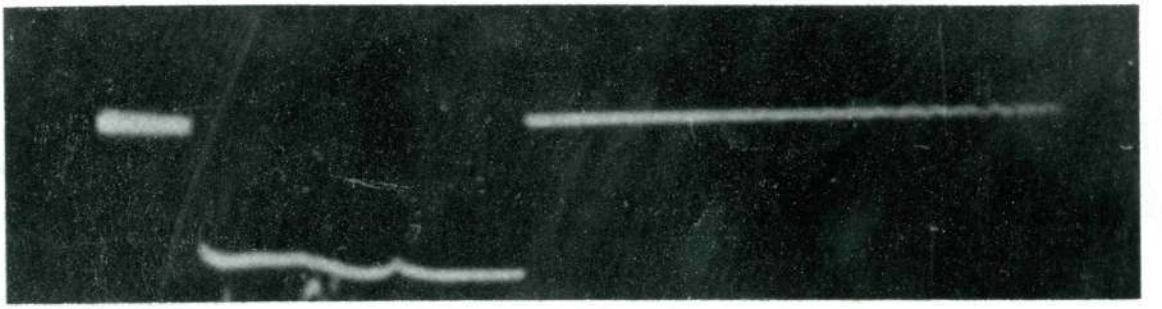

I C 10

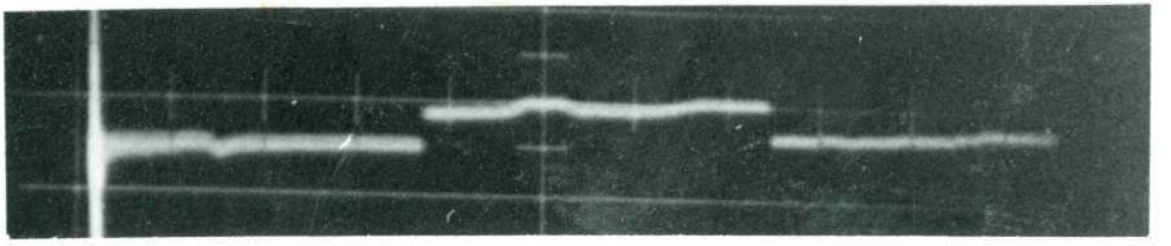

I C 10

SERIES III

Load Applied: 5.0 in. from centerline toward gages

Pendulum Distance: 15.00 in.

III M1 300 10

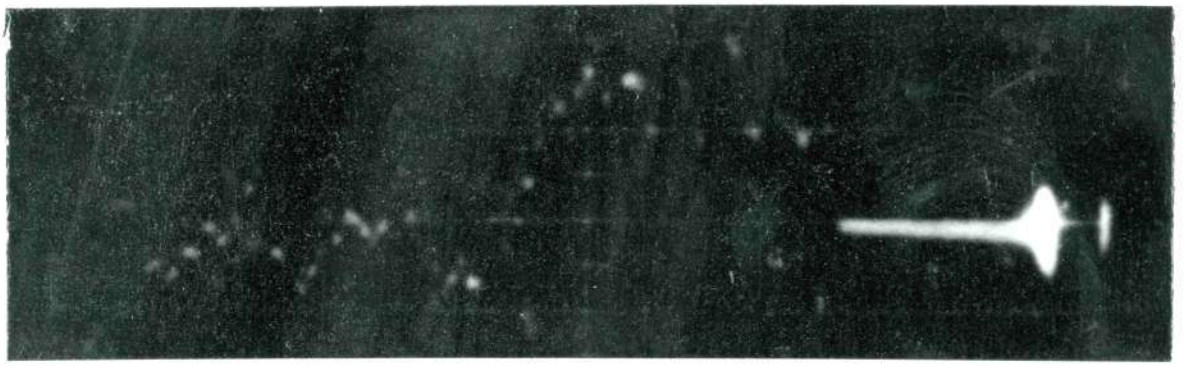

III M2 200 10

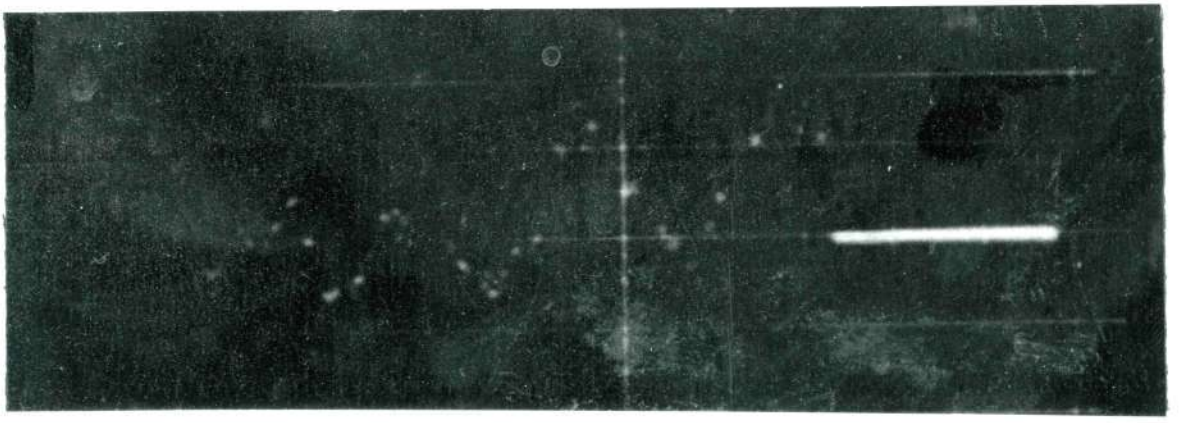

III M3 200 10

III M4 200 10

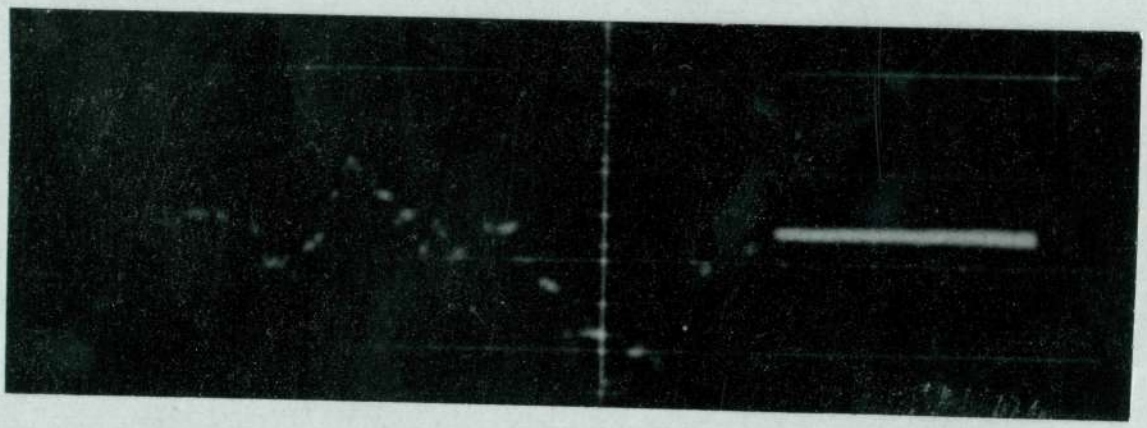

III M5 250 10

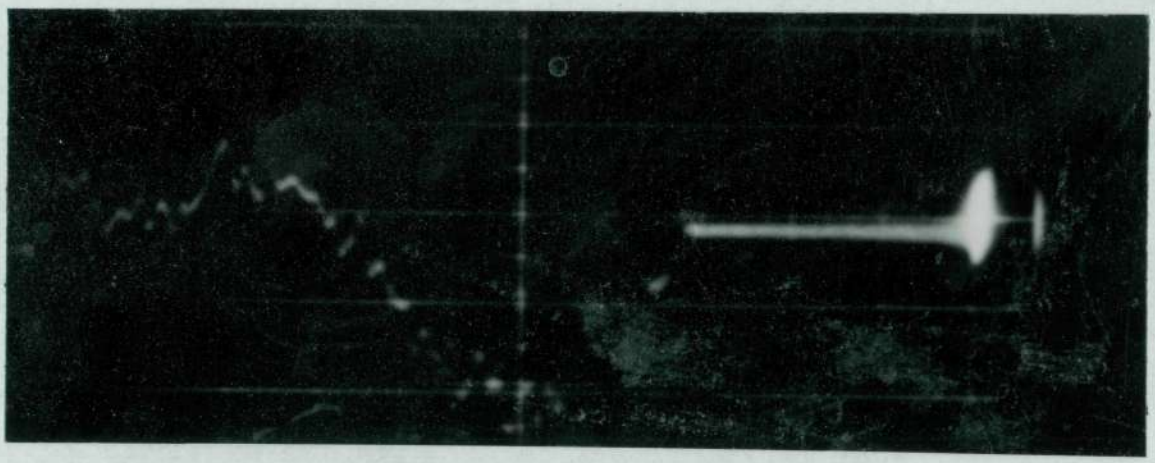

III M6 300 10

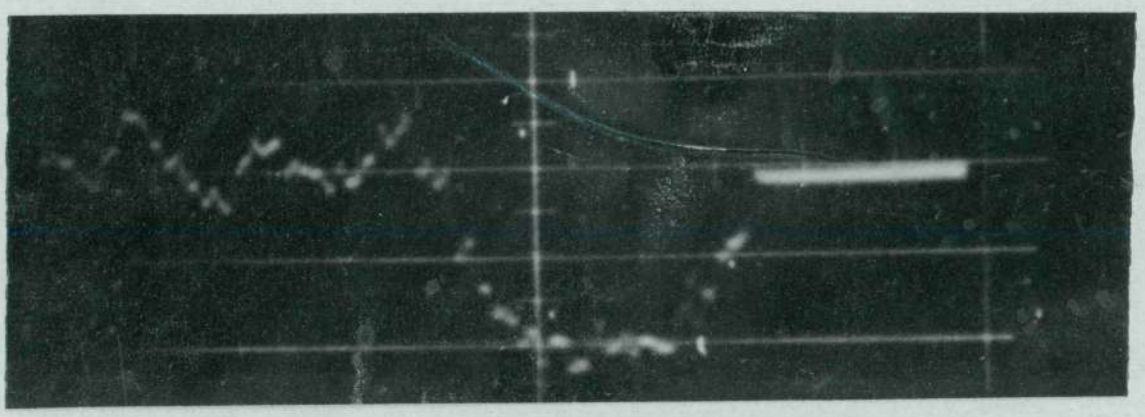

III M7 300 10

III M8 200 10

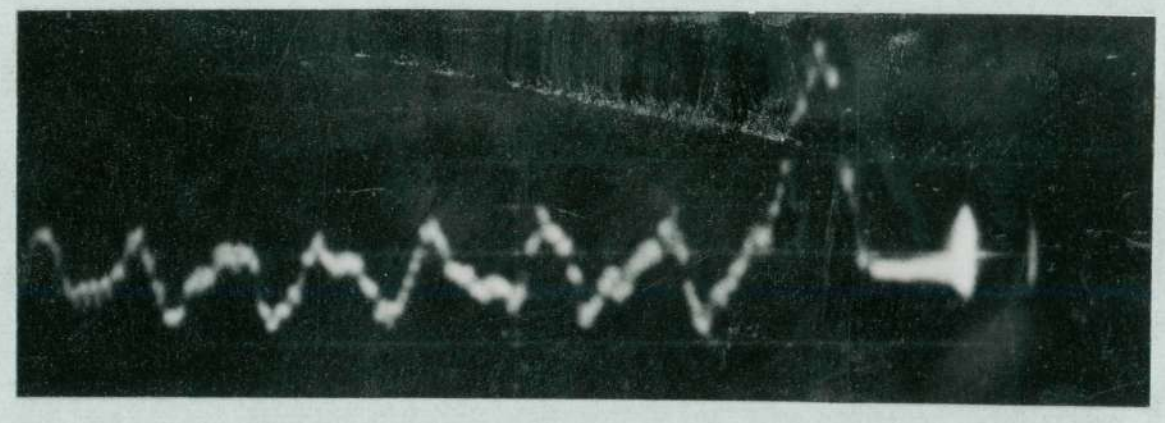

III M1 200 25

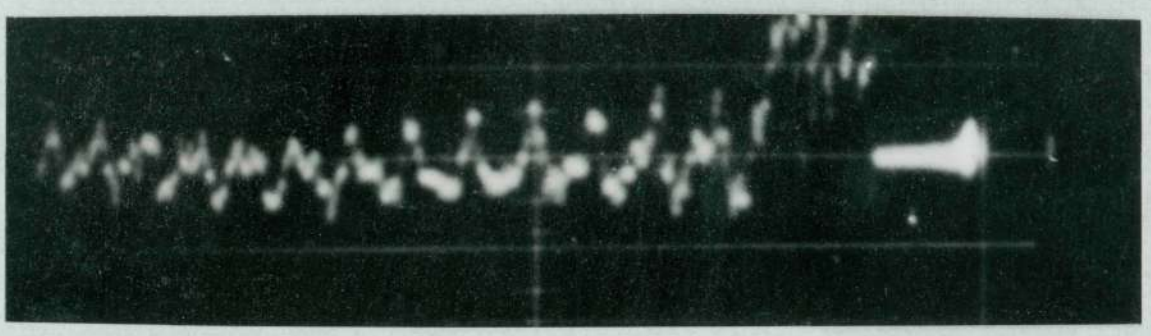

III M2 200 25

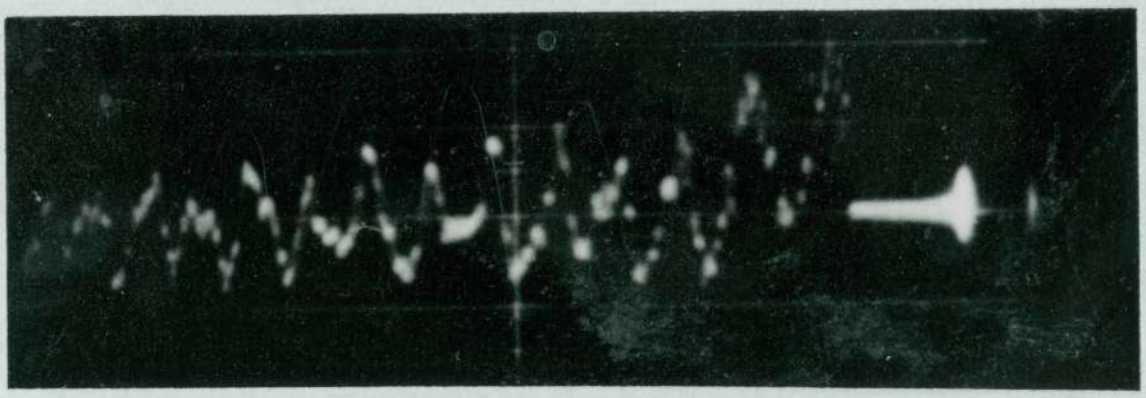

III M3 200 25

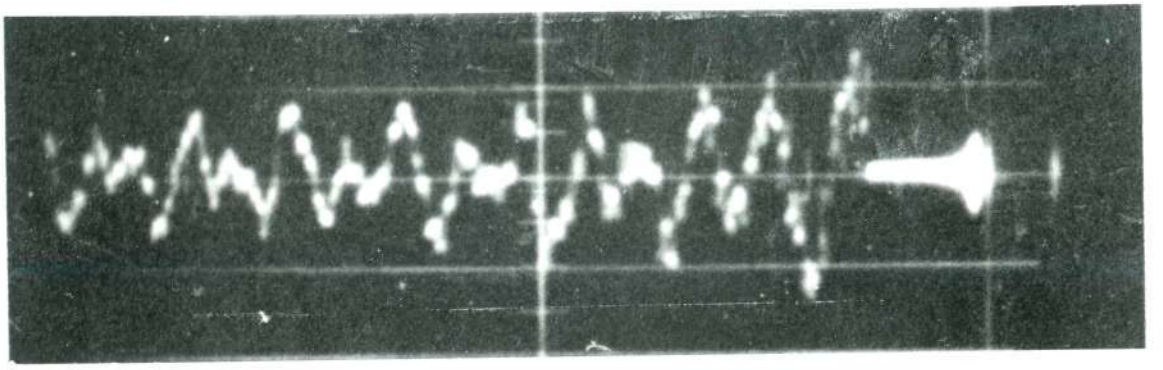

III M4 200 25

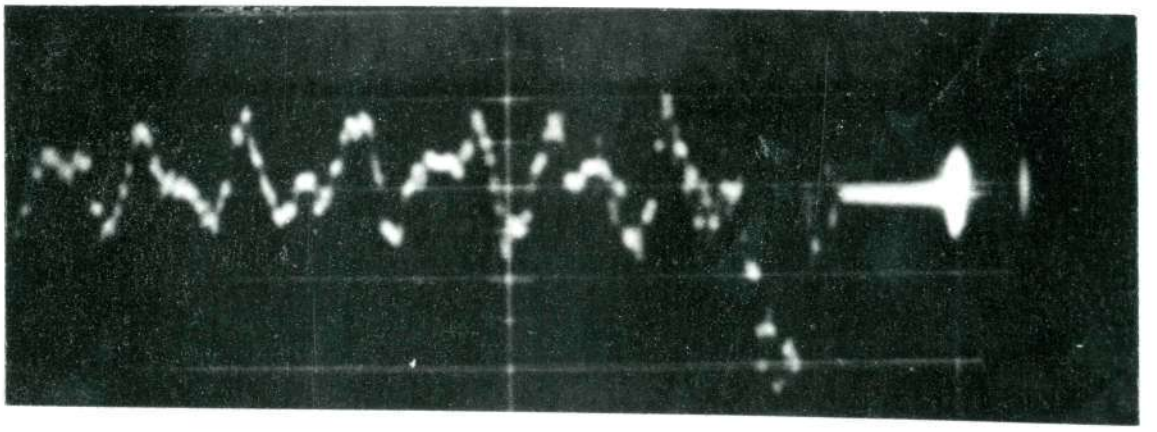

III M5 200 25

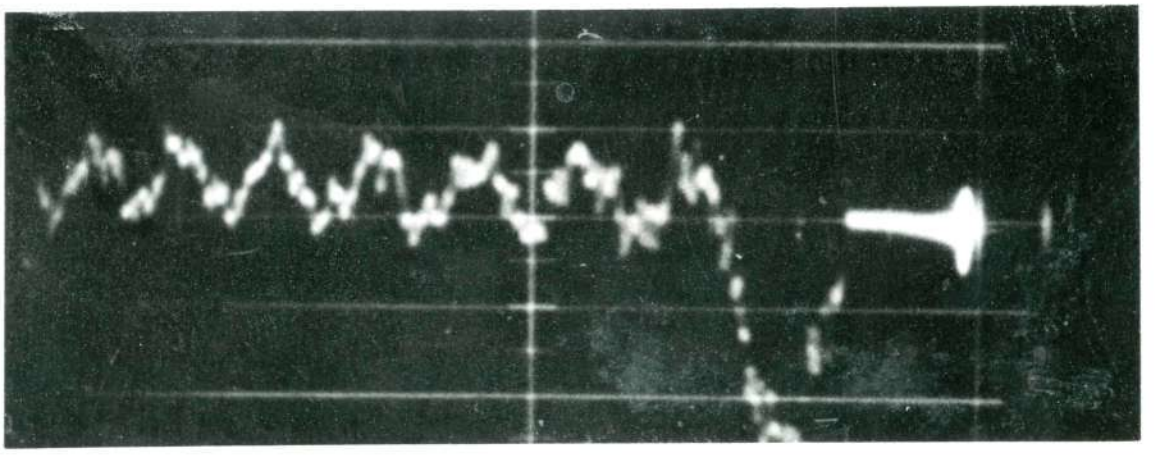

III M6 200 25

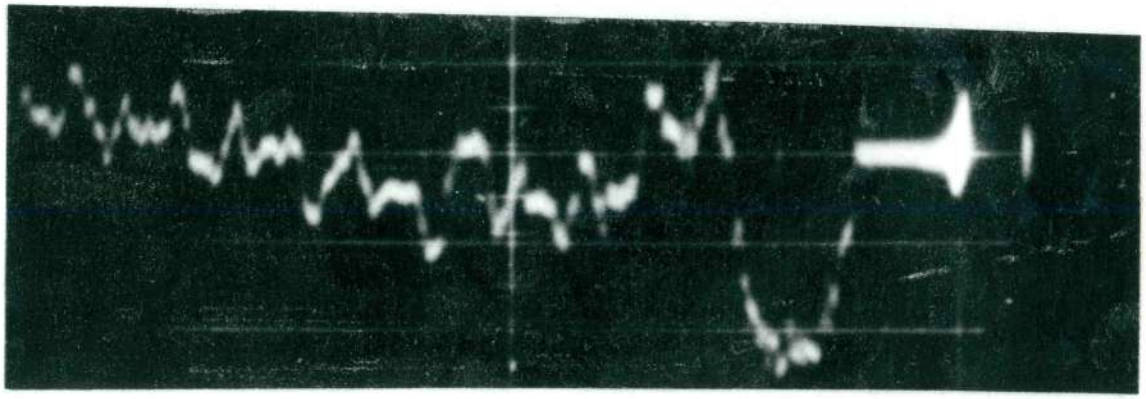

III M7 200 25

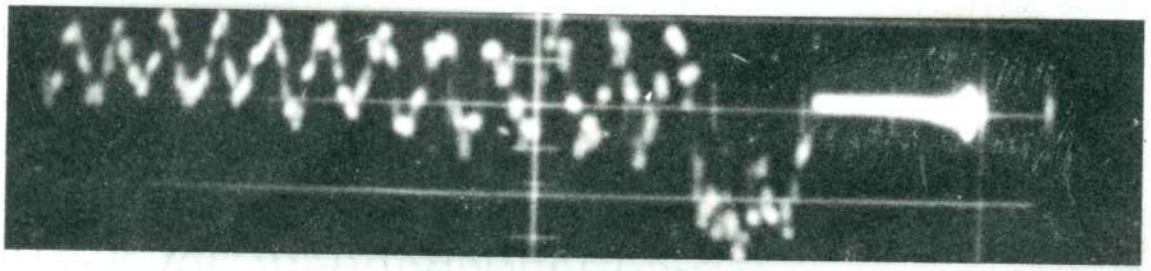

III M8 200 25

III M1 C 300 9

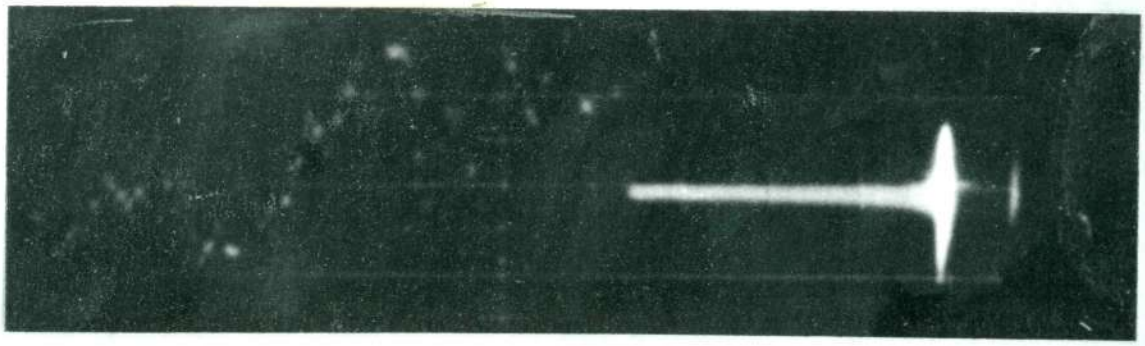

III M2 C 200 9

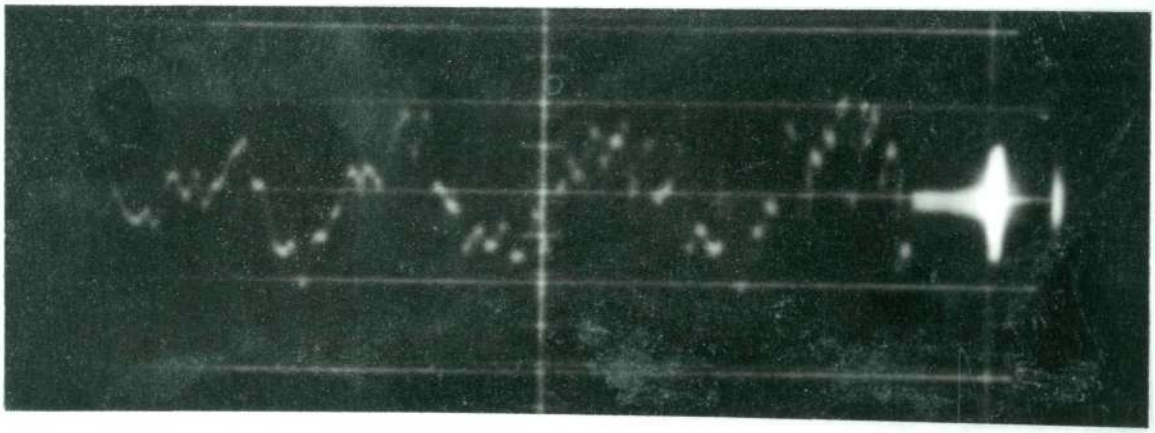

III M3 C 200 9

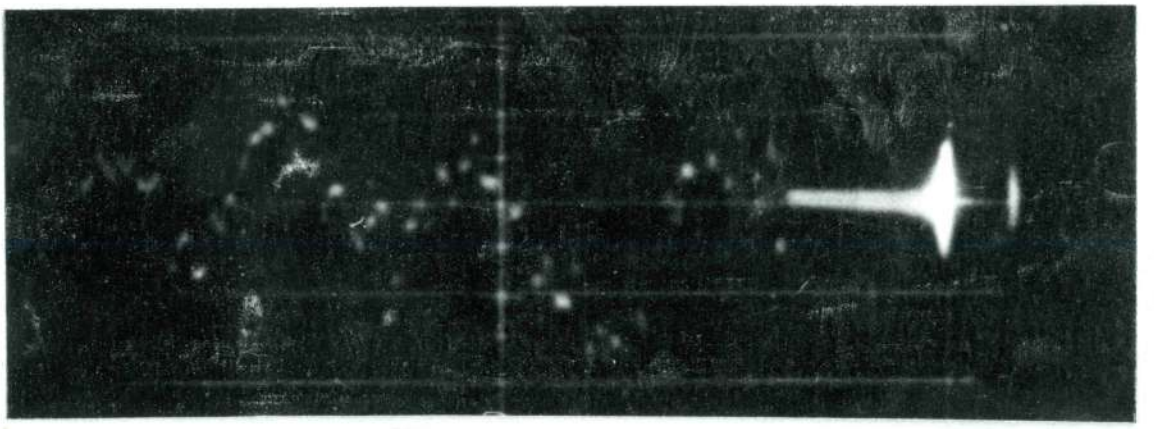

III M4 C 200 9

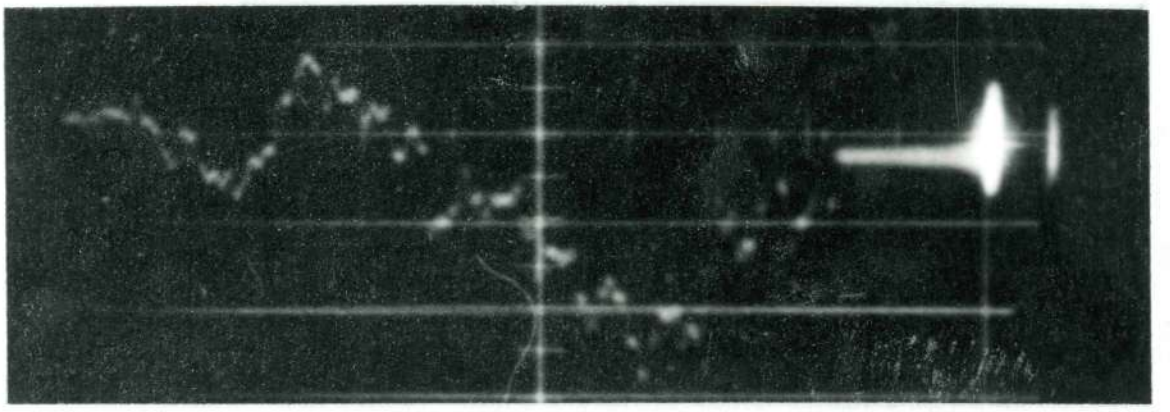

III M5 C 200 9

III M6 C 300 9

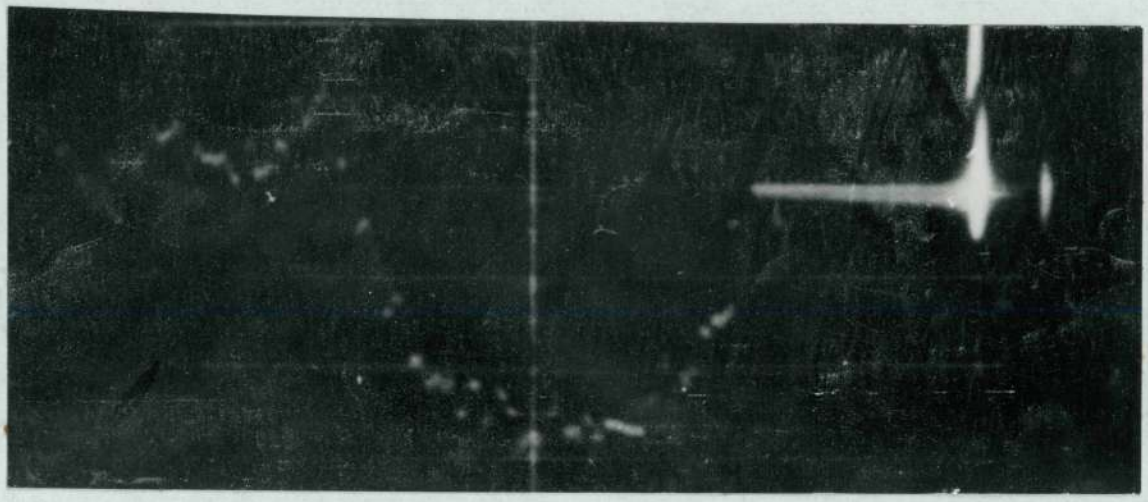

III M7 C 300 10

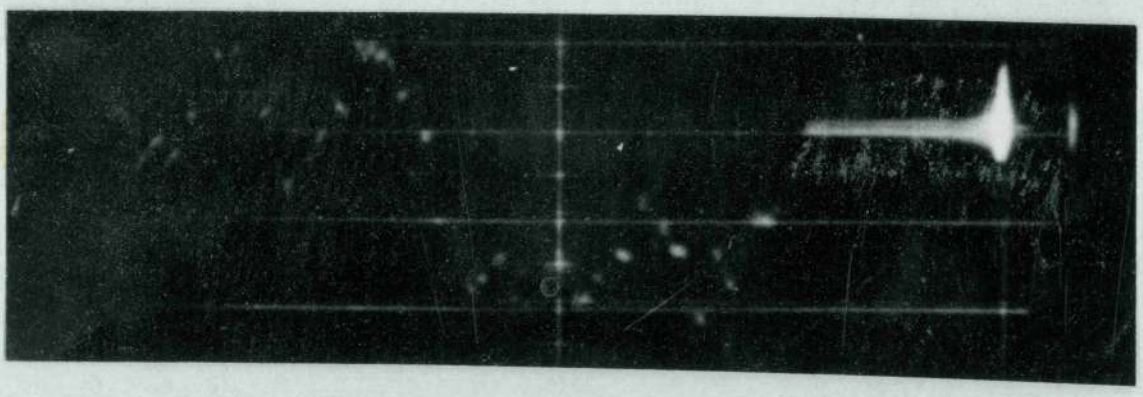

III M8 C 200 9

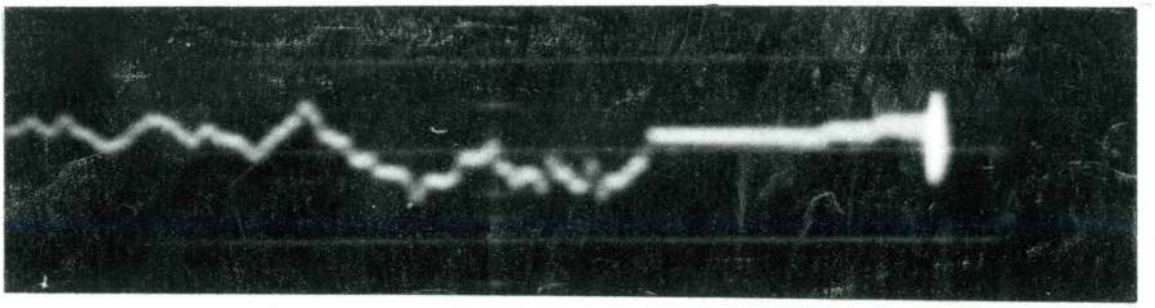

III T1 200 10

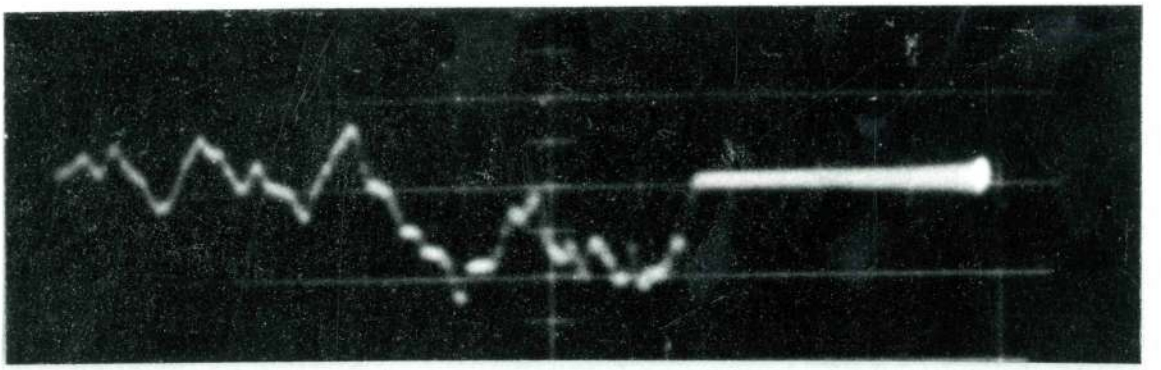

III T2 100 10

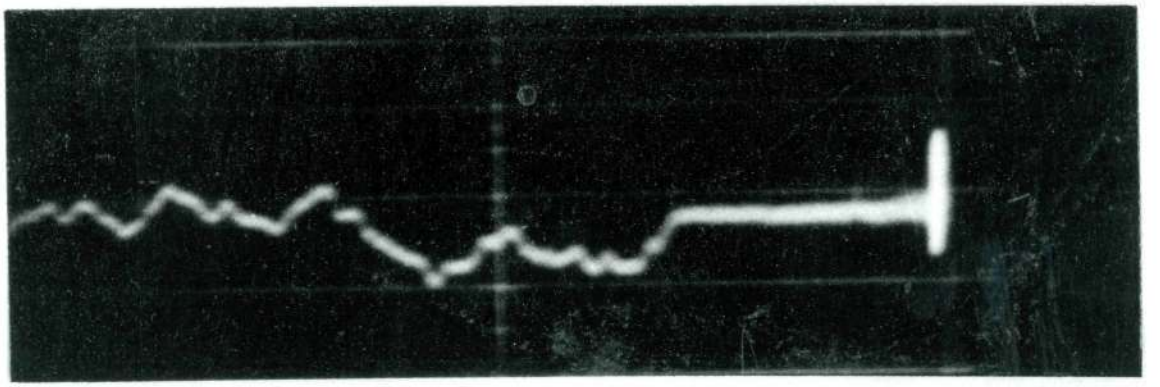

III T3 200 10

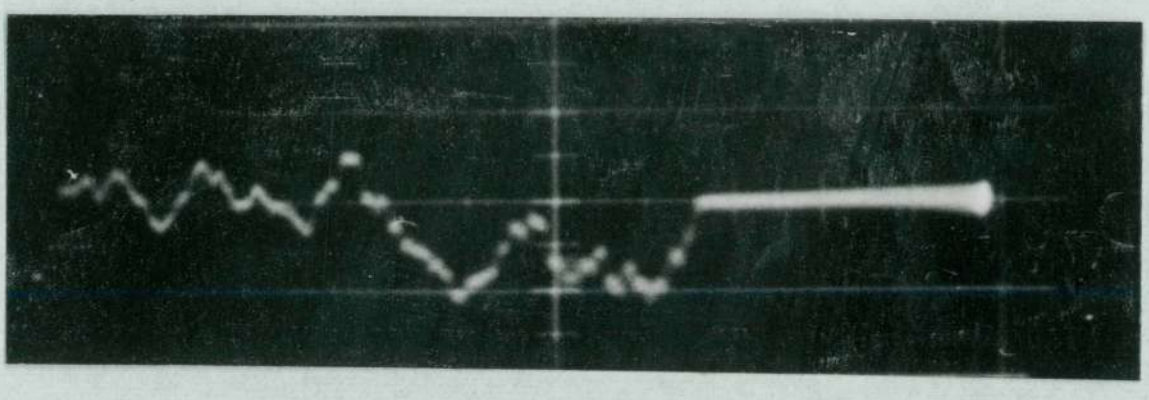

III T4 100 10

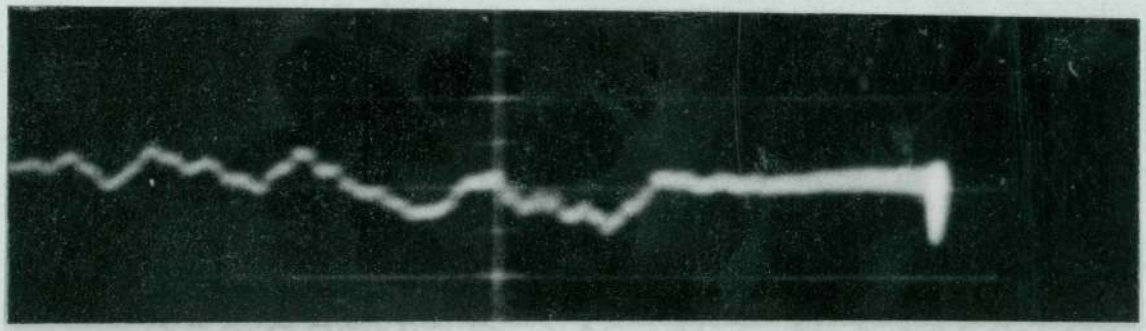

III T5 200 10

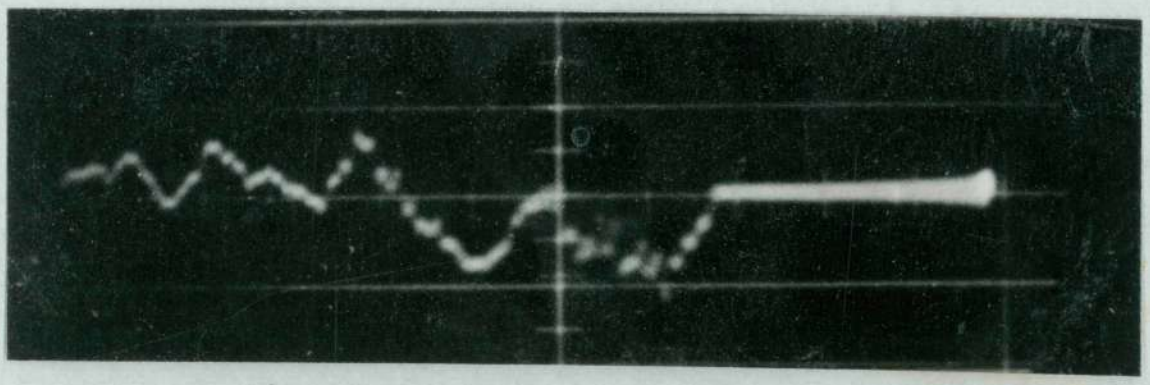

III T6 100 10

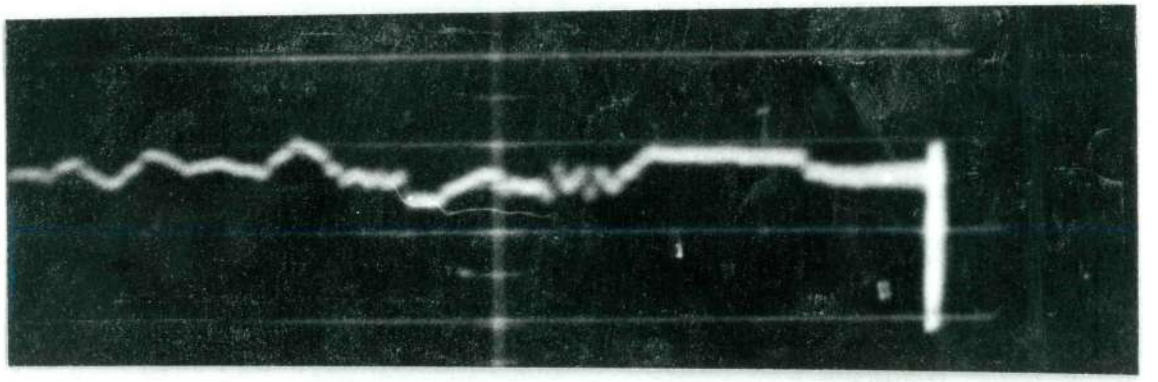

III T7 200 10

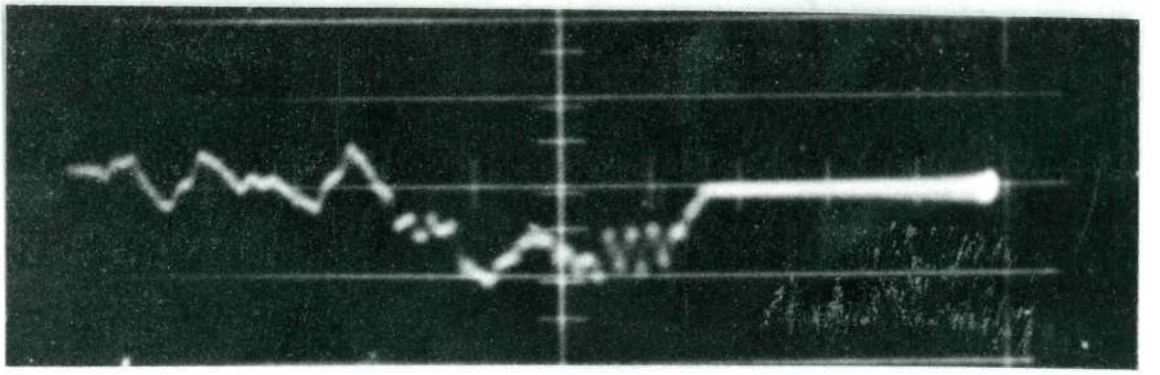

III T8 100 10

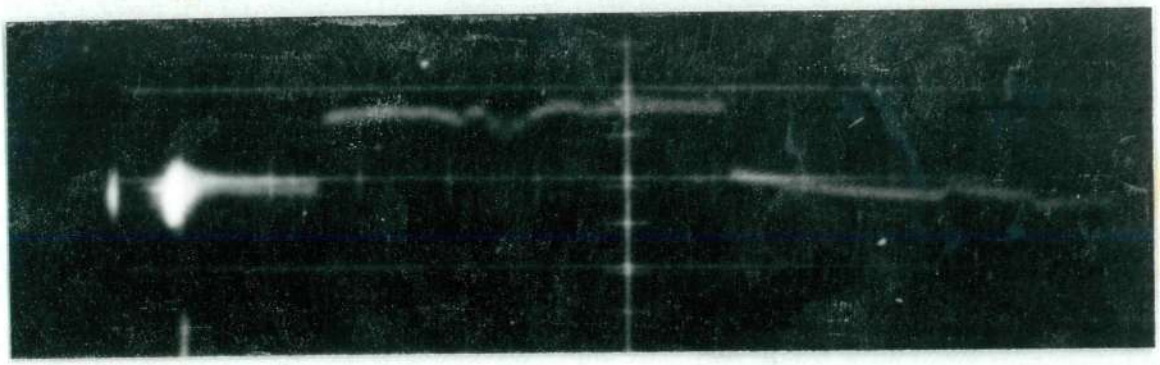

III C 9

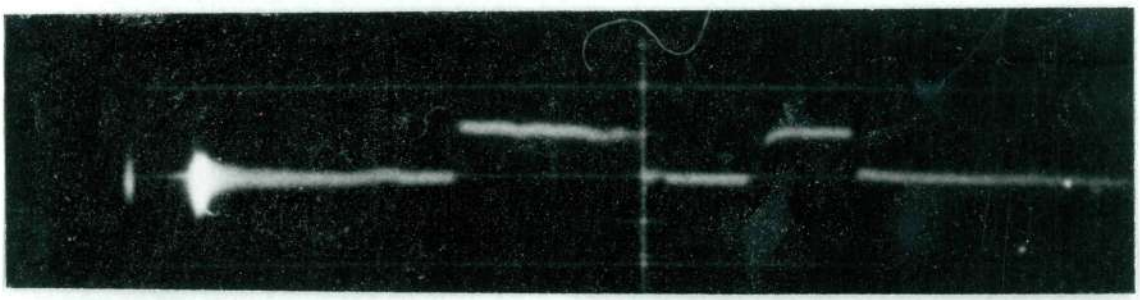

III C 9

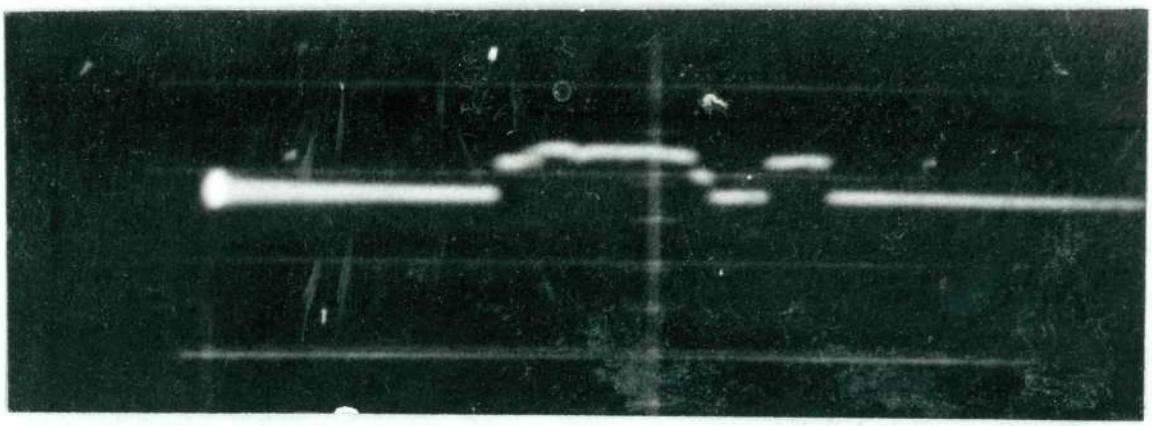

III C 10

BIBLIOGRAPHY

Literature Cited

1. Timoshenko, S., Vibration Problems in Engineering, 2nd ed., New York, D. Van Nostrand Company, Inc., 1937, p. 393.

2. Salvadori, M. G., "A Mathematical Treatment of the Generalized Hertz Impact of a Mass on a Simply Supported Beam", reprint from Welding Research Supplement, Welding Research Council, New York, July, 1953.

3. Zener, C. and Feshbach, H., "A Method of Calculating Energy Losses During Impact", Journal of Applied Mechanics, Vol. 62, p. A-129, 1940.

4. Timoshenko, op. cit., p. 394 ff.

5. Lamb, H., "On the Flexure and Vibrations of a Curved Bar", London Mathematical Society Proceedings, Vol. 19, p. 365, 1888.

6. Den Hartog, J. P., "The Lowest Natural Frequencies of Circular Arcs", Philosophical Magazine, Vol. 5, p. 400 ff, 1928.

7. Den Hartog, J. P., "Vibrations of Frames of Electrical Machines", Transactions American Society of Mechanical Engineers, Vol. 49-50, pp. APM-50-60 and APM-50-11, 1927 and 1928.

8. Timoshenko, op. cit., p. 408.

Other References

9. Hetenyi, M., Handbook of Experimental Stress Analysis, New York, John Wiley and Sons, Inc., 1950.

10. Den Hartog, J. P., Mechanical Vibrations, New York, McGraw-Hill Book Company, Inc., 1947.

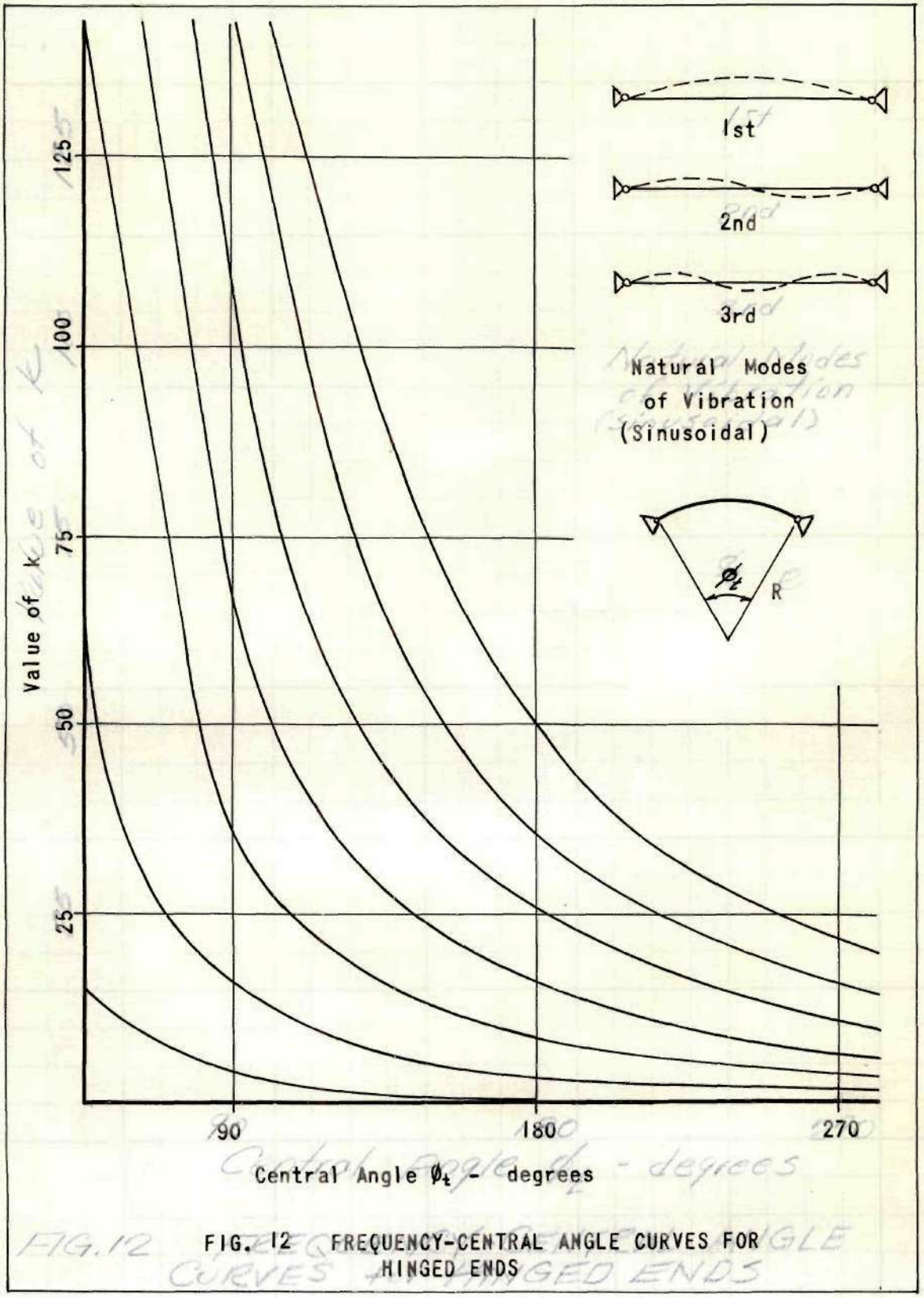

FIG. 12 FREQUENCY-CENTRAL ANGLE CURVES FOR HINGED ENDS

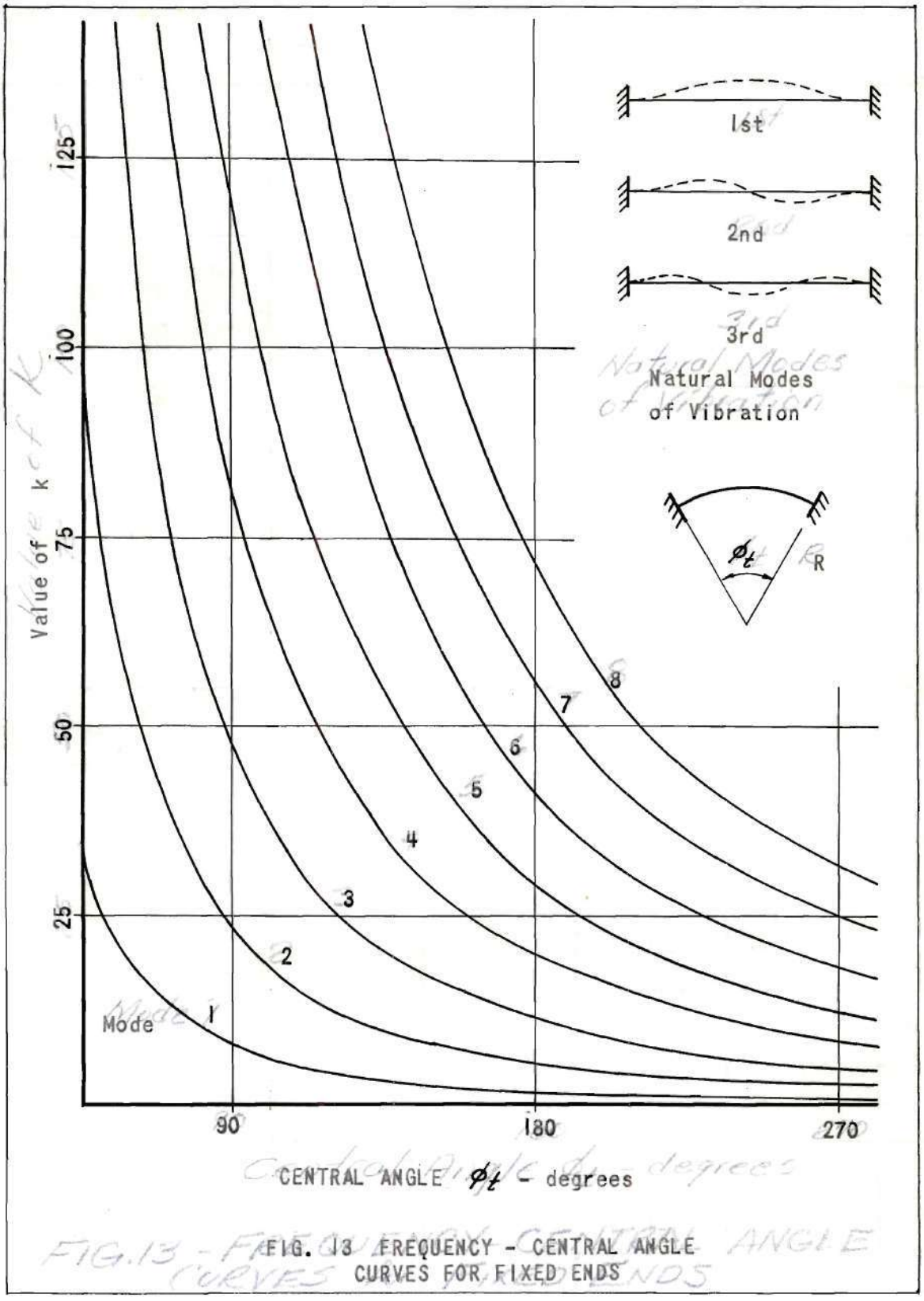

FIG. 13 FREQUENCY - CENTRAL ANGLE CURVES FOR FIXED ENDS

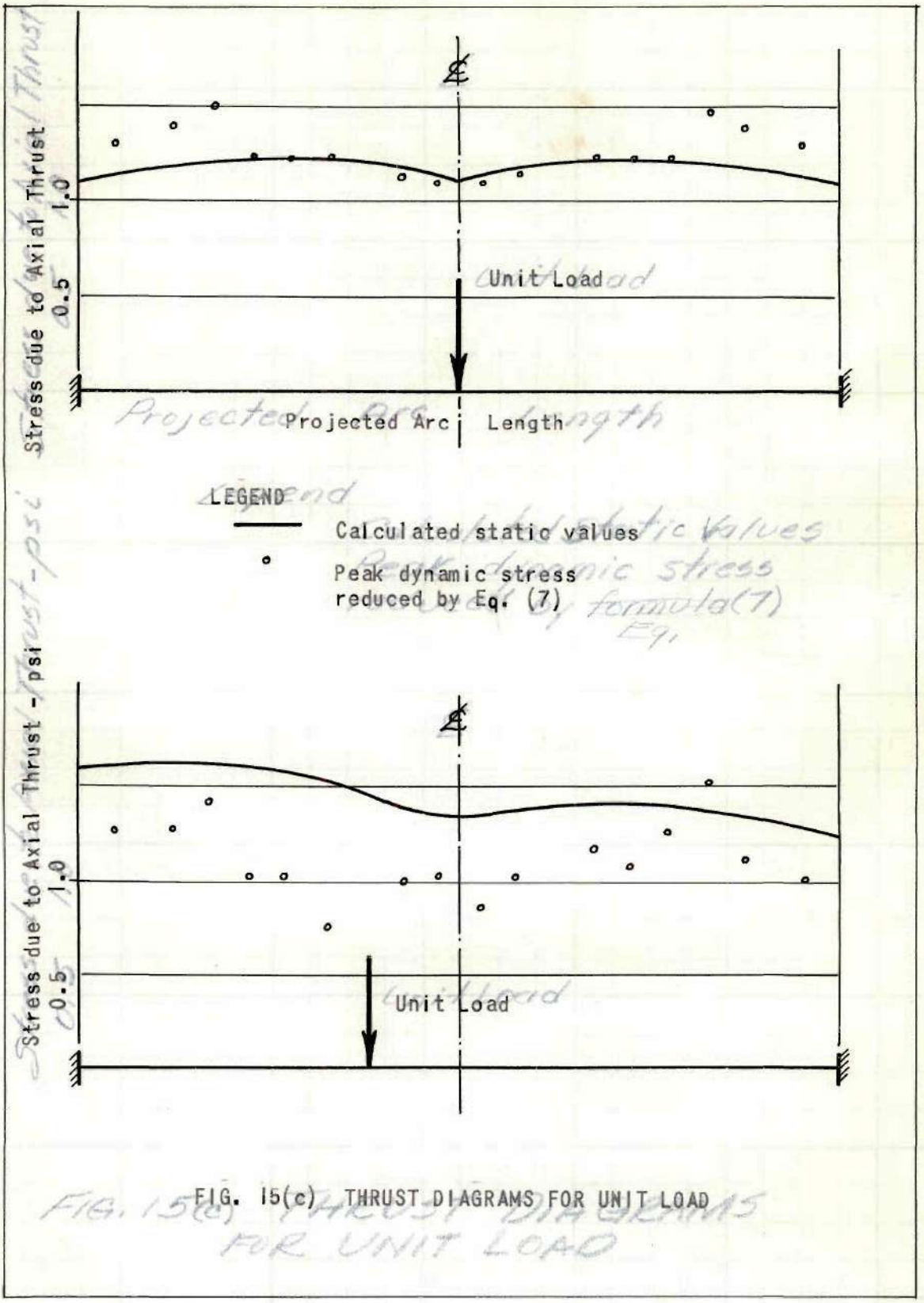

FIG. 15(c) THRUST DIAGRAMS FOR UNIT LOAD

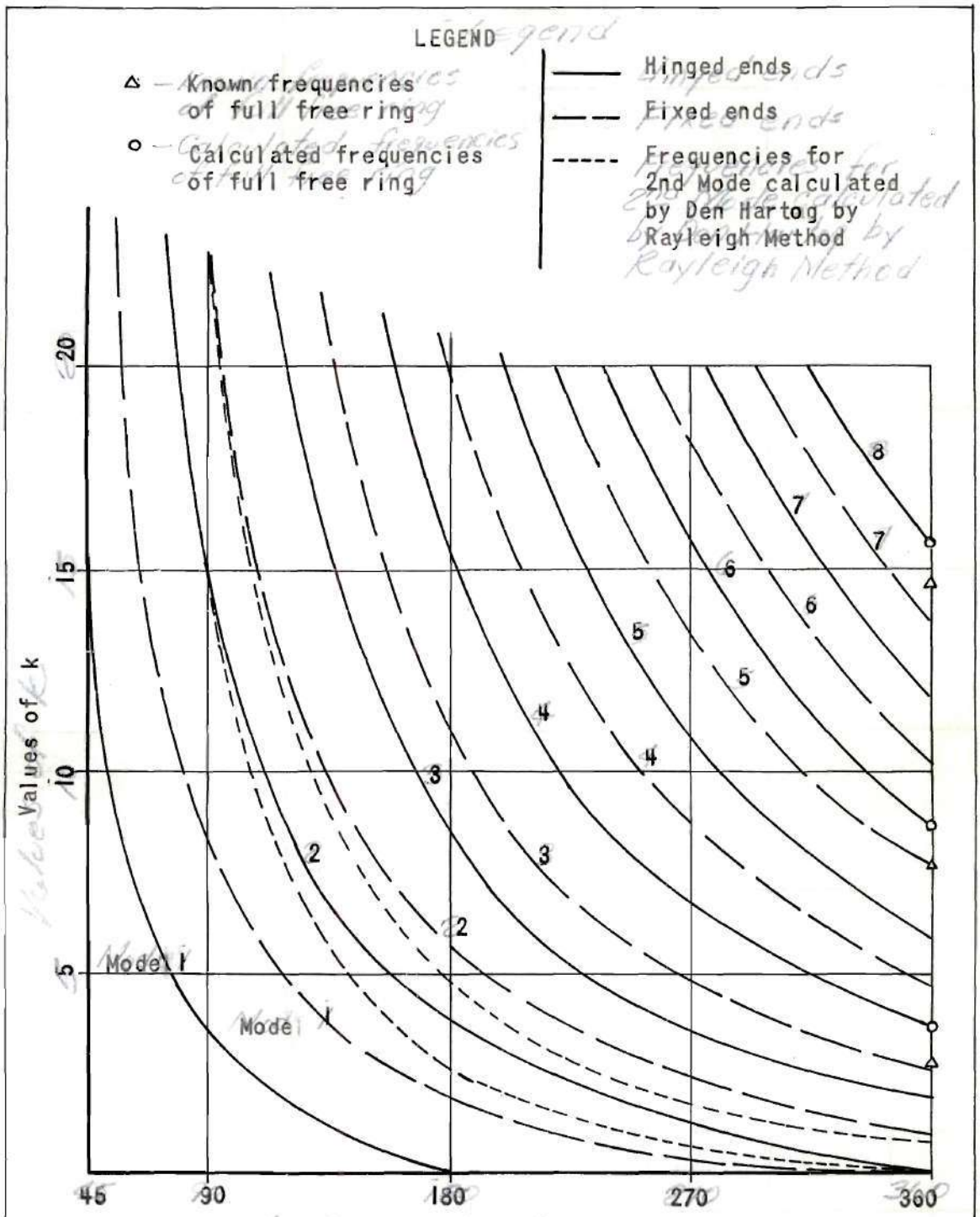

FIG. 14 FREQUENCY - CENTRAL ANGLE CURVES FOR HINGED ENDS AND FIXED ENDS

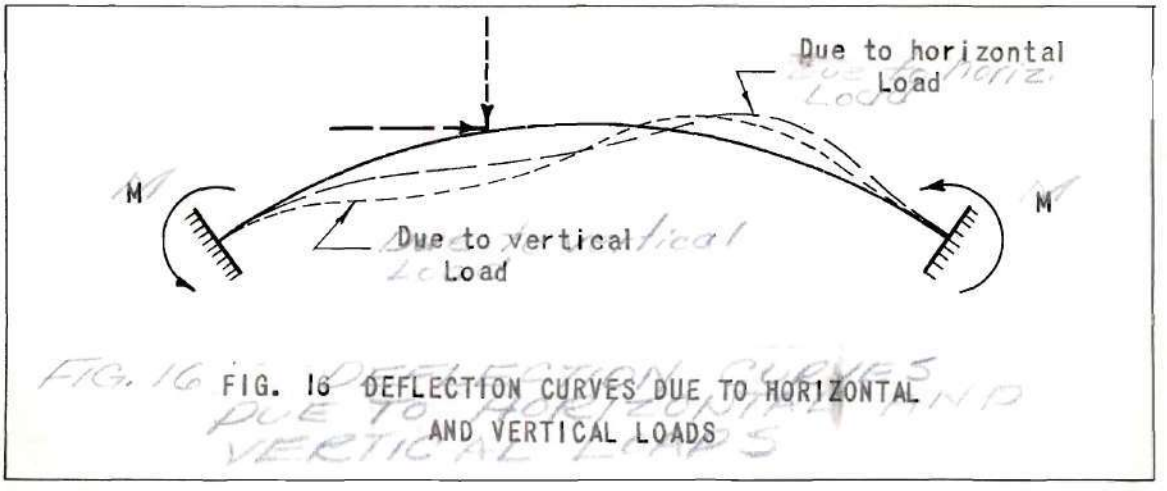

FIG. 16 DEFLECTION CURVES DUE TO HORIZONTAL AND VERTICAL LOADS

Trim off all pencil lines

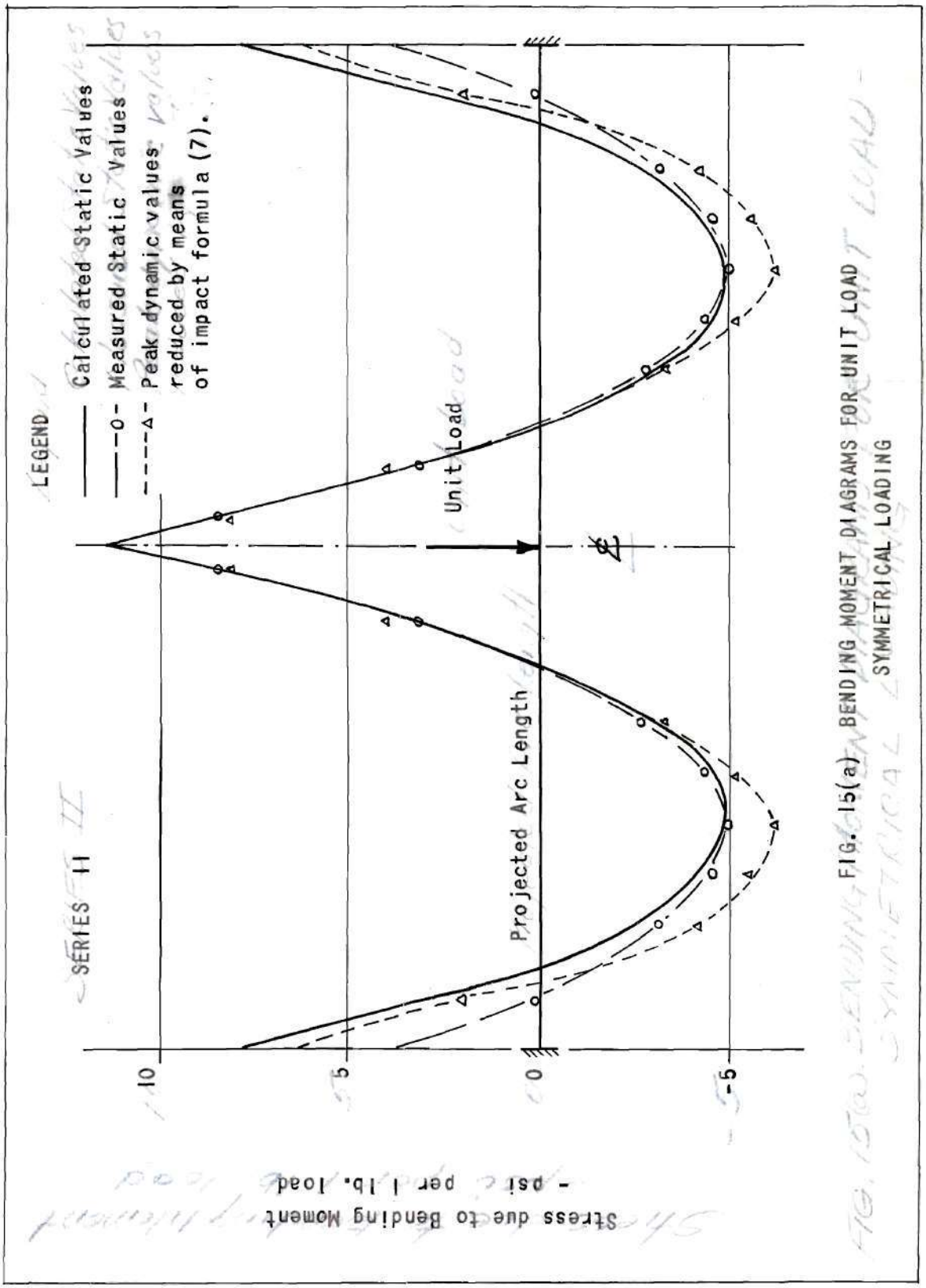

FIG. 15(a) BENDING MOMENT DIAGRAMS FOR UNIT LOAD SYMMETRICAL LOADING

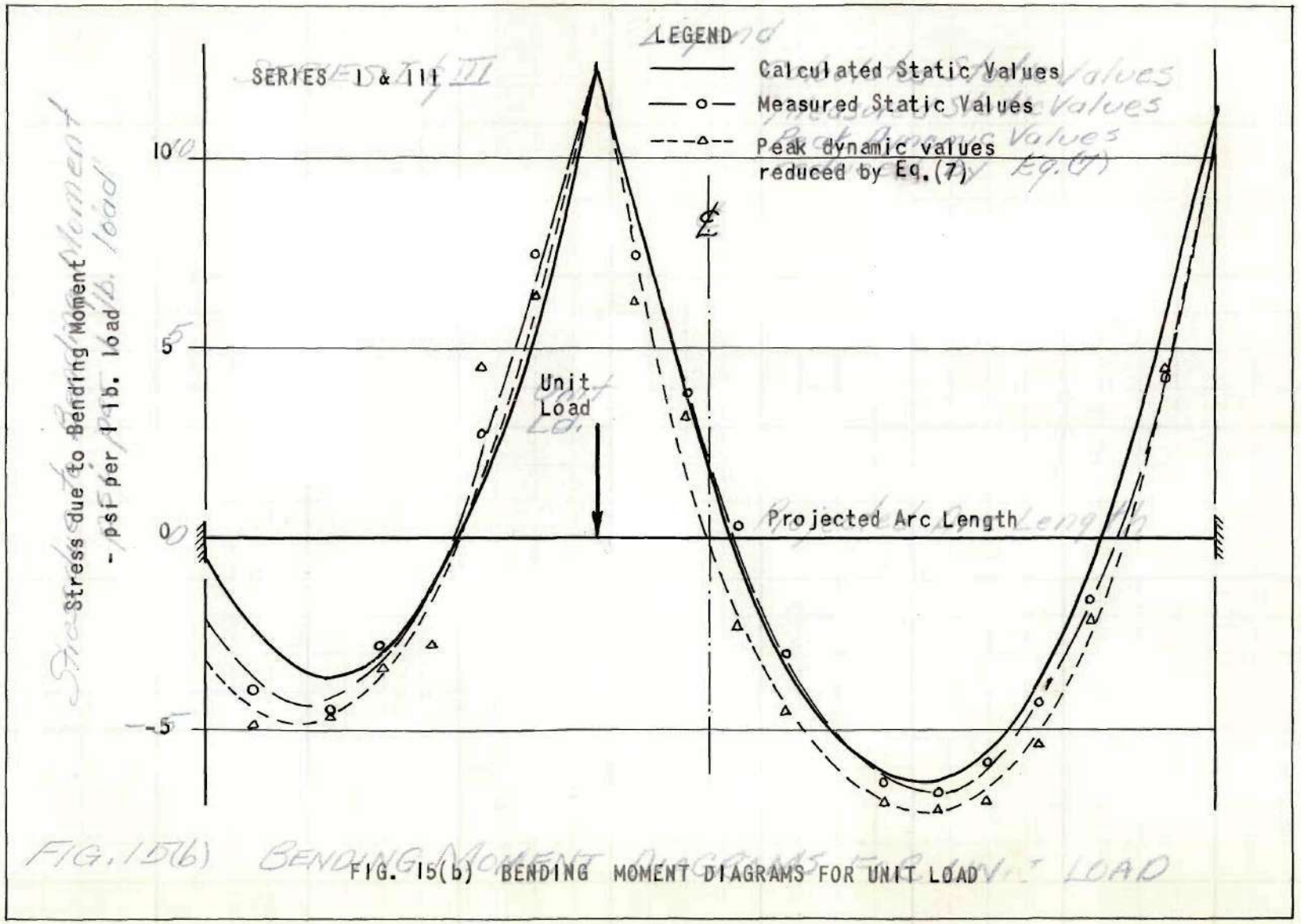

FIG. 15(b) BENDING MOMENT DIAGRAMS FOR UNIT LOAD

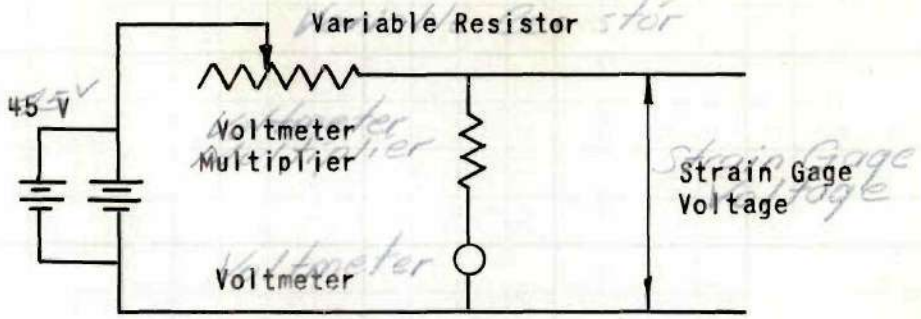

FIG. 7 STRAIN GAGE POWER SUPPLY

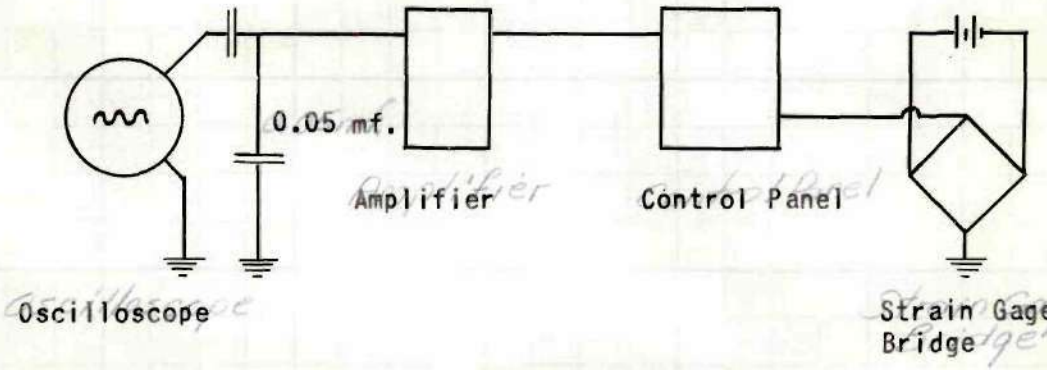

FIG 8 OVERALL CIRCUIT

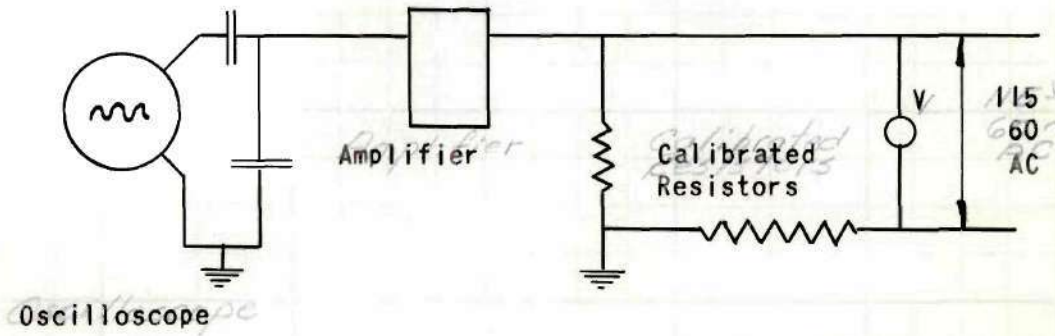

FIG. 9 CALIBRATION CIRCUIT FOR OSCILLOSCOPE

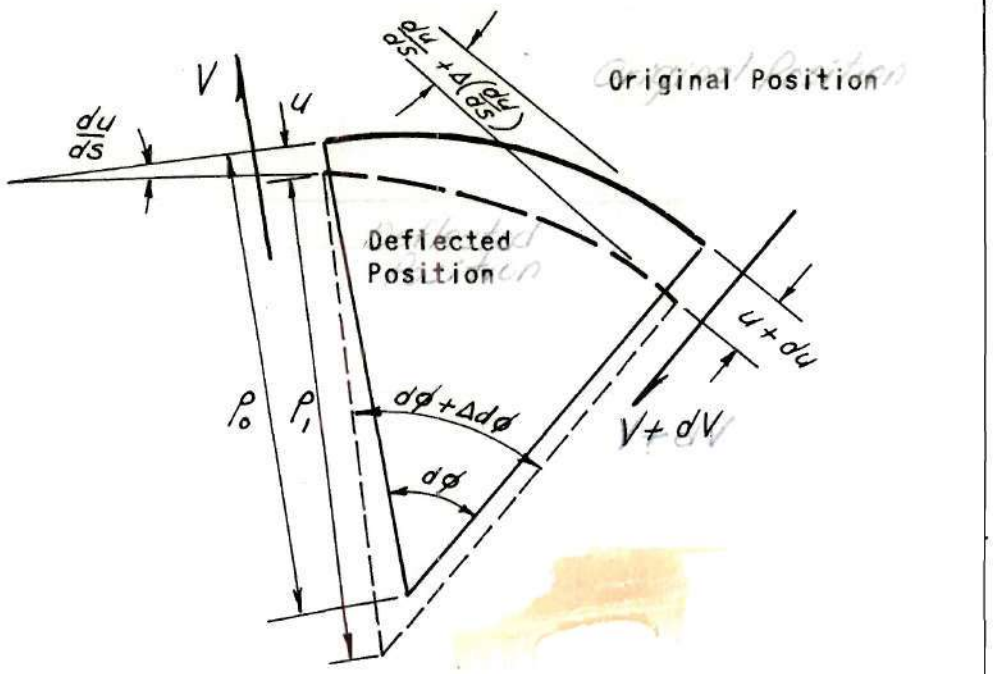

FIG. 10 DISPLACED ELEMENT OF ELASTIC CURVE OF A CIRCULAR ARC

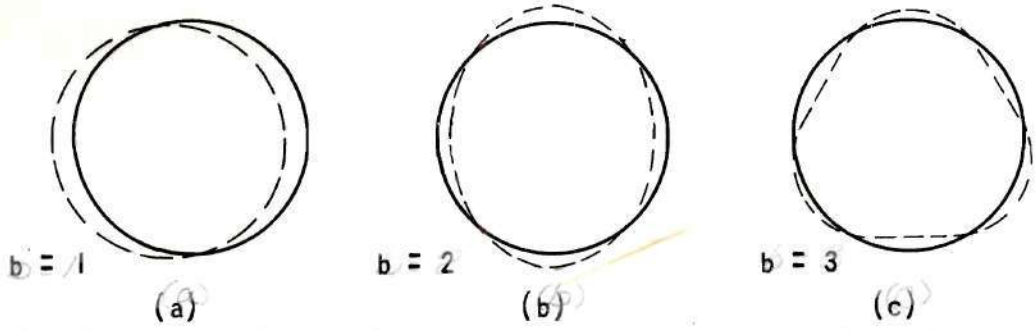

FIG. 11 MODES OF FREE VIBRATION OF A FULL RING

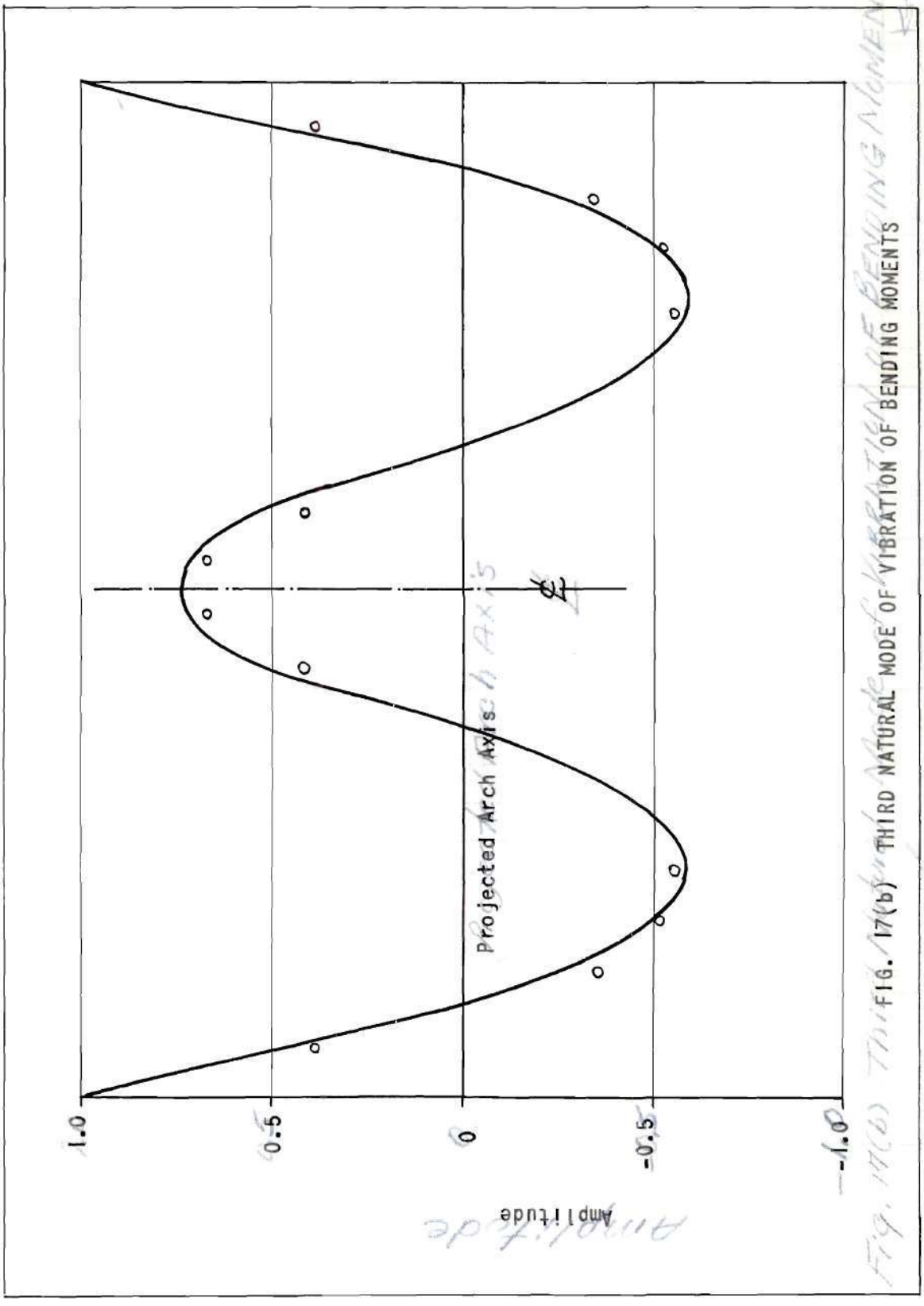

FIG. 17(b) THIRD NATURAL MODE OF VIBRATION OF BENDING MOMENTS

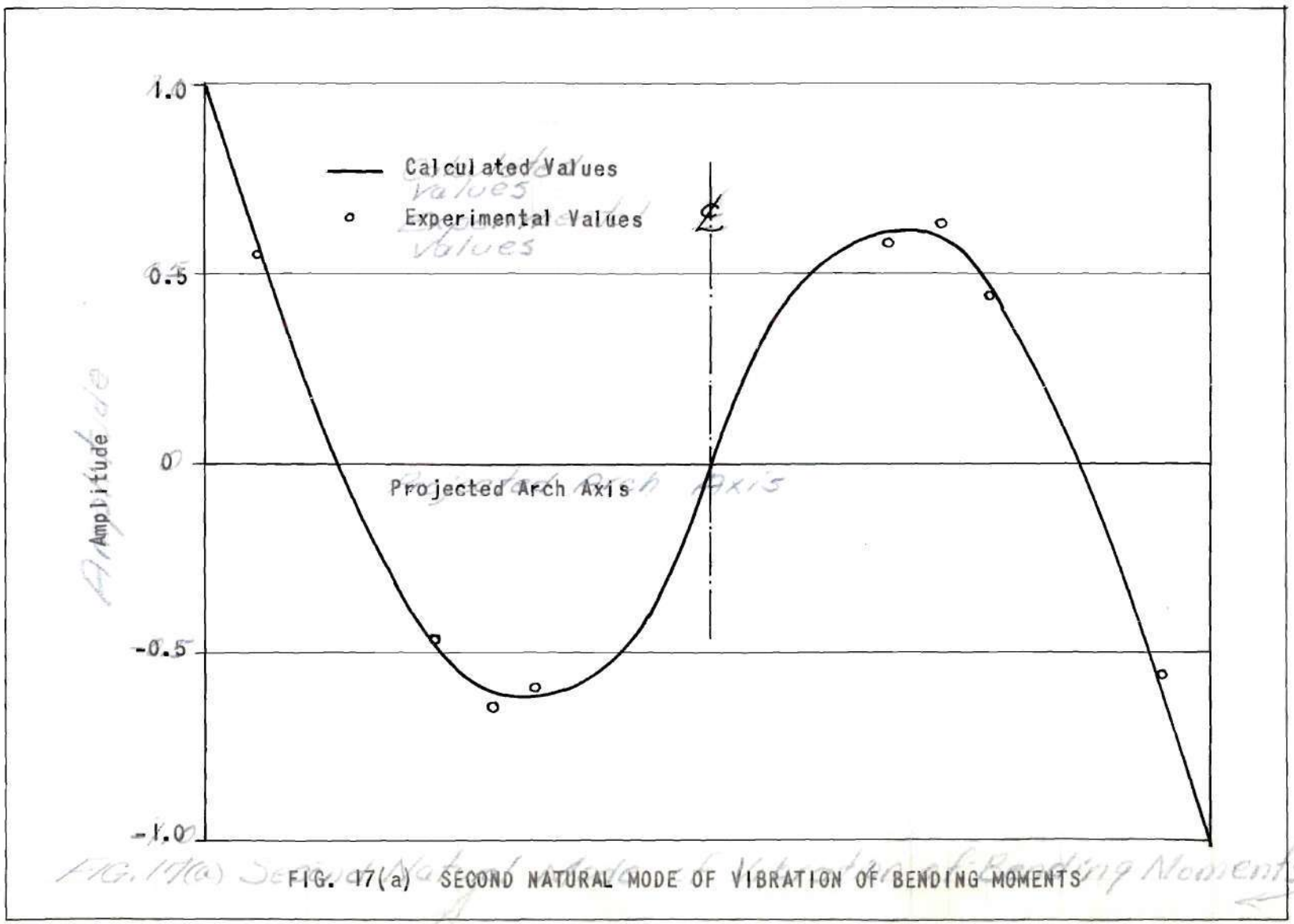

FIG. 17(a) SECOND NATURAL MODE OF VIBRATION OF BENDING MOMENTS

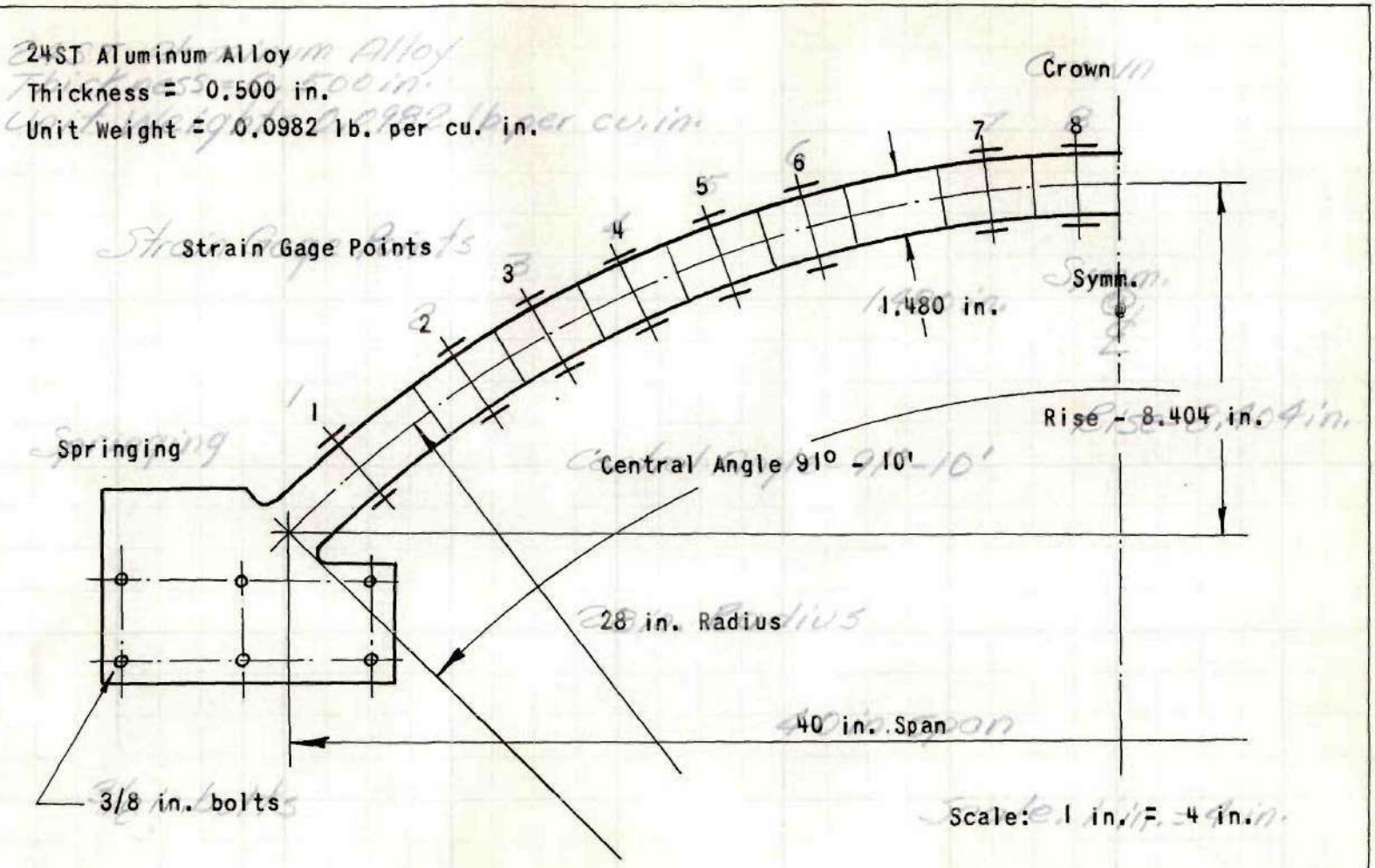

FIG. 5 DETAIL DRAWING OF MODEL

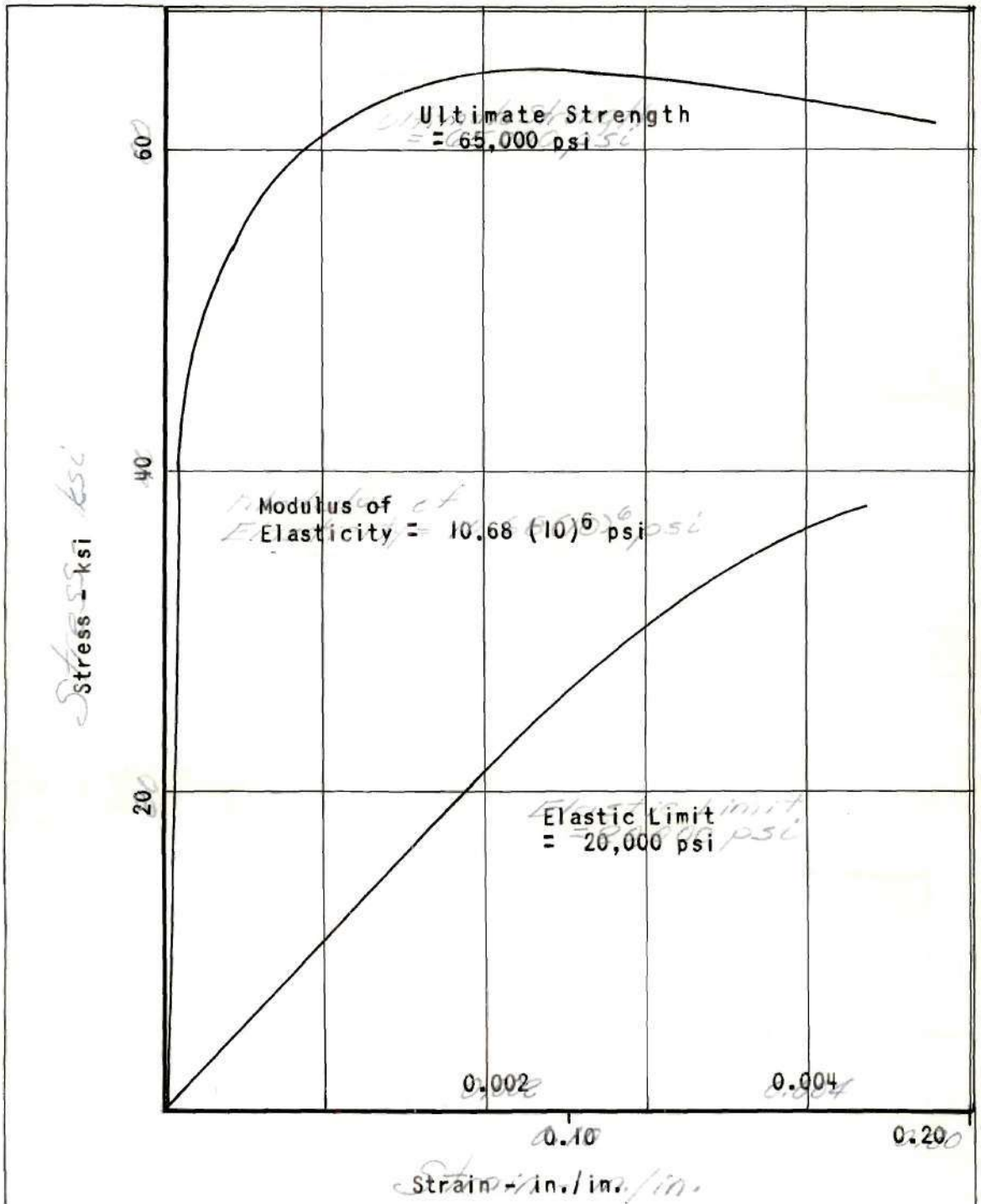

FIG. 4 STRESS - STRAIN CURVE FOR SPECIMEN OF MODEL, 24ST ALUMINUM IN TENSION

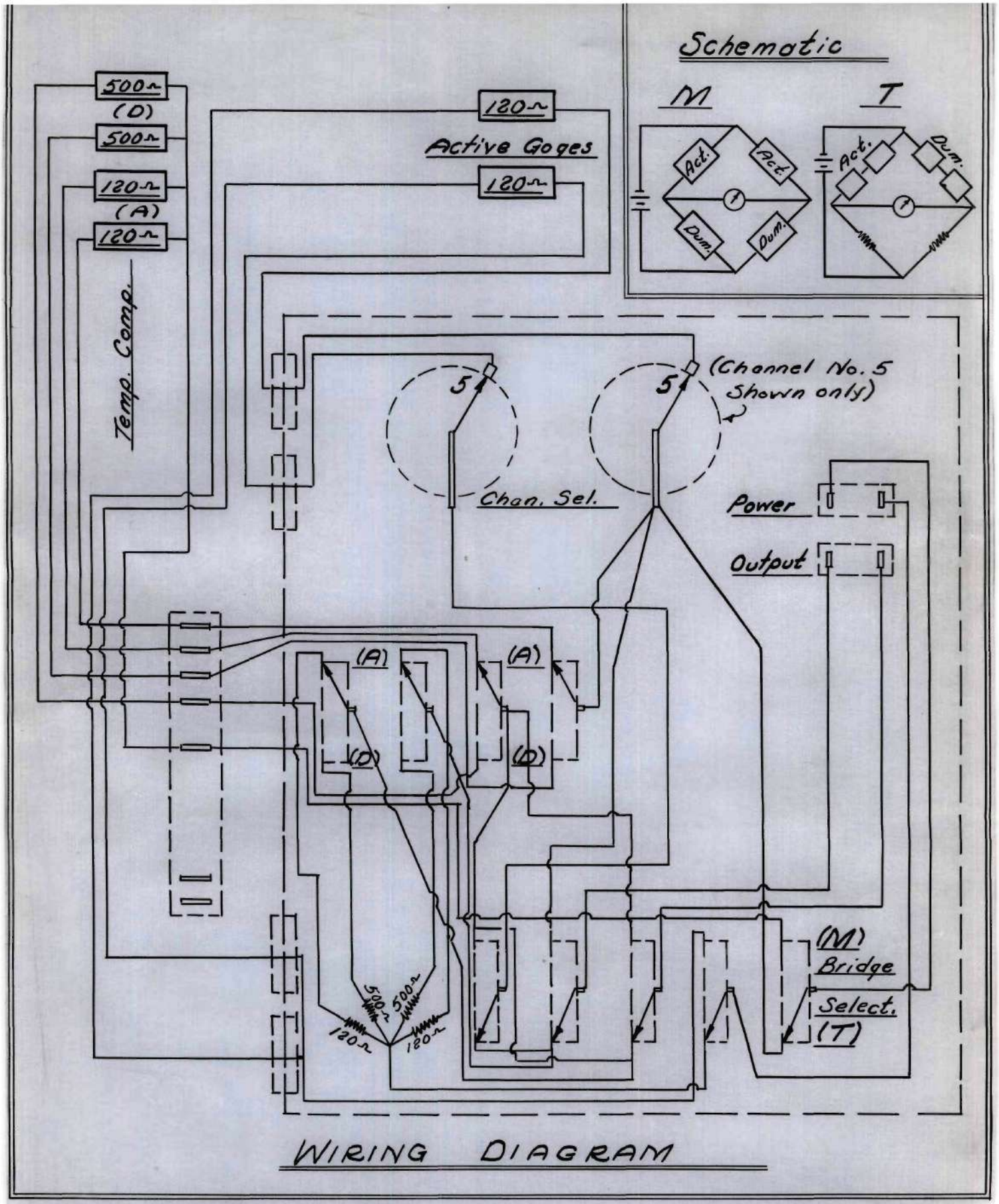

FIG.6 CONTROL BOX WIRING DIAGRAM